Fate and Transport of PFASs in the Landfill — Impact of the Perfluoroalkyl Chain Length

August 31, 2024

Gang Chen
Scott Wasman
Lin Qi

Department of Civil and Environmental Engineering
FAMU-FSU College of Engineering

Hinkley Center for Solid and Hazardous Waste Management
University of Florida
P. O. Box 116016
Gainesville, FL 32611
www.hinkleycenter.org

Report #

FINAL REPORT

September 1, 2023 to August 31, 2024

PROJECT TITLE: Fate and Transport of PFASs in the Landfill — Impact of the Perfluoroalkyl Chain Length

PRINCIPAL INVESTIGATOR(S): Gang Chen and Scott Wasman
AFFILIATION: Department of Civil and Environmental Engineering, FAMU-FSU College of Engineering

COMPLETION DATE: August 31, 2024

PHONE NUMBER: 850-410-6303

TAG MEMBERS: Bruce Marvin (Geosyntec Consultants), Chao Zhou (Geosyntec Consultants), Kevin Warner (Geosyntec Consultants), Gary Williams (Florida Rural Water Association), Paul E. Seaver (Palm Beach Springs Water Company Inc.), Sterling Carroll (Florida Rural Water Association), Owete S. Owete (WSP USA), Natalia Soares Quinete (Florida International University), Joseph Dertien (Florida Department of Environmental Protection), Shanin Speas-Frost (Florida Department of Environmental Protection), Walsta Jean-Baptiste (Florida Department of Environmental Protection)

KEY WORDS: Fate, Transport, PFASs, Chain Lenth, Landfill

ABSTRACT (1 page only)

Per- and polyfluoroalkyl substances (PFASs) are synthetic chemicals that lead to adverse human health effects. PFASs are introduced to landfills from waste such as water-repellent household products as well as waste streams such as fire protection practices. PFASs of concern are non-polymer PFASs including perfluoroalkyl acids (PFAA), perfluoroalkane sulfonyl fluoride (PASF), perfluoroalkyl iodides (PFAI), and per- and polyfluoroalkyl other-based substances such as per- and polyfluoroether carboxylic acids (PFECA) and per- and polyfluoroether sulfonic acids (PFESA). PFAS compounds are mainly acids that contain a carbon chain fully saturated with fluorine atoms and a polar head (i.e., carboxylic acid or sulfonic acid functional group, etc.). The fluorocarbon chain is hydrophobic and lipophobic because the fluorocarbon tail is non-polar and less susceptible to the London dispersion force than hydrocarbons, and the polar head is hydrophilic and interacts strongly with polar groups, specifically water. The hydrophobic chain promotes PFAS adsorption to the organic fraction of the solid waste in the landfill. This research investigated the impact of the perfluoroalkyl chain length on PFAS fate and transport in landfills. Fate and transport of PFASs with variable perfluoroalkyl chain lengths were investigated in laboratory columns. In addition, fate and transport of PFASs with different functional groups, i.e., cationic and anionic functional groups were also investigated.

Metrics:

1. List graduate or postdoctoral researchers funded by this Hinkley Center project

Last name, first name	**Rank**	**Department**	**Professor**	**Institution**
Lin Qi	Ph.D. Candidate	Civil and Environmental Engineering	Gang Chen	Florida State University
Shahin Alam	Ph.D. Student	Civil and Environmental Engineering	Gang Chen	Florida State University

2. List undergraduate researchers working on this Hinkley Center project

N/A

3. List research publications resulting from this Hinkley Center project
Qi, L., Alam, S. and Chen, G., 2024, PFAS Adhesion to Porous Media: A Surface Thermodynamic Exploration, in Kash Mittal (Editor), Progress in Adhesion and Adhesives, Scrivener Publishing LLC.

Alam, S. and Chen, G., 2024, PFAS research trend, concern and removal from the environment: A review, Environmental Science and Pollution Research, under review.

Alam, S. and Chen, G., 2024, PFAS health impacts of humans and ecosystem emerging contaminants: A review, Emerging Contaminants, under review.

4. List research presentations resulting from this Hinkley Center project
Chen, G., 2024, Fate and transport of PFASs in the landfill — Impact of the perfluoroalkyl chain length, Food-Energy-Water-Climate Nexus, July 2-4, Durban, South Africa.

5. List who has referenced or cited your publications from this project?
Current research is in process. Our related published work on PFASs has been cited from 10 times to 21 times:
Qi, L., Li, R., Wu, Y., Lin, X. and Chen, G., 2022, Effect of solution chemistry on the transport of short-chain and long-chain perfluoroalkyl carboxylic acids (PFCAs) in saturated porous media, Chemosphere, 303, 135160. Cited by 10
Wu, Y., Qi, L. and Chen, G., 2022, A mechanical investigation of perfluorooctane acid adsorption by engineered biochar, Journal of Cleaner Production, 340, 130742. Cited by 21

6. How have the research results from this Hinkley Center project been leveraged to secure additional research funding?
"Destructing PFAS in Landfill Leachate by in Situ Treatment Train: Selective Adsorption and Hydrothermal Treatment" by Yudi Wu and Gang Chen was Environmental Research and Education Foundation.

7. What new collaborations were initiated based on this Hinkley Center project?
We have initiated collaboration with Florida Rural Water Association (FRWA), a nonprofit and non-regulatory professional association which was originally formed for the benefit of small water and wastewater systems throughout Florida. The primary purpose of this organization is to assist water and wastewater systems with every phase of the water and wastewater operations. This research is of interest to the active members of this organization, who are associated with water and wastewater systems. We have also been contacted by professionals from Carollo Engineers, an environmental engineering firm that specializes in the planning, design, and construction of water and wastewater facilities regarding our work on landfill leachate treatment.

8. How have the results from this Hinkley Center funded project been used (not will be used) by the FDEP or other stakeholders? (1 paragraph maximum).
We keep close contact with managers of Leon County Landfill, Springhill Regional Landfill (Jackson County), and Perdido Landfill (Escambia County). In addition, we work closely with Thomas P. Smith Water Reclamation Facility located in Tallahassee, FL. We discuss the technical achievement of this project with the managers and request suggestions to further our research. We also share the results with FDEP through TAG members and discuss the results with FRWA, which services water and wastewater systems.

EXECUTIVE SUMMARY

September 1, 2023 to August 31, 2024

PROJECT TITLE: Fate and Transport of PFASs in the Landfill — Impact of the Perfluoroalkyl Chain Length

PRINCIPAL INVESTIGATOR(S): Gang Chen and Scott Wasman

AFFILIATION: Department of Civil and Environmental Engineering, FAMU-FSU College of Engineering

PROJECT WEBSITE ADDRESS (URL):
https://web1.eng.famu.fsu.edu/~gchen/index_files/Page1986.htm

PROJECT TAG MEMBERS: Bruce Marvin (Geosyntec Consultants), Chao Zhou (Geosyntec Consultants), Kevin Warner (Geosyntec Consultants), Gary Williams (Florida Rural Water Association), Paul E. Seaver (Palm Beach Springs Water Company Inc.), Sterling Carroll (Florida Rural Water Association), Owete S. Owete (WSP USA), Natalia Soares Quinete (Florida International University), Joseph Dertien (Florida Department of Environmental Protection), Shanin Speas-Frost (Florida Department of Environmental Protection), Walsta Jean-Baptiste (Florida Department of Environmental Protection)

COMPLETION DATE: August 31, 2024

Objective:
Per- and polyfluoroalkyl substances (PFASs) are synthetic chemicals that lead to adverse human health effects. PFASs are introduced to landfills from waste such as water-repellent household products as well as waste streams such as fire protection practices. PFASs of concern are non-polymer PFASs including perfluoroalkyl acids (PFAA), perfluoroalkane sulfonyl fluoride (PASF), perfluoroalkyl iodides (PFAI), and per- and polyfluoroalkyl other-based substances such as per- and polyfluoroether carboxylic acids (PFECA) and per- and polyfluoroether sulfonic acids (PFESA). PFAS compounds are mainly acids that contain a carbon chain fully saturated with fluorine atoms and a polar head (i.e., carboxylic acid or sulfonic acid functional group, etc.). The fluorocarbon chain is hydrophobic and lipophobic because the fluorocarbon tail is non-polar and less susceptible to the London dispersion force than hydrocarbons, and the polar head is hydrophilic and interacts strongly with polar groups, specifically water. The hydrophobic chain promotes PFAS adsorption to the organic fraction of the solid waste in the landfill. The objective of this research was to investigate the impact of the perfluoroalkyl chain length on PFAS fate and transport in landfills. Subsequently, fate and transport of PFASs with variable perfluoroalkyl chain lengths were investigated in laboratory columns. In addition, fate and transport of PFASs with different functional groups, i.e., cationic and anionic functional groups were also investigated.

Methodology:

Saturated PFAS transport was conducted in acrylic columns (0.75-inch diameter × 12-inch length). Before the experiments, the sand was soaked in concentrated hydrochloric acid overnight to minimize the influence of inorganic and organic impurities on the surface. The hydrodynamic properties of the sand columns were characterized via a nonreactive tracer of NaBr. Following the tracer test, a pulse of 3 PVs of PFASs with target pH and ionic strengths was injected to columns in upward mode by a peristaltic pump. Then, several PVs of background solution were pumped through columns at the same velocity until the background signal was detected. Effluent solutions were collected continuously in polypropylene tubes using a fraction collector and then transferred into chromatography vials for PFCA concentration quantification.

Unsaturated PFAS transport was conducted using unsaturated columns, and inflow was applied from the top using a sprinkler consisting of 12 hypodermic needles (30-gauge) by a peristaltic pump. The bottom of the column was equipped with two layers of a nylon membrane. Water content was monitored using tensiometers by CR-7X data logger. The effluent was collected and analyzed for PFASs.

Results:

Undersaturated conditions, transport of PFPeA, PFHxA, and PFOA were similar to that of the tracer, whereas PFDA was asymmetrical and displayed delays, indicating that PFPeA, PFHxA, and PFOA were slightly retarded upon passing through the sand column, while PFDA exhibited enhanced retardation due to sorption to the minerals. Increasing pH had a relatively minor effect on the transport of PFPeA, PFHxA, and PFOA. On the other hand, an increase in pH yielded a substantially higher mitigation of PFDA transport. Retardation factor was observed to be smaller for short-chain PFASs than that of long-chain PFASs. When the fluorocarbon chains contained eight or less carbons, the impact of solution chemistry had minimal impact on their transport. However, when the fluorocarbon chains contained carbon numbers greater than eight, such as PFDA, the retardation became significant. In addition, the presence of the divalent cation of Ca^{2+} inhibited the transport of both short-chain and long-chain PFASs, which was more pronounced for the long-chain ones.

Under saturated conditions, there was minimal difference of PFBS, PFPeS, PFHxS, and PFOS. Under high saturation conditions, breakthrough delays were observed for PFHxS and PFOS, which was more pronounced for PFOS as compared to PFHxS. Under low saturation conditions, similarly, breakthrough delays were observed for PFHxS and PFOS with PFOS more pronounced. The delays of the breakthrough curves of PFOS and PFHxS clearly indicated that the perfluoroalkyl chain length played significant roles of PFAS retention in the porous media, with enhanced effects with increased C-F chain length. The results also indicated that the impact of C-F chain length on PFAS retention started to be observed with C-F chain length greater than 6. With increased input concentration, PFASs formed micelles or hemi-micelles, which promoted PFAS transport in the form of micelles with the flowing solution, leading to advection.

TABLE OF CONTENTS

TABLES

FIGURES

1. Introduction

1.1 PFAS overview

Per- and polyfluoroalkyl substances (PFASs) are synthetic chemicals that are used for consumer products such as nonstick pans, food packaging, and waterproof clothing as well as industrial purposes such as chrome plating, electronics manufacturing, and oil recovery (Gluge et al., 2020; Zhu et al., 2021). They have also been extensively used as firefighting foam (de Vries et al., 2017; Hoisaeter et al., 2019). PFASs have been manufactured and used in a variety of industries since the 1940s. So far, more than 3,000 different PFAS compounds have been detected with varying number of carbon atoms and functional groups, of which only 24 are routinely measured (Lang et al., 2017). Due to their thermal stability and hydrophobic properties, they have been determined by regulators to be persistent, bioaccumulative, and toxic substances. There is evidence that exposure to PFASs can lead to adverse human health effects and subsequently they are currently considered emerging contaminants of concern (Boone et al., 2019). Because of the toxicity concerns, management actions to curtail manufacture of long-chain PFASs and their precursors have been taken (Brendel et al., 2018). Although they are no longer manufactured in the US, they are still produced internationally and imported into the US in consumer goods.

Landfills are the ultimate repositories for PFAS-contaminated industrial waste as well as PFAS-treated consumer waste such as goods treated with hydrophobic, stain-resistant coatings (Coffin et al., 2023; Vo et al., 2023; Zhang et al., 2023a). The type and amount of PFASs deposited in landfills vary greatly among landfills due to variations in the waste streams. Domestic household waste as well as C&D waste that may contain firefighting foam waste can be a significant source of PFASs in landfills. Inside the landfills, PFASs may leach out and accumulate in the landfill leachate or be retained in the waste depending on the perfluoroalkyl chain length. For those leached to the leachate, they are typically sent directly to wastewater treatment plants for further treatment, although some landfills practice pre-treatment before discharge (Benskin et al., 2012; Lang et al., 2017; Solo-Gabriele et al., 2020). PFASs may also get into the wastewater treatment processes as a result of down-the-drain disposal from sources such as food and laundry wastewater and disposal of products treated with PFASs (Coggan et al., 2019). However, conventional wastewater treatment processes are often ineffective degrading PFASs with PFASs escaping the treatment processes in the effluent or associated with biosolids (i.e., sewage sludge), which are deposited back to the landfills.

Adsorption of PFASs is the currently the most cost-effective method for PFAS removal, especially when using activated carbon and ion exchange (Carter and Farrell, 2010). However, although adsorption can be cost-effective, treatment processes should consider sorbent regeneration and further destruction of adsorbed PFASs. For most cases, the sorbent with adsorbed PFASs is recycled back to the landfills. Adsorbed PFASs can be destructed by thermal treatment, which involves breaking the C–C and C–F bonds with high temperature to produce perfluoroalkyl radicals that will subsequently be decomposed (Merino et al., 2016; Ross et al., 2018; Wang et al., 2015). By incineration, PFASs are destructed to produce volatile 1-H-substituted perfluoroalkyl substances such as 1-H-perfluoroheptane (Merino et al., 2016). Other harmful emissions, including strong greenhouse gases such as tetrafluoromethane (CF_4) and hexafluoroethane (C_2F_6) can also be produced.

A comprehensive understanding of the impact of carbon chain length on PFAS contamination is crucial for making regulatory frameworks, developing effective remediation strategies, and mitigating the environmental impact (Sun et al., 2024). Ongoing research continues to refine our knowledge of PFAS behavior, providing valuable insights into the complex interplay between carbon chain length and the fate and transport of these persistent pollutants. The carbon chain length of PFAS compounds plays a role in their fate and transport, influencing their behavior in various environmental compartments. The perfluoroalkyl chain length of PFAS determines PFAS solubility and their hydrophobic interactions with the sorbent (Coppola et al., 2022). An increase in the perfluoroalkyl chain length will decrease their solubility and increase their hydrophobic interactions. There is a general trend that the hydrophobicity of PFASs increases with the rise of the carbon numbers in the C-F chain, and so does the PFAS adsorption capacity (Herath et al., 2010).

It should be noted that although interactions of C-F with water are more attractive than those of C-H with water, the fluorocarbon surfaces are more hydrophobic than those of the corresponding hydrocarbons because of the enhanced hydrophobicity of fluorinated surfaces. The fluorocarbons have a molecular cross-section of 28.3 Å2 and occupy sufficiently more volume and surface area in water than the corresponding hydrocarbons with a molecular cross-section of 18.9 Å^{2}. Subsequently, fluorocarbons pack less densely on the surfaces, leading to poorer van der Waals interactions with water (Gagliano et al., 2020). Long-chain PFASs are more accessible to absorb than short-chain PFASs because of the more significant decrease of the cross-section area after adsorption (i.e., a more substantial reduction of Gibbs free energy). Branched isomers have less sorption than linear ones because of the decrease in the contact area (Shimoaka et al., 2017).

Depending on the perfluoroalkyl chain length, PFASs would exhibit different fate and transport. PFASs with fewer carbons tend to dominate in the landfill leachate because they are less hydrophobic and more likely to partition to the aqueous phase. On the contrary, longer-chain PFASs are more prevalent in the waste and less prone to release and leaching (Tolaymat et al., 2023). This project determined what kinds of PFASs (i.e., with what perfluoroalkyl chain lengths) would possibly be in the landfill leachate and what kinds of PFASs would be retained in the landfill. In addition, the impact of PFAS functional groups on PFAS leaching was investigated.

1.2 PFASs in the landfill

Among the typical domestic solid waste deposited in landfills, textiles have PFAS content of 450-2100 ug/Kg, carpeting has PFAS content of 350-1100 ug/Kg, and sludge has PFAS content of 50-250 ug/Kg (Yu, 2020). Averagely, the daily dumping of PFASs from the above waste is 9 g/day for textiles, 7.5 g/day for carpet, and 1.7 g/day for sludge (Liu et al., 2022; Robey et al., 2020). Among the food waste and compostable food services, perfluorohexanoic acid (PFHxA) is in the range of 10-37.5 ug/kg, perfluorooctanesulfonic acid (PFOS) is up to 2.5 ug/Kg, and perfluorooctanoic acid (PFOA) is up to 7.5 ug/kg.

PFAS composition and concentration in the landfill leachate vary depending on the waste type, age, and climate. Inside the landfill, PFASs can also be produced from polyfluorinated substances (i.e., precursor PFASs) by chemical and biological transformation such as hydrolysis, photolysis, and oxidation under ambient environmental conditions (Capozzi et al., 2023). As fully fluorinated molecules, perfluoroalkyl acids (PFAAs) are basic PFAS structures with a formula of C_nF_{2n+1}-R, where "C_nF_{2n+1}" represents the carbon-fluorine chain and "R" represents the attached functional group head (Figure 1). PFAA precursors are also important in the landfill since they can be biotically and abiotically transformed into PFAAs. Many polyfluoroalkyl substances are PFAA precursors, which are not fully fluorinated with a non-fluorine atom (i.e., hydrogen or oxygen) attached to at least one, but not all, of the carbon atoms, while at least two or more of the remaining carbon atoms in the carbon chain tail are fully fluorinated. For instance, heat and persulfate generate hydroxyl radicals, which react with the PFAA precursors to break them down to perfluorinated carboxylic acids (PFCAs) (Dombrowski et al., 2018). Similarly, PFAA precursors can also be biotransformed to PFCAs and perfluoroalkyl sulfonic acids (PFSAs) (Chen et al., 2019; Eriksson et al., 2017; Yi et al., 2018). The most studied and usually the primary indicators of PFASs are perfluorooctanesulfonic acid (PFOS), perfluorooctanoic acid (PFOA), and perfluorohexane sulfonate (PFHxS). This is because PFOS and PFHxS are found in the breakdowns of firefighting foam (i.e., aqueous film-forming foam or AFFF) and PFOA can be found in the older formulation of AFFF.

Although carbon-fluorine chains of PFASs are hydrophobic, the functional groups (e.g., sulfonate, carboxyl, etc.) of PFASs are hydrophilic, which make them potential water soluble and mobile in the aqueous phase. For modern landfills designed with liners and leachate collection systems, PFASs are found to have elevated concentrations in the landfill leachate. The perfluoroalkyl chain length of PFASs largely determines their solubility properties. Typically, PFASs with short perfluoroalkyl chain length tend to dominate in the landfill leachate because they are less hydrophobic and therefore more likely to partition to the aqueous phase (Ateia et al., 2019). On the contrary, longer-chain PFASs tend to be retained in the landfill for a longer term (Stebel et al., 2019). Further research is needed to characterize the composition of PFASs with different perfluoroalkyl chain lengths in the landfill and landfill leachate.

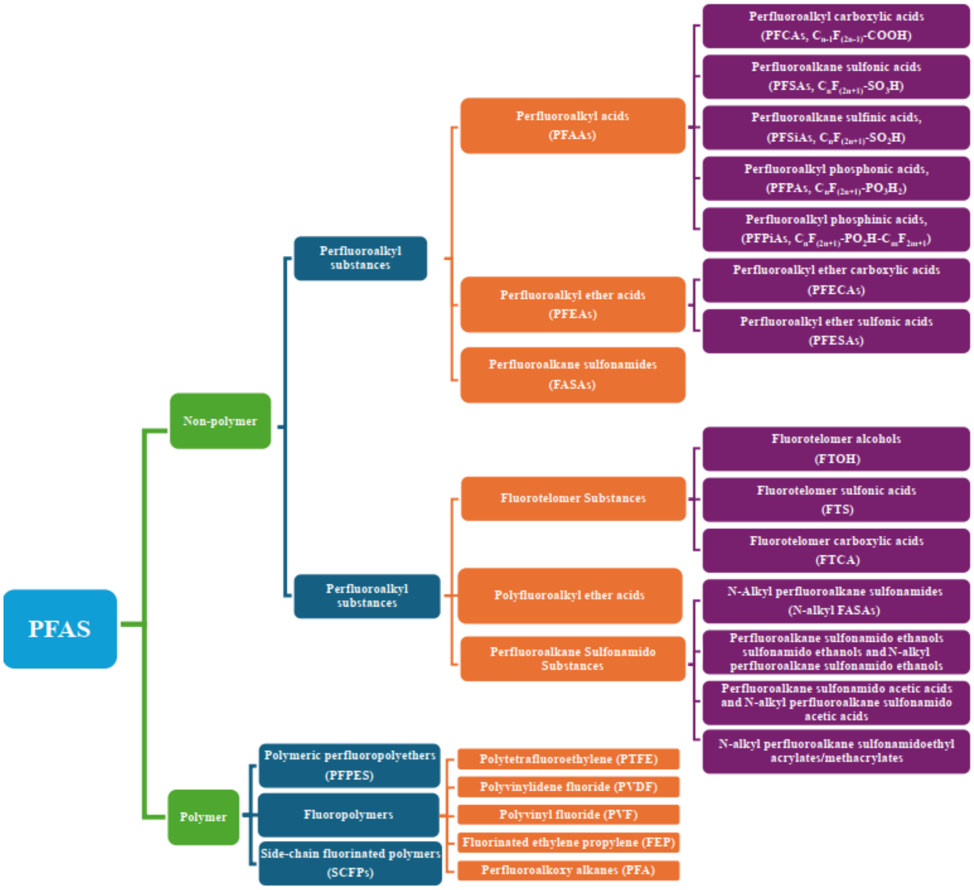

Figure 1. PFAS Classification

Typically, the leached PFASs are around 1.6 g/day in the landfill leachate. Based on prior study, the total PFAS concentration reported for untreated landfill leachate is 2.8-18 µg/L and 0.3-66 µg/L (Solo-Gabriele et al., 2020). Inside the landfill, PFASs continue to be leached from the PFAS-containing waste, which are subject to further adsorption. The landfills themselves are considered to consist of three phases, i.e., a solution phase, a solid phase, and a gas phase. It should be noted that the gas phase interacts with liquid and solid phases to form liquid-gas interface, solid-gas interface, and liquid-gas-solid three-phase interface. Since most PFASs contain the hydrophobic C-F chain and a hydrophilic polar functional head group, they display amphiphilic properties, which enable them to attach to the liquid-gas interface in addition to the solid surfaces in the landfill (Brusseau, 2018a; Brusseau, 2019; Wei et al., 2017). Again, since the adsorption of PFASs to the solid and liquid-gas interface depends on the perfluoroalkyl chain length, PFASs would exhibit different fate and transport. Further research is thus needed to characterize the impact of the perfluoroalkyl chain length on PFAS attachment to the liquid-gas interface, which subsequently affects their fate and transport in the landfill.

1.3 PFAS chain length and PFAS fate and transport

Studies reported short-chain PFASs transported long distances. On the contrary, long-term retention of longer-chain PFASs was commonly observed (Ateia et al., 2019; Stebel et al., 2019). The perfluoroalkyl chain length of PFASs determines PFAS solubility and their hydrophobic interactions with the sorbent. Increase in the perfluoroalkyl chain length decreases their solubility and increases their hydrophobic interactions. There is a general trend that the hydrophobicity of PFASs increases with the increase of the carbon numbers in the C-F chain and so is the PFAS adsorption capacity. It should be noted that although interactions of C-F with water are more attractive than those of C-H with water, the fluorocarbon surfaces are more hydrophobic than those of the corresponding hydrocarbons because of the enhanced hydrophobicity of fluorinated surfaces (Dalvi and Rossky, 2010). The fluorocarbons have a molecular cross-section of 28.3 $Å^2$ and occupy sufficiently more volume and surface area in water than the corresponding hydrocarbons that have a molecular cross-section of 18.9 $Å^2$. Subsequently, fluorocarbons pack less densely on the surfaces, leading to poorer van der Waals interactions with water. Long-chain PFASs are more easy to be adsorbed than those of short-chain PFASs because of the greater decrease of the cross-section area after adsorption (i.e., greater decrease of Gibbs free energy). Branched isomers have less sorption than linear ones because of the less decrease of the contact area (Brendel et al., 2018).

The length of the PFAS carbon chain also affects their mobility in the environmental media. Longer-chain PFAS compounds often exhibit a higher affinity for organic matter in soils and sediments, resulting in stronger adsorption (Zhang et al., 2023b). The enhanced adsorption can lead to the accumulation of PFASs in specific environmental compartments, raising concerns about potential long-term retention and exposure. Shorter-chain PFAS compounds are generally more mobile and may exhibit stronger transport through aquatic systems. The volatility of PFASs is also influenced by carbon chain length. Shorter-chain PFAS compounds are generally more volatile and can readily attach to air-water interfaces, which may lead to atmospheric deposition, contributing to the widespread distribution of PFASs in various environmental compartments. The degradation and transformation of PFASs is also influenced by carbon chain length.

Studies suggested that shorter-chain PFAS compounds were more prone to specific transformation processes, potentially forming degradation byproducts with different environmental fates and toxicological properties based on the investigation of the impact of perfluorinated carbon chain length on PFCA transport in the soil by using PFPeA, PFHxA, PFOA, and PFDA as model PFCA compounds (Gagliano et al., 2020). In addition, solution chemistry, including pH, ionic strength, and cationic type, was also found to have significant impact on their transport. These studies also concluded that the chain length had limited impacts on PFCA transport when the fluorocarbon chains contained eight or fewer carbons, such as PFPeA, PFHxA, and PFOA, under various pH and ionic strength conditions (Bigler et al., 2024). In contrast, when the fluorocarbon chains contained carbon numbers greater than eight, such as PFDA, the mobility was significantly affected by pH and ionic strength. The presence of the divalent cation of Ca^{2+} inhibited the transport of both short-chain and long-chain PFCAs, which was more pronounced for the long-chain ones.

The adsorption of PFASs to the organic fraction of the sorbent is determined by the sorbent organic carbon content. Research demonstrated a general increase of PFAS adsorption with the increase in chain length. This also indicated greater leaching potentials of short-chain PFASs under equilibrium conditions. The difference in the relative partitioning affinity of the PFASs with variable chain lengths also reflected that hydrophobicity was crucial in PFAS retention in the soil. In other words, the partition of PFASs to the organic fraction in the soil controlled PFAS transport, which depended on the perfluorinated chain length (Viticoski et al., 2022). PFSAs partition to the organic fraction more than PFCAs of equal C-F chain length. It should be noted that although eight perfluorinated carbons are mentioned as the threshold between short- and long-chain PFASs, the actual threshold of perfluorinated carbons is less clear. For instance, PFOA (8 perfluorinated carbons) and PFHxS (6 perfluorinated carbons) were typically considered “long-chain” PFASs. However, they partitioned into organic fractions similarly to conventional short-chain PFASs (lower than six perfluorinated carbons). Studies on PFAS fate and transport with dynamic soil column tests were conducted to assess the retardation of 10 classical PFAA (C5–C11 PFCA and C4, C6, C8 PFSA) and two alternative PFAS (6:2 and 8:2 fluorotelomer sulfonates), and the results highlighted substantial retardation for long-chain PFASs. Competitive effects were also noted by replacing shorter-chain PFCA, such as PFPeA, with longer-chained PFASs. Calculated partitioning coefficients (K_d) ranged from ∼103 to 105 L/kg for individual PFASs, and a significant positive correlation ($p < 0.05$) was derived for perfluorocarbon chain length and K_d (Niarchos et al., 2022).

1.4 PFAS characteristics and retention

PFASs of concern are PFAAs, including PFCAs, PFSAs, perfluoroalkyl phosphonic acids (PFPAs), perfluoroalkyl phosphonic acids (PFPiAs), etc. Among these PFASs, the perfluoroalkyl chains are hydrophobic and the acidic functional groups are hydrophilic. The hydrophilic polar head functional groups exist in equilibrium between the neutral and the anionic forms, which influences their solubility in water, i.e., the anionic form leads to greater water-solubility than that of the neutral form. The hydrophobic perfluoroalkyl chains make it possible for PFASs to adsorb on the organic fraction of the solid waste. At the same time, the polar heads of PFASs interact strongly with polar groups, making PFASs to attach the oppositely charged surfaces in the landfill (Sundstrom et al., 2012). The amphiphilic properties of PFASs complicate their adsorption behaviors such as partitioning coefficients, which also make them adsorb to the liquid-gas interface.

Currently, adsorption of PFASs in the landfill can be explained by three mechanisms: 1) hydrophobic interactions of the fluorinated carbon tail with the organic carbon fraction of the sorbent, 2) electrostatic interactions of the polar head group with the sorbent charged fraction, and 3) hydrogen bonding of the acidic head group with functional groups such as carboxylic on the sorbent surfaces (Figure 2). It should be noted that theoretically, hydrophobic interactions are not an attractive force, but rather a thermodynamically driven process. Electrostatic interactions become important when sorbents contain positively charged sites and PFASs exist primarily as anions. Hydrogen bonding plays a key role of PFAS adsorption when the sorbents are saturated with carboxylic functional groups.

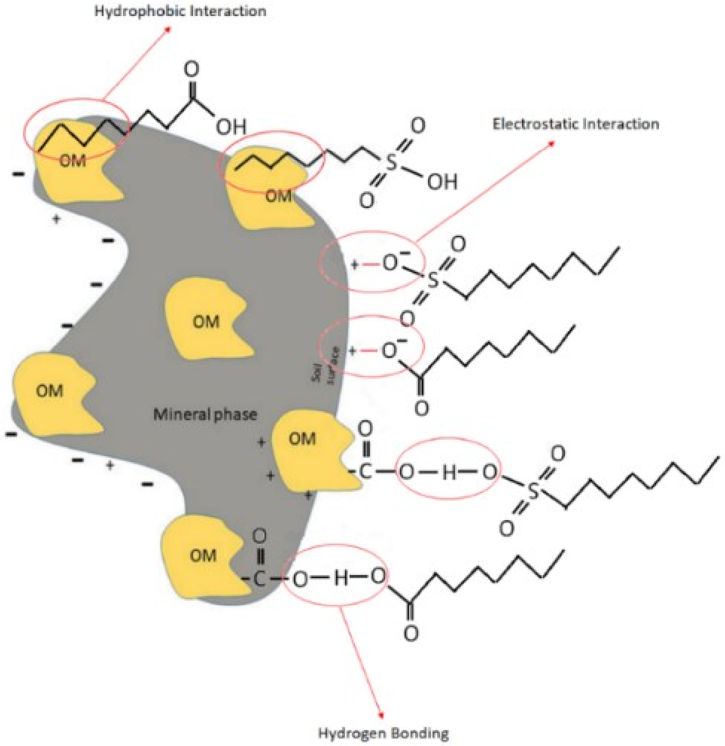

Figure 2. PFAS Adsorption Mechanisms

Solution chemistry is important in terms of pH and ionic strength for electrostatic interactions. At the environmental pH values, PFASs exist primarily as anions, making them potential water soluble. At these pH values, PFASs will likely to sorb strongly to positively charged materials by electrostatic interactions. Thus, pH plays an important role in PFAS adsorption in the landfill since it affects the sorbents' surface charges. For instance, increase of pH causes minerals such as goethite and kaolinite to become negatively charged, decreasing PFAS adsorption (McFarlan and

Lemke, 2024). On the other hand, greater acidity increases the potential magnitude of PFAS adsorption by electrostatic attraction. Similarly, different ionic strength leads to variable electrical double layer thickness, and eventually the electrostatic interactions between PFASs and the sorbent. Higher ionic strength leads to lower electrostatic interactions and subsequently less adsorption. Different PFASs display different adsorption under the same water chemistry conditions. For instance, PFSAs sorb more strongly than PFCAs through electrostatic interactions. Co-contaminants in the landfill also affect PFAS adsorption since they compete for the adsorption sites.

2. Background

PFASs are a group of thousands of chemicals utilized in a wide range of consumer and commercial products since the 1940s. Concerns about the persistence of PFASs and the scarcity of information about the properties, applications, and toxicological profiles of PFASs in use urge more research on PFAS fate and transport (Scher et al., 2018). To argue that PFASs cannot be considered a single class, PFAS manufacturers routinely pointed to the diversity of PFAS structures, features, and behaviors. The high persistence of PFASs is cited as a reason to regulate the class of chemicals and phase out non-essential PFAS applications. However, several applications for which a complete ban on all PFASs is unfeasible. Some PFAS applications are considered imperative for health, safety, or the proper running of today's society, for which there are no viable alternatives.

On the other hand, PFASs are phased out when their use is determined to be non-essential. By the Montreal Protocol, the essential use has further expanded for PFASs with illustrative case studies for various important use categories. PFASs are 100 to 1000 times more expensive per unit volume than conventional hydrocarbon compounds, and are often used when other substances fail to deliver the desired results (Hamdani et al., 2024). Therefore, PFASs can be used in much smaller quantities while providing the same results that require more significant quantities of non-fluorinated chemicals. Since PFAS molecules are made up of C–F bonds, they are highly stable, which also accounts for their persistence in the environment. PFASs have hydrophobic and oleophobic hydrocarbon moieties, making them suitable surfactants and surface protectors. Compared to hydrocarbon surfaces, fluorinated polymers have about half the surface tension of hydrocarbon surfaces (Pinkard et al., 2021). Subsequently, PFAS-based fluorosurfactants can reduce water surface tension twice as much as hydrocarbon surfactants.

PFASs are used in a plethora of applications due to their attractive qualities. Perfluorooctanoic acid (PFOA), perfluorooctane sulfonic acid (PFOS), perfluorohexane sulfonic acid (PFHxS), and GenX are the common PFAS chemicals (Furlow, 2024). PFASs have become a global pollutant that threatens the health of humans and wildlife because of their persistence and mobility. Meanwhile, PFAS use reduces the expenses of our daily lives and industry. PFASs are common in rural freshwater resources, especially near biosolids application sites, which manage beneficial land use in the United States. Eventually, accumulation of PFASs in oceans and marine food chains, as well as groundwater contamination, pushes unnecessary PFASs to phase out from production. However, PFAS exposures caused by accumulated PFASs in oceans and marine food chains, as well as groundwater contamination, persist over long-time scales.

PFAS concentrations and trends in water resources vary depending on many factors, and there are not enough data of PFAS contamination to determine human PFAS exposure (Brusseau and Guo, 2023b). Many communities across the country have discovered the presence of PFASs in various water resources. To develop pollution control and treatment approaches that protect human and ecosystem health, it is necessary to characterize the level of PFAS contamination in water resources and identify the PFAS sources and subsequent their fate and transport. Because of their persistence, PFASs tend to affect human health through the food chain, by accumulating in fish or aquatic organisms, or in edible plants and grains when PFAS-contaminated water is used for irrigation. To accurately assess exposure risks, data collection and interpretation are important in understanding the impact of PFASs on human health.

In 2009, the United States Environmental Protection Agency (US EPA) issued provisional Health Advisories for PFOA and PFOS (USEPA, 2009). Subsequently, in 2012, public water supplies underwent testing under the Safe Drinking Water Act. In 2016, the US EPA recommended drinking water health advisories for PFOS and PFOA, known carcinogens (USEPA, 2016). In the same year, the EPA established a national Lifetime Health Advisory (LHA) of 70 ng/L, with approximately 28 states subsequently setting guidance values for PFAS concentrations. The United States Office of Water recommended a lifetime health advisory for drinking water in 2016 of 70 ng/L for both PFOA and PFOS, as well as a total of 70 ng/L for PFOA and PFOS. The Office of Land and Emergency Management made interim recommendations regarding PFOA and PFOS in groundwater at 40 ng/L, as well as the sum of PFOA and PFOS in 2020. The US EPA published updated health advisories for PFOA, PFOS, GenX, and PFBS on June 15, 2022, with PFOA interim concentration of 0.04 parts per trillion (ppt) or ng/L, PFOS interim concentration of 0.02 ppt or ng/L, GenX chemicals final concentration of 10 ppt or ng/L, and PFBS final concentration of 2,000 ppt or ng/L. There was a reporting limit of 4 ppt or ng/L for PFOA, 4 ppt or ng/L for PFOS, 5ppt or ng/L for GenX, and 3 ppt or ng/L for PFBS (Furlow, 2024). Health recommendations from EPA reflected peer-reviewed science and are non-regulatory. The USEPA's revised interim health advisories for PFOA and PFOS overrode those issued by the EPA in 2016.

In March 2023, the US EPA proposed the National Primary Drinking Water Regulation (NPDWR) for six PFAS chemicals, including PFOA, PFOS, perfluorononanoic acid (PFNA), perfluorohexanesulfonic acid (PFHxS), PFBS, and HFPO-DA or GenX. For PFOA, Maximum Contaminant Levels (MCL) and MCL Goals (MCLG) are 4 ng/L and 0 ng/L. For PFOS, MCL and MCLG are 4 ng/L and 0 ng/L. PFNA, PFHxS, PFBS, and HFPO-DA or GenX have a hazard index MCL of 1 and a hazard index MCLG of 1. On April 10, 2024, EPA announced the final National Primary Drinking Water Regulation (NPDWR) for six PFASs, including perfluorooctanoic acid (PFOA), perfluorooctane sulfonic acid (PFOS), perfluorohexane sulfonic acid (PFHxS), perfluorononanoic acid (PFNA), hexafluoropropylene oxide dimer acid (HFPO-DA, commonly known as GenX Chemicals), and mixtures containing two or more of PFHxS, PFNA, HFPO-DA, and PFBS, with enforceable levels of Maximum Contaminant Levels (MCLs) of 4.0 ppt for PFOA and PFOS, 10 ppt for PFHxS, PFNA, and HFPO-DA, and 1 hazard index for mixtures containing two or more of PFHxS, PFNA, HFPO-DA, and PFBS (Furlow, 2024). The US EPA identified the regulatory hazard index for PFAS mixture, which is calculated by (USEPA, 2023):

$$\frac{HFPO-DA}{10} + \frac{PFBS}{2000} + \frac{PFNA}{10} + \frac{PFHxS}{10} = \text{Hazard Index Value}$$

All units are parts per trillions (ppt) or nanogram per litter (ng/L).

PFASs contain a carbon-fluorine chain with a hydrophilic functional group head (Panieri et al., 2022). The substitution of hydrogen atoms entirely or partly by fluorine atoms makes the fluorinated carbon hydrophobic. The nature of being both hydrophobic and hydrophilic makes PFASs a functional surfactant. PFASs are also thermally stable with highly enduring properties, enabling them to function as polymers in various applications (Hamid et al., 2024; Lukic Bilela et al., 2023; Panieri et al., 2022). PFASs have been used in industries such as chrome plating, electronics manufacturing, oil recovery, etc. They have also been used in consumer products such as nonstick pans, food packaging, waterproof clothing, cosmetics, greases, lubricants, paints, polishes, adhesives, etc. (Gluge et al., 2020; Zhu et al., 2021). PFASs are well-known and have been extensively used as firefighting foam (de Vries et al., 2017; Hoisaeter et al., 2019). Among the PFASs, perfluoroalkyl acids (PFAAs), including perfluoroalkyl carboxylic acids (PFCAs) and perfluoroalkyl sulfonic acids (PFSAs), are the most commonly used ones.

PFASs have been a part of a wide range of consumer and commercial products since their introduction in the 20th century. The family of perfluorinated compounds was introduced on April 6, 1938, when, by coincidence, Roy J. Plunkett invented polytetrafluoroethylene (PTFE), a wholly saturated fluorocarbon polymer. Since its registration in 1945, the Teflon™ trademark had gained global recognition for its superior cookware nonstick properties, ability to repel textile stains, and commercial coatings (Teflon™, 2024). Perfluorooctane sulfonic acid (PFOS) and perfluorooctanoic acid (PFOA) are the most commonly used PFAS compounds, which were introduced into the production of polytetrafluoroethylene (PTFE) nonstick coatings between the 1940s and the 1950s (Teflon™, 2024). Between the 1950s and 1960s, PFOS and PFOA were further used in water- and stain-resistant products and protective coatings (Buck et al., 2011; Teflon™, 2024). The widespread use of PTFE started in industrial cookware in 1961, completely changing the culinary industry. Perfluorinated substances significantly transformed their usage due to their outstanding capacity to repel water and grease. PFOS was further introduced to firefighting in the 1960s and 1970s (Liuzza, 2024).

Since the 1940s, more than 3,000 PFASs have been detected with varying numbers of carbon atoms and functional groups. In 2021, the Organization for Economic Co-operation and Development (OECD) updated the definition of PFASs, resulting in the discovery of over 7 million PFAS compounds in PubChem, one of the largest open chemical collections (Lang et al., 2017; Schymanski et al., 2023). Because of the toxicity concerns, management actions have been implemented to restrict the manufacturing of long-chain PFASs and their precursors (Brendel et al., 2018). Although they are no longer manufactured in the US, they are still produced internationally and imported into the US as consumer goods.

With their popular applications, many consumer goods and drinking water additives in the twenty-first century contained different types of PFASs at variable concentrations. During the 1970s to 1980s, certain manufacturers acknowledged the toxic characteristics of PFASs, prompting the voluntary phase-out of Class A forms by 2000 (Hilton, 1972; ITRC, 2024). Due to the concern of the presence of PFASs in the environment, regulatory agencies established drinking water standards for several PFAS compounds. US EPA issued updated health advisories for several PFAS compounds, including PFOA, PFOS, GenX or hexafluoropropylene oxide dimer acid (HFPO-DA), and perfluorobutanesulfonic acid (PFBS) with 4.0 ppt for PFOA and PFOS, 10 ppt for PFHxS, PFNA, and HFPO-DA, and 1 hazard index for mixtures containing two or more of PFHxS, PFNA, HFPO-DA, and PFBS (Furlow, 2024).

PFASs are known as “forever chemicals” due to their strong carbon and fluorine bonding. Regulators have determined that PFAS are persistent, bioaccumulative, and toxic substances, and they are currently considered emerging contaminants of concern (Boone et al., 2019).

Polyfluorinated substances can be precursors for PFASs of concern, including PFCAs, PFSAs, etc. Polyfluoroalkyl substances are compounds that are not fully fluorinated. For these compounds, at least one, but not all, non-fluorine atoms (i.e., hydrogen or oxygen) attach to the carbon atoms, while at least two or more of the remaining carbon atoms in the carbon chain are fully fluorinated. By chemical and biological transformation, such as hydrolysis, photolysis, and oxidation under ambient environmental conditions, stable PFAS compounds, such as PFAAs, can be generated from these precursors. For instance, hydroxyl radicals released by strong oxidants can break down the precursors to PFCAs (Dombrowski et al., 2018). Similarly, PFAA precursors can be biotransformed to PFCAs and PFSAs (Chen et al., 2019; Eriksson et al., 2017; Yi et al., 2018). Because perfluorooctanesulfonic acid (PFOS), perfluorooctanoic acid (PFOA), and perfluorohexane sulfonate (PFHxS) are commonly found in the breakdowns of firefighting foam (i.e., aqueous film-forming foam, or AFFF), they are the primary indicators of PFAS and are the most studied PFAS compounds.

2.1 Water surface tension and PFAS partitioning to the air-water interface

Water surface tension results from imbalanced inter-molecular attractive interactions or cohesive forces of water molecules at the air-water interface. At the air-water interface, the water molecular interactions differ from those of the bulk solution, i.e., the water molecules strongly attract hydrogen bonding towards the bulk liquid, forming surface tension (Menger et al., 2009). When PFASs are present in water, they can interact with the water molecules at the air-water interface. PFAS molecules have hydrophobic (water-repelling) tails and hydrophilic (water-attracting) heads. At the air-water interface, PFAS molecules tend to align themselves such that their hydrophobic tails are oriented away from the water and their hydrophilic heads are in contact with the water. PFASs tend to attach to the air-water interface due to their surfactant properties. In the presence of PFASs, the cohesive forces of water molecules at the air-water interface decrease owing to the change in the molecular composition of the air-water interface (Lenard et al., 1924). At the air-water interface, the higher the PFASs accumulate, the lower the surface tension is (Figure 3).

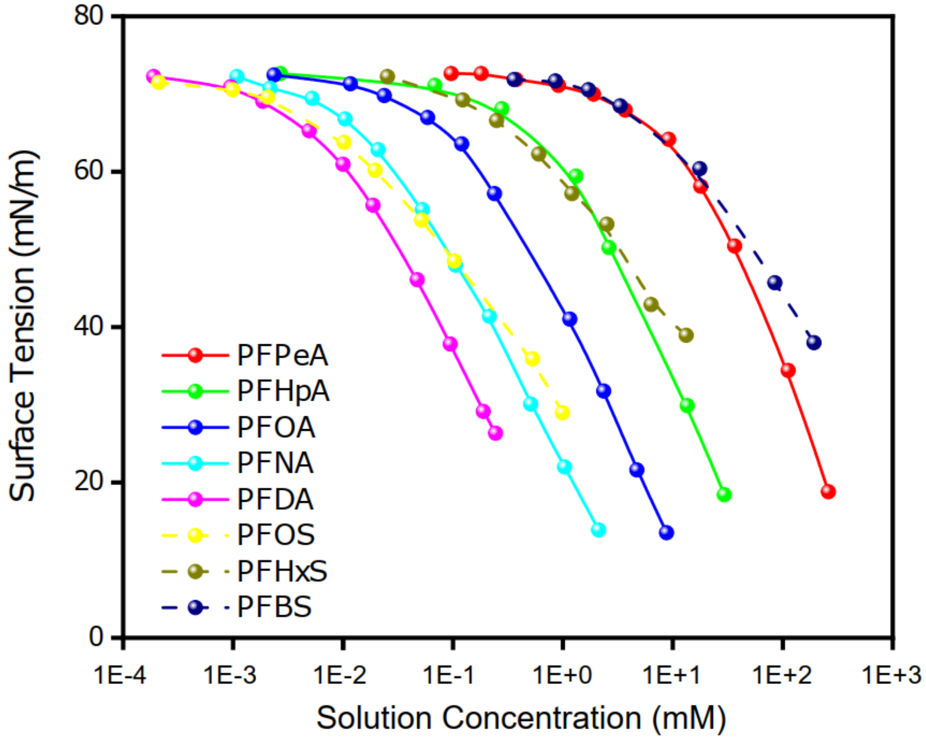

Figure 3. Water Surface Tension Drop as a Function of PFAS Concentration (Silva et al., 2021)

Air at the air-water interface behaves like a flat hydrophobic surface, making the air-water interface attractive to hydrophobic substances such as PFASs. Once accumulated at the air-water interface, the hydrophilic heads of PFASs immerse in water while the hydrophobic tails extend to the air. The degree of PFAS adsorption at the air-water interface is controlled by PFAS hydrophobicity, solution ionic strength, PFAS charges, surface tension, pH of the water, presence of other solutes, temperature, concentration of PFASs, etc. Because of the surfactant properties of PFASs and their preference for the air-water interface, the adsorption of PFASs to the air-water interface is essential, which strongly influences the movement and spatial distribution of PFASs in the unsaturated subsurface matrices, especially the vadose zone and the capillary fringe.

In the presence of PFAAs, surface tension reduces with effects more pronounced for PFAAs with increased C-F chain length. For instance, perfluorodecanoic acid (PFDA) (C10) decreases water surface tension more significantly than PFAAs with shorter C-F lengths, such as perfluorononanoic acid (PFNA) (C9), perfluoroheptanoic acid (PFHpA) (C7), and perfluoropentanoic acid (PFPeA) (C5). Similarly, water surface tension is further dropped in the presence of PFOS (C8), PFHxS (C6), and perfluorobutanesulfonic acid (PFBS) (C4). pH plays an essential role in PFAS surfactant functions since pH determines whether a PFAS compound exists in an anion or molecular form. Decreasing pH makes PFASs exist in an ionic form and soluble in water. At the same time, pH influences the water surface tension, with a lower pH resulting in a lower surface tension. For instance, the electro-kinetic data indicate that the isoelectric point of the air-water interface is pH 3.8, at which the air-water interface exhibits a minimum surface tension (Colussi, 2018). It should be noted that water surface tension also increases with the increase in solution ionic strength (Bulavin et al., 1998). Since soluble PFASs are in the ionic form with negative charges, PFAS accumulation at the air-water interface is reflected by zeta potential, a function of surface conductivity induced by the air and the excess of electrical charges at the interface. Zeta potential is thus an essential physicochemical parameter to describe PFAS adsorption at the air-water interface (Manciu and Ruckenstein, 2012).

The subsurface vadose zone serves as a significant PFAS reservoir. Specifically, the air-water interface created by the trapped air in the pore space creates an extra sink for PFASs to adsorb. Recent studies have demonstrated that the adsorption of PFASs at air-water interfaces can be an important retention process for PFAS transport in the vadose zone (Brusseau, 2018b). Because of the capillary force, which holds the PFAS molecules on the air-water interface, desorption of PFASs attached to the air-water interface is difficult (Wan and Tokunaga, 1998; Wan and Tokunaga, 2002). Surface tension measurements combined with the Gibbs energy calculation could explain the adsorption of PFASs at the air-water interface.

In practice, surface tension measurement can be conducted by techniques such as the Wilhelmy plate method, spinning drop method, maximum bubble pressure method, Du Nouy ring method, capillary rise method, and pendant drop method. Surface thermodynamic properties of PFASs can be characterized by the DLVO theory through contact angle measurements. PFAS accumulation at air-water interfaces can thus be quantified based on surface tension and PFAS thermodynamic data by the Langmuir adsorption equation (Pauletto and Bandosz, 2022; Silva et al., 2021):

$$\Gamma = \Gamma_{max} \frac{K_{eq} C_w}{1 + K_{eq} C_w}$$

where Γ is PFAS surface excess at concentration of C_w, Γ_{max} is the maximum PFAS surface excess, and K_{eq} is the equilibrium adsorption constant. Table 1 summarizes the typical K_{eq} values and Γ_{max} values for some typical PFASs.

Table 1. K_{eq} and Γ_{max} Values for Typical PFAS (Silva et al., 2021)

PFAS Compounds	K_{eq} (L/mol)	Γ_{max} (mol/m^2)	A_{min} (nm^2)
PFPeA	83	6.42×10^{-6}	0.237
PFHpA	1053	6.42×10^{-6}	0.285
PFOA	6667	5.54×10^{-6}	0.300
PFNA	90909	4.67×10^{-6}	0.325
PFDA	138889	4.96×10^{-6}	0.335
PFOS	136986	3.50×10^{-6}	0.474

According to the Gibbs adsorption equation, the surface excess can be quantified by (Yan et al., 2020):

$$\Gamma = \frac{-1}{xRT}\frac{\partial\gamma}{\partial InC_w}$$

where γ is the surface tension, x is the coefficient, which equals 1 for nonionic PFAS or ionic PFAS surfactants with excess solution electrolyte and equals 2 for ionic PFAS surfactants without excess solution electrolyte, R is the universal gas constant, and T is the temperature.

By combining the Gibbs adsorption equation and the Szyszkowski equation, PFAS adsorption at the air-water interface is described by the Langmuir−Szyszkowski isotherm (Brusseau and Van Glubt, 2019; Brusseau and Van Glubt, 2021):

$$\gamma_0 - \gamma = aRT\Gamma_{max}Ln\left(1 + K_{eq}C_w\right)$$

where γ_o is the surface tension of pure water, and a is a constant. Based on the above equation, it can be seen that higher PFAS concentration leads to a lower surface tension, which is a function of the molecular structure of PFASs, such as the length of the fluoroalkyl chain. This explains the observations discussed previously. At too high concentrations, i.e., critical micelle concentrations (CMCs), surface excess decreases the effectiveness of further surface tension decrease by PFASs. It should be noted that there is a limitation to use the above equations for low PFAS concentrations.

For low PFAS concentrations, $K_{iw\text{-}0}$ is introduced, which is defined as the ratio of PFAS surface excess to the corresponding aqueous concentration at low concentration (Le et al., 2021):

$$K_{iw-0} = \lim_{C_w \to 0} \frac{\Gamma}{C_w} = \Gamma_{max} K_{eq}$$

PFAS adsorption to the air-water interfaces results in standard free energy change, which is linked to the partition coefficient between water and the air-water interface (Le et al., 2021):

$$\Delta G_0^{ads} = -RTLn\left(K_{eq}\omega\right)$$

where ΔG_0^{ads} is the change of standard free energy to transfer a PFAS molecule from the bulk aqueous phase to the interface, and ω is the PFAS molar concentration at the air-water interface, which decreases with increasing PFAS concentration.

The values of Γ_{max} and K_{eq} can be established by minimizing the root mean square error (RMSE) between the observed and modeled surface tension for individual PFAS and hydrocarbon surfactants. To achieve this, a modified version of the Szyszkowski equation can be used (Le et al., 2021):

$$\gamma_2 - \gamma_1 = aRT\Gamma_{max} Ln\left(\frac{1 + K_{eq}C_1}{1 + K_{eq}C_2}\right)$$

This equation enables fitting between two points on the surface tension curve without presuming a pure water surface tension. This method helps mitigate potential errors in the derived parameters, which may arise from fitting data with minor errors in instrument calibration.

2.2 PFAS adsorption isotherm

Batch sorption experiments are usually conducted with PFAS solutions in the presence of soil matrices. The initial solution pH and ionic strength can be adjusted to investigate the impact of pH and ionic strength on PFAS adsorption. Adsorbed PFAS at time t, q_t is calculated using the following equation:

$$q_t = \frac{(C_0 - C_t)V}{m}$$

where C_0 is the initial PFAS concentration in the solution, C_t is the PFAS concentration in the solution at time t, V is the volume of the solution, and m is the weight of the media matrix. This measurement can determine the time required to reach equilibrium for the adsorption isotherm determination. Following the above experiment, adsorption isotherm experiments can be conducted. PFAS adsorption on solid surfaces is typically described by the Langmuir adsorption isotherm (Adachi et al., 1997; Hajratwala, 1982) (Figure 4) (Kancharla et al., 2022):

$$q_e = \frac{K_L q_m C_e}{1 + K_L C_e}$$

where q_e is the adsorbed PFAS, K_L is the Langmuir constant, q_m is the maximum adsorption capacity, and C_e is the equilibrium solution concentration of PFAS. K_L is linked to the adsorption reaction thermodynamics through the Gibbs free energy change, which is a function of ΔH and ΔS (i.e., $\Delta G = \Delta H - T\Delta S$). According to the van't Hoff equation, K_L from the Langmuir adsorption is also linked to ΔH and ΔS:

$$Ln(K_L) = -\frac{\Delta H}{RT} + \frac{\Delta S}{R}$$

where ΔG is the Gibbs free energy change of PFAS adsorption, R is the universal gas constant, T is the absolute temperature, ΔH is the change in enthalpy, and ΔS is the change of entropy associated with adsorption. Thermodynamic indicators of enthalpy and entropy reveal the driving forces governing adsorption, whether enthalpy-driven or entropy-driven. Eventually, a negative Gibbs free energy change indicates an exergonic reaction occurring during adsorption.

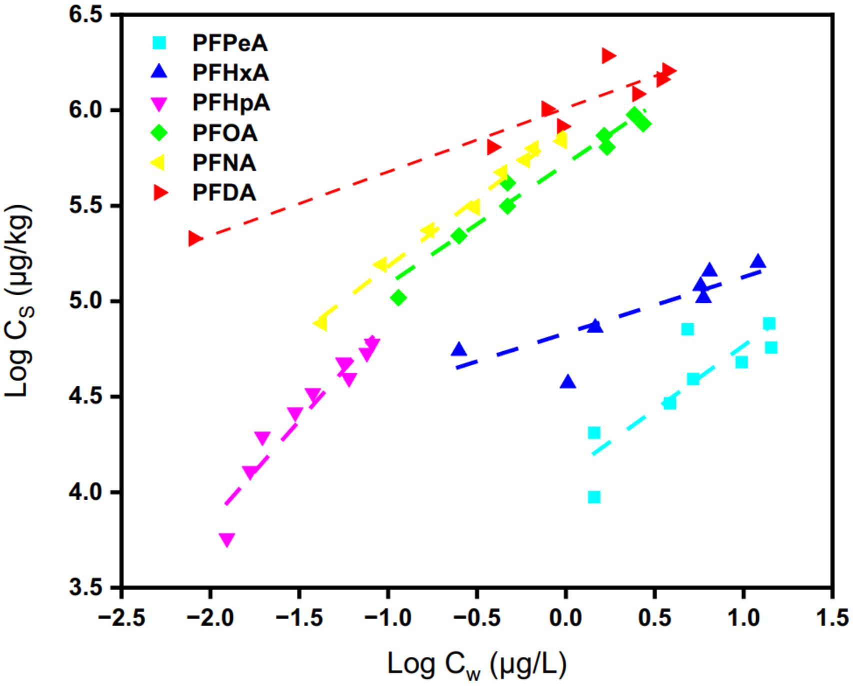

Figure 4. PFAS Adsorption Isotherms on Biochar Produced from Ullensaker Sludge (Krahn et al., 2023b)

2.3 PFAS transport

Fate and transport of PFAS as emerging contaminants are of critical concern. It is now clearly established that soil serves as a long-term source for many sites contaminated by PFAS. Hence, there is great interest in the transport behavior of PFAS in the vadose zone, which can be considerably more complex than in groundwater. PFAS transport in the vadose zone reflects the complexity of PFAS transport under water-unsaturated conditions, which includes the air-water interface as an extra sink term for accumulation or adsorption of PFAS.

Studies have reported that short-chain PFAS can transport long distances with low retardation. On the contrary, long-term retention of longer-chain PFAS is commonly observed (Ateia et al., 2019; Stebel et al., 2019). Investigation of the impacts of perfluorinated carbon chain length on PFCA transport, such as PFPeA, PFHxA, PFOA, and PFDA, indicated that the chain length had limited impacts on PFCA transport when the fluorocarbon chains contained eight or less carbons under various pH and ionic strength conditions. In contrast, when the fluorocarbon chains contained carbon numbers greater than eight, such as PFDA, the mobility was significantly affected by pH and ionic strength (Figure 5 and Figure 6).

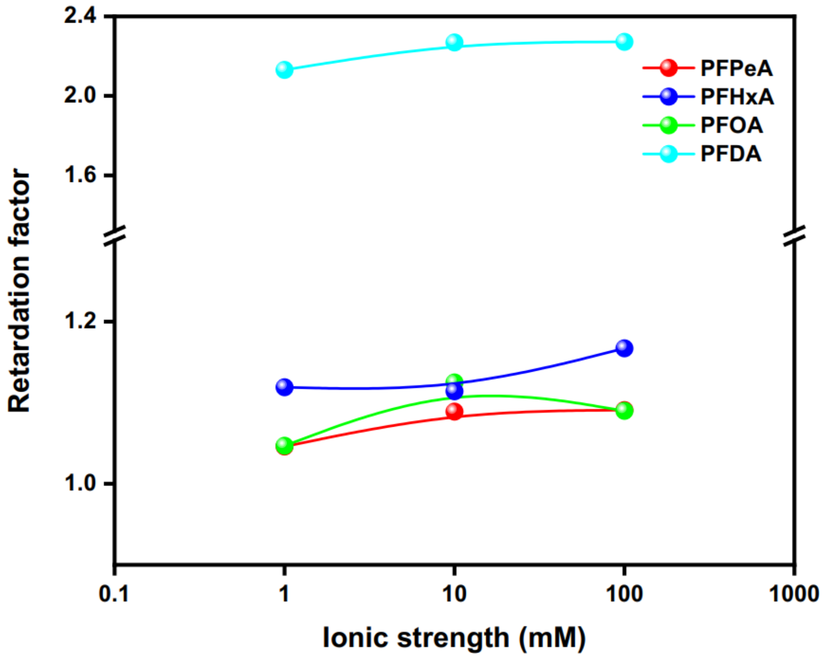

Figure 5. Impacts of Solution Ionic Strength on PFAS Retardation (Qi et al., 2022)

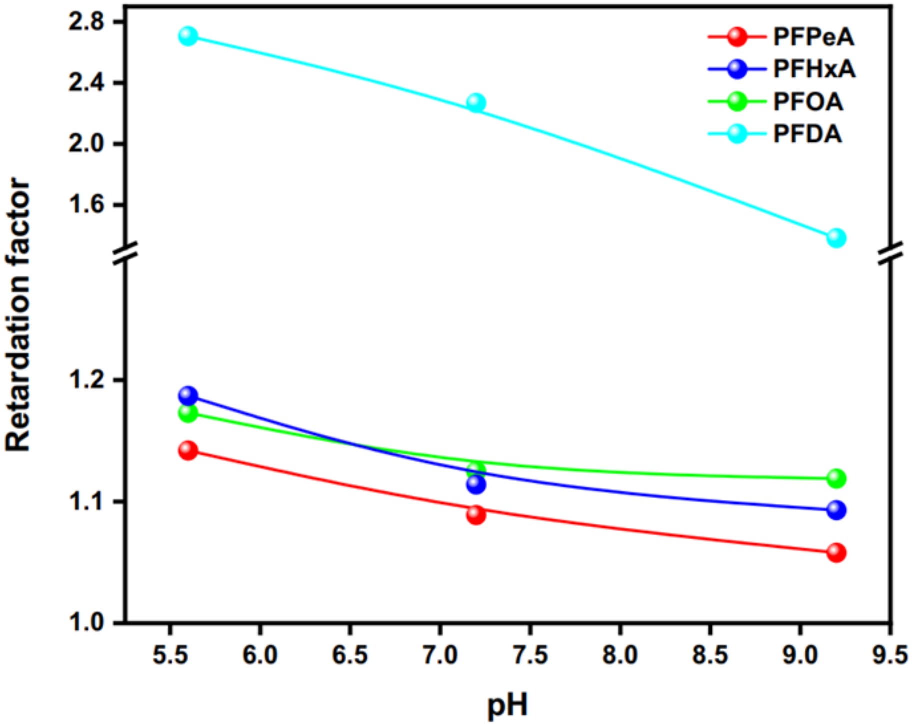

Figure 6. Impacts of Solution pH on PFAS Retardation (Qi et al., 2022)

PFAS transport in the subsurface varies with loading rates, with the transport level of PFAS decreasing with the depth (Figure 7) (Sepulvado et al., 2011). More PFAS were retained in the top layers than those in the lower ones because the organic content was higher in the top layers. This is consistent with the presumption that hydrophobic adsorption increases with increased organic content. PFSAs (i.e., PFOS) were transported to a lesser extent than PFCAs (i.e., PFOA) because PFSAs had stronger adsorption. Subsequently, PFSAs displayed a more significant partition coefficient than those of PFCAs with equal C-F chain length (Figure 8) (Rayne and Forest, 2009). Figure 11 also demonstrated that the partition coefficient increased with the increase of C-F chain length for PFAS.

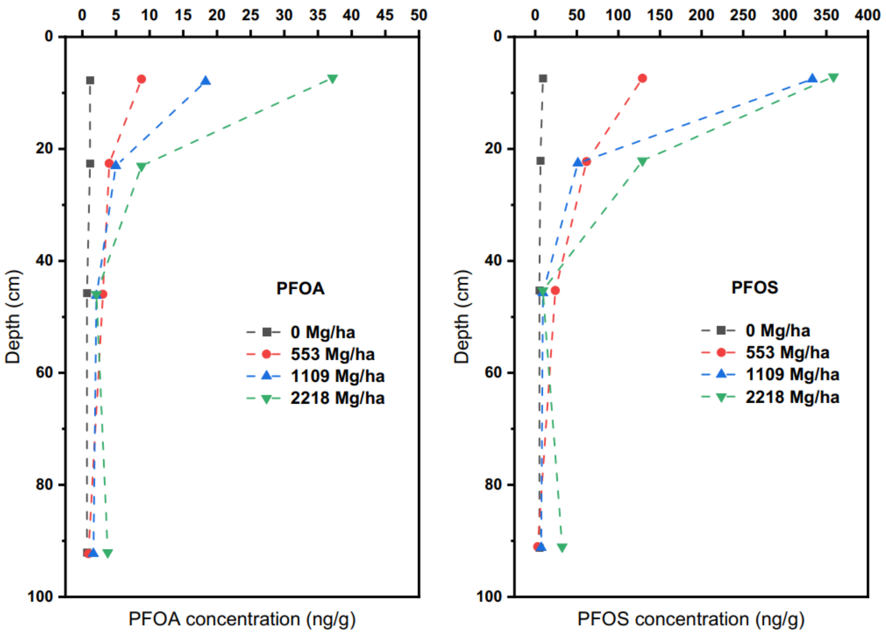

Figure 7. PFOS and PFOA Transport underneath the Soil at Various Loading Rates (Sepulvado et al., 2011)

(The loading rate is expressed as PFAS-containing biosolid per ha.)

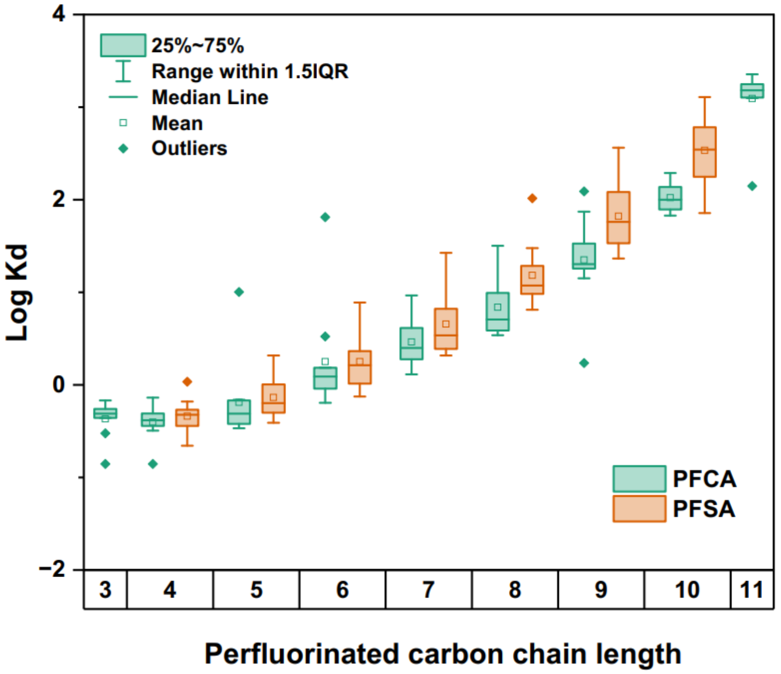

Figure 8. Log K_d of PFASs with Different Chain Lengths (Nguyen et al., 2020)

2.4 PFAS transport under unsaturated conditions

Since the air-water interface plays a crucial role in PFAS transport in the soil, unsaturated conditions of the soil environment are essential. The unsaturated conditions can be monitored by tensiometers and time domain reflectometer (TDR) for different soil depths. The matric potential and water content are related to each other by the van Genuchten equation:

$$S_e = [1 + (\alpha h)^n]^{\left(\frac{1}{n-1}\right)}$$

where S_e is the effective saturation, α is the inverse of the air-entry potential, h is the water potential, and n is the parameter related to pore size distribution. S_e is related to the water content as follows:

$$S_e = \frac{\theta - \theta_r}{\theta_s - \theta_r}$$

where θ is the water content, θ_r is the residual water content, and θ_s is the saturated water content. An example of soil matric potential vs. volumetric water content is presented in Figure 9.

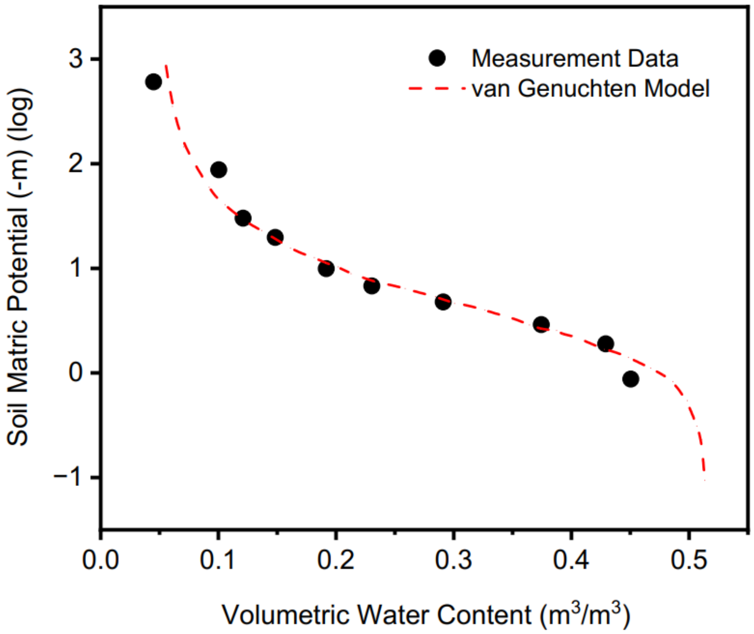

Figure 9. Soil Matric Potential vs. Volumetric Water Content (Tuller et al., 2004)

2.5 Modeling of PFAS transport in unsaturated zone

Since PAFS are hydrophobic by the perfluoroalkyl chain and hydrophilic by hydrophilic functional groups, PFAS act as surfactants in the solution, absorbing them to the air-water interface in the vadose zone. For PFAS transport, the following one-dimensional transport model with a sink term of air-water interface for PFAS retention is commonly used (Simunek et al., 2005):

$$\frac{\partial}{\partial t}[\theta C_R] = \frac{\partial}{\partial z}\left[D_z \theta \frac{\partial C_R}{\partial z}\right] - \frac{\partial}{\partial z}[q C_R] - k_1 \theta C_R + k_{des}\frac{\rho_b A_s}{S_e} C_{Rr} - k_d \theta C_R$$

$$\frac{\partial C_{Rr}}{\partial t} = k_1 \frac{\theta S_e}{\rho_b A_s} C_R - k_{des} C_{Rr}$$

where C_R is the PFAS concentration in the solution, D_z is the apparent dispersion coefficient, θ is the moisture content (moisture volume divided by the total volume of the porous media), q is the specific discharge (Darcian fluid flux), k_1 is the deposition rate coefficient, k_{des} is the desorption rate coefficient, k_d is the obliterating rate, ρ_b is the bulk density, A_S is the air-water interfacial area, S_e is the effective saturation, C_{Rr} is the retained PFAS concentration, z is the axial coordinate, and t is the time.

By considering the NAPL formation, transport of a PFAS in the vadose zone may be further described by the advection-dispersion equation with appropriate sink terms to account for the PFAS retention associated with NAPL formation:

$$\frac{\partial(\theta_w C_w)}{\partial t} + \rho_b \frac{\partial C_s}{\partial t} + \frac{\partial C_{aw}}{\partial t} + \frac{\partial C_{nw}}{\partial t} + \frac{\partial C_{an}}{\partial t} + \frac{\partial C_{deg}}{\partial t} + \frac{\partial C_{up}}{\partial t} + \frac{\partial C_{Bac}}{\partial t}$$

$$+ \frac{\partial}{\partial x}(\theta_w V_w C_w) - \frac{\partial}{\partial x}\left(\theta_w D \frac{\partial C_w}{\partial x}\right) = 0$$

where C_w is the aqueous PFAS concentration, C_s is the solid-phase adsorbed PFAS concentration, C_{aw} is the adsorbed PFAS concentration at air-water interfaces, C_{nw} is the adsorbed PFAS concentration at NAPL-water interfaces, C_{an} is the adsorbed concentration at air-NAPL interfaces, C_{deg} is the degradation, C_{up} is the plant uptake, C_{Bac} is the bacteria biomass adsorption, ρ_b is the bulk density of soil, θ_w is the volumetric water content, v_w is the interstitial pore water velocity, and D is the dispersion coefficient.

When linear sorption isotherm is used for interfacial sorption and partition, the advection-dispersion equation may be written as:

$$\frac{\partial(\theta_w R C_w)}{\partial t} + \rho_b \frac{\partial C_s}{\partial t} + \frac{\partial C_{deg}}{\partial t} + \frac{\partial C_{up}}{\partial t} + \frac{\partial}{\partial x}(\theta_w V_w C_w) - \frac{\partial}{\partial x}(\theta_w D \frac{\partial C_w}{\partial x}) = 0$$

where R is the nondimensional retardation, which is calculated by (Brusseau and Guo, 2022; Brusseau and Guo, 2023a):

$$R = 1 + K_d \frac{\rho_b}{\theta_w} + H\frac{\theta_a}{\theta_w} + K_n\frac{\theta_n}{\theta_w} + K_{aw}\frac{a_{aw}}{\theta_w} + K_{nw}\frac{a_{nw}}{\theta_w} + K_{an}\frac{a_{an}}{\theta_w} + K_c X_c$$

where a_{an} is the specific air-NAPL interfacial area, a_{aw} is the specific air-water interfacial area and is the particular NAPL-water interfacial area, K_{an} is the air-NAPL interfacial adsorption coefficient, K_{aw} is the air-water interfacial adsorption coefficient, K_c is the distribution coefficient of colloids for sorption, K_d is the solid-phase adsorption coefficient, K_n is the NAPL-water partition coefficient, K_{nw} is the NAPL-water interfacial adsorption coefficient, X_c is the concentration of colloidal material in porewater, and θ_n is volumetric NAPL content. The term R describes the delay of PFAS by adsorption and desorption in the soil phase as compared to that of the aqueous phase, considering the presence of PFASs in all pertinent retention domains. The total mass of a select PFAS constituent in a volume of soil is given by:

$$M_t = C_p \theta_w V_t R$$

where the total sample volume is V_t, so the total soil concentration of select PFASs, C_t (M/M) is:

$$C_t = \frac{C_p V_t}{\rho_b}$$

The ratio of soil concentration and pore water concentration can thus be expressed as:

$$\frac{C_t}{C_p} = \frac{\theta_t}{\rho_b} R$$

The retardation factor equation can be adjusted site-specific by incorporating only the terms applicable to that site. In cases where the air-water interface serves as the sole additional source of retention beyond solid-phase sorption and partitioning to the soil matrices, the following equation expresses the modified distribution term for this scenario (Brusseau and Guo, 2023a):

$$R = 1 + K_d \frac{\rho_b}{\theta_w} + H \frac{\theta_a}{\theta_w} + K_{aw} \frac{a_{aw}}{\theta_w}$$

The EPA soil screening level (SSL) in terms of the nondimensional distribution factor is given by (Brusseau and Guo, 2023a):

$$SSL = C_{soil} = C_{gw} DAF \frac{\theta_w}{\rho_b} R$$

where C_{gw} is the target groundwater concentration deemed to be protective of groundwater quality, C_{pw} = vadose zone porewater concentration, C_{soil} = soil concentration, $C_{pw} = C_{gw}DAF$, K_d is the sorption coefficient, and H is Henry's law constant. DAF comprises the product of two components, the dilution factor (DF) and the attenuation factor (AF), i.e., DAF = DF × AF. The soil concentration determined from this calculation is SSL. The DAF SSL model is thus presented in the following format:

$$SSL = C_{gw} DAF [K_d + \frac{K_{aw} a_{aw} + \theta_w + \theta_w H}{\rho_b}$$

The adsorption of PFAS in the subsurface has the effect of slowing, or retarding, the rate of PFAS transport during unsaturated transport. Additionally, interfacial adsorption could serve as an environmental sink for PFASs, providing an additional sink source. PFAS transport is commonly illustrated by breakthrough curves, which are expressed in terms of the ratio of breakthrough concentration to the input concentration, C/C_0. The time scale is commonly expressed in terms of pore volume, which is calculated as:

$$Pore\ Volume = \frac{v \cdot A}{\theta \cdot V}$$

where v is the flow velocity, A is the cross area, and V is the volume of the system. Transport observations of PFOA at different concentration conditions are illustrated in Figure 10. It is obvious for PFAS compounds that the breakthrough is a function of the input concentration. A high concentration is easier to breakthrough than a low concentration.

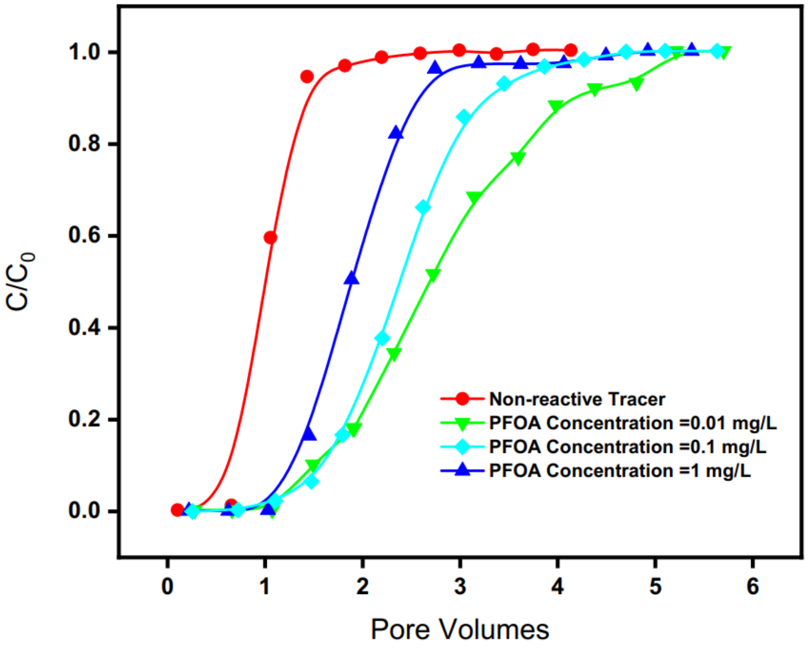

Figure 10. PFOA Transport Breakthrough Curves for Different Input Concentrations (Lyu et al., 2018)

Delay of PFAS transport, as described by the retardation factor, can be evaluated by integration of the breakthrough curves:

$$R = \frac{\int_0^{\infty} C(\sigma)\sigma d\sigma}{\int_0^{\infty} C(\sigma) d\sigma} - \frac{v_p}{2}$$

where σ is the pore volume and v_p is the pulse length of the PFAS input. It is observed that the PFAS retardation factor increases with the increase of the C-H chain length (Figure 11).

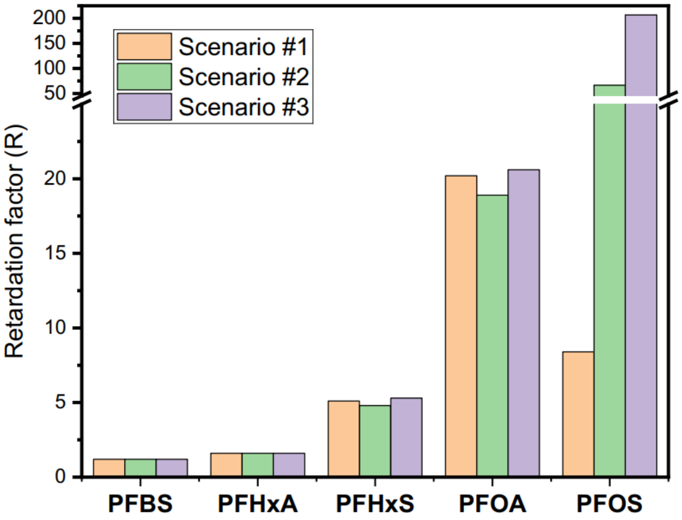

Figure 11. Retardation Factor of Typical PFAS (Guo et al., 2023)

Under unsaturated conditions, PFAS adsorption to the soil matrices can be described by integrating the breakthrough curves (Burgisser et al., 1993). Based on this method, the concentration of equilibrium adsorbed PFAS in the soil matrices, *S*, can be obtained by integrating the experimental record of the retention time if the dispersion term can be neglected (D = 0) (Burgisser et al., 1993):

$$S = \frac{\theta}{\rho_b(1-\theta)} \int_0^{C} (\frac{t(C')}{t_0} - 1) dC' - \int_0^{C} t(C') K_p dC'$$

where $t_0 = L/v$ is the average PFAS travel time in the column and $K_p = dS/dC$ is the partition coefficient of PFAS between soil matrices and water. The insignificant role of hydrodynamic dispersion on solution transport in columns has been proven to be valid (Unice and Logan, 2000).

2.6 PFAS removal by adsorption

2.6.1 PFAS adsorption to activated carbon

PFASs can be absorbed by traditional filtration media such as granular activated carbon (GAC). In practice, PFASs have been demonstrated to be adsorbed by carbon, clay minerals, ion-exchange resins, biochar, etc. The shorter-chain PFASs are more challenging to remove due to their increased solubility and mobility. The hydrophilic polar head functional groups also influence the adsorption. For instance, PFSAs tend to adsorb more strongly than PFCAs of equal chain length (Francis et al., 2017). As the polarity of PFAS decreases with increasing chain length, GAC is more effective in absorbing long-chain PFAS than short-chain PFAS. The non-polar and hydrophobic surface of GAC significantly interacts with hydrophobic PFASs, leading to its extensive usage in PFAS adsorption. GAC has become the most widely utilized sorbent for PFAS removal. Prior research has demonstrated that PFOA is readily absorbed compared to PFHxA, PFPeA, and PFBA. However, adsorption by GAC is ineffective for PFBA and PFPeA.

To compare the affinity of different PFASs for GAC, PFAS removal percentages by GAC were plotted as a function of PFAS C-F chain length for PFCAs and PFSAs (Figure 12) (Sun et al., 2016a). The PFAS adsorption capacity increased with increasing C-F chain length. PFSAs were more readily removed than PFCAs of matching C-F chain length. Perfluoroalkyl ether carboxylic acids (PFECAs) exhibited lower adsorption capacity than those of PFCAs of the same chain length, suggesting that the replacement of a CF_2 group with an ether oxygen atom decreased the affinity of PFAS for activated carbon. However, the replacement of additional CF_2 groups with ether groups resulted in minor affinity changes among the studied PFECAs (Sorengard et al., 2020) (Krahn et al., 2023a) (Alves et al., 2020).

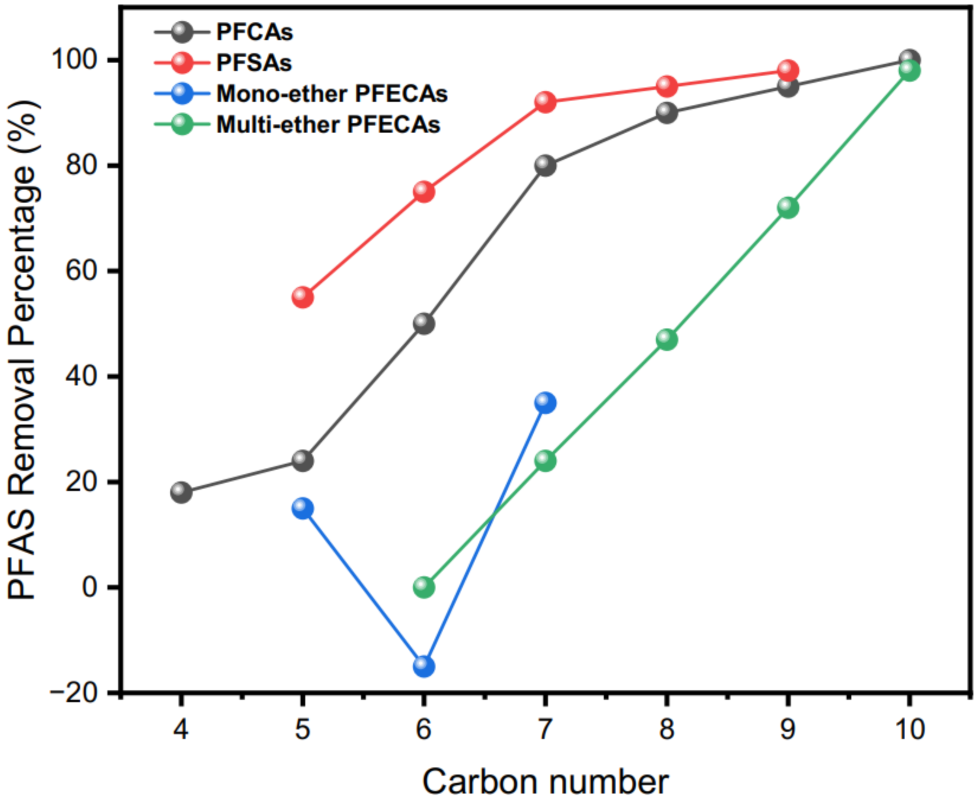

Figure 12. PFAS Removal as a Function of PFAS Chain Length (Sun et al., 2016b)

2.6.2 PFAS removal by biochar

Biochar can replace GAC for PFAS retention to save costs. Biochar is a carbon-enriched and stable material derived from the energy conversion process of pyrolysis, during which organic materials (such as crop stubble, wood chips, and biosolids) are heated in the complete or near absence of oxygen (Manya, 2012). Different physicochemical properties of feedstocks lead to variable carbon availability, molecular structure, and pore size distribution of biochar. The temperature of pyrolysis is another important factor of biochar surface characteristics. Biochar derived from relatively low-temperature pyrolysis is characterized by a high content of volatile matter that contains easily decomposable substrates, which can support typical microbial activities (Mukherjee and Zimmerman, 2013). In contrast, biochar derived from relatively high-temperature pyrolysis is more depleted of H and O but possesses a larger proportion of aromatic C than that of a lower temperature. The structure of biochar is thus characterized by a large surface area and aromatic carbon content, which may increase the adsorption capacity.

As a carbonaceous, highly stable, porous, and environment-friendly material, biochar is primarily made from abundant, low-cost, and widely available agricultural biomass. The biochar surface is saturated with heterocyclic and aromatic functional groups, including hydroxyl, carboxyl, carbonyl, etc., which help the formation of hydrogen bonding. Hydrophobic and electrostatic interactions and hydrogen bonding are the main mechanisms of PFAS adsorption. The chemical structures of biochar are affected by feedstocks and pyrolysis temperature, which is reflected by FT-IR spectrum analysis as evidenced by the spectral peaks (Li and Chen, 2018; Li et al., 2019). For instance, unstable functional groups such as O–H (near 3400 cm^{-1}) and aliphatic C–C (near 3000 cm^{-1}) exist for biochar derived at 200°C (Figure 13). When the pyrolysis temperature is raised to 600°C, almost no aliphatic functional groups can be found in the biochar. Instead, aromatic structures begin to dominate, resulting in the increased presence of phenolic functional groups and ethers (1000–1250 cm^{-1}). The spectra of the biochar derived at 800°C demonstrates the formation of graphite-like structures due to the high degree of carbonization.

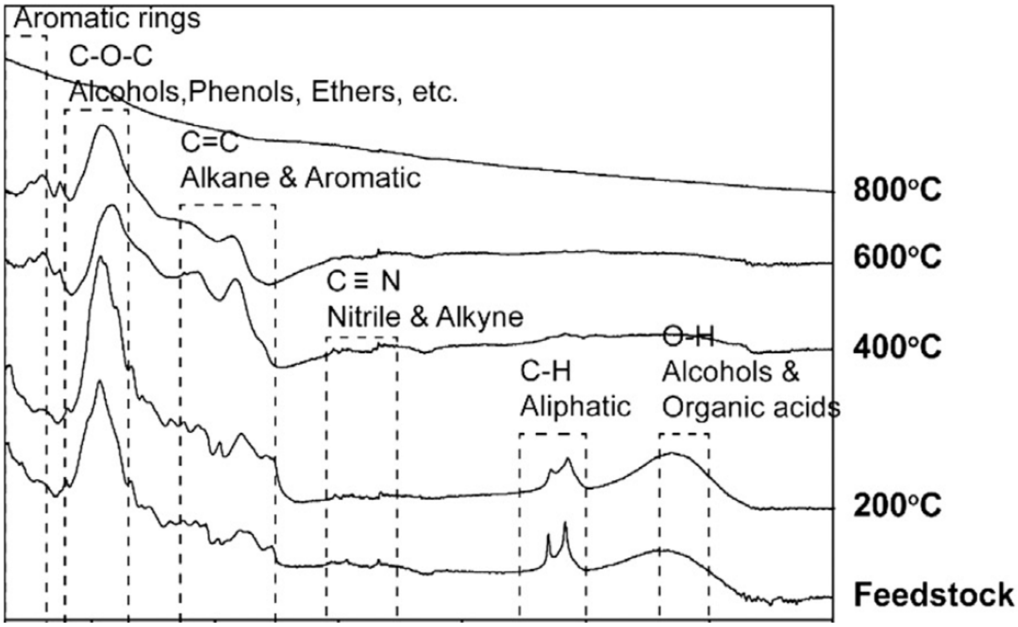

Figure 13. FTIR Spectra of the Switchgrass and Resulting Biochar Produced by Pyrolysis at 200, 400, 600, and 800ºC (Li and Chen, 2018)

Multi-element scanning thermal analysis (MESTA) shows the thermochemical transformation of specific elements, such as C, for the biochar (Figure 16) (Li and Chen, 2018). The results showed that a pyrolysis temperature of 160ºC is required to provide enough activation energy to initiate the decomposition of C structures. The biochar derived from low-temperature pyrolysis (< 400ºC) has at least two thermal peaks of C, indicating the presence of more diverse C structures such as methyl (–CH_3), methylene (–CH_2–), and carbonyl (C–O–C). However, the high pyrolysis temperature (> 600ºC) causes intensive thermochemical transformation through demethyloxylation, demethylation, and decarboxylation. As more and more aliphatic structures are cracked and more thermostable aromatic structures remain, the diversity of C structures decreases, which is reflected by the single thermal peak in the MESTA thermogram. Moreover, the single thermal peak of the biochar derived from a relatively higher pyrolysis temperature shifts towards a higher combustion temperature, which conforms to the formation of aromatic structures that require higher activation energy for their thermal decomposition. Biochar pyrolyzed at high temperatures had more PFAS adsorption, which is attributed to high surface area and increased pore size. This is especially the case for long-chain PFAS. However, ionic interaction is more crucial for the adsorption of short-chain PFAS.

2.6.3 PFAS removal by engineered biochar

Biochar can be further engineered by Fe_2O_3 and/or Al_2O_3-impregnation and coating with graphene oxide and carbon nanotubes (CNTs) to strengthen PFAS adsorption (Figure 14). Iron and aluminum contents contribute to the electrostatic interactions between PFAS and engineered biochar. The carboxylic functional group on biochar surfaces added by graphene oxide and nanotube coating enhances hydrogen bonding between PFAS and engineered biochar. Graphene oxide is a unique material that can be viewed as a single monomolecular layer of graphite with various oxygen-containing functionalities such as epoxide, carbonyl, carboxyl, and hydroxyl groups. As an oxidized form of graphene, graphene oxide is laced with oxygen-containing groups. Graphene-coated biochar has various functional groups, including -OH (at approximately 3450 cm^{-1}), C=C (at approximately 1630 cm^{-1}), C-OH (at approximately 1400 cm^{-1}), and C-O-C groups (at approximately1050 cm^{-1}).

Most importantly, absorption peaks in the wave numbers of 3450 cm^{-1}, 1630 cm^{-1}, 1400 cm^{-1}, and 1050 cm^{-1} have been observed, indicating the surface contains carboxyl, phenolic hydroxyl, and oxygen-containing groups. Carbon nanotubes are cylindrical molecules that consist of rolled-up sheets of single-layer carbon atoms (i.e., graphene). They can be single walled with a diameter of less than 1 nanometer (nm) or multi-walled, consisting of several concentrically interlinked nanotubes with more than 100 nm diameters. Their length can reach several micrometers or even millimeters. Similar to graphene oxide, carbon nanotubes can saturate biochar surfaces with carboxylic acid functional groups. In practice, enhanced retention of PFAS has been observed with biochar saturated with carboxyl functional groups (Aly et al., 2019).

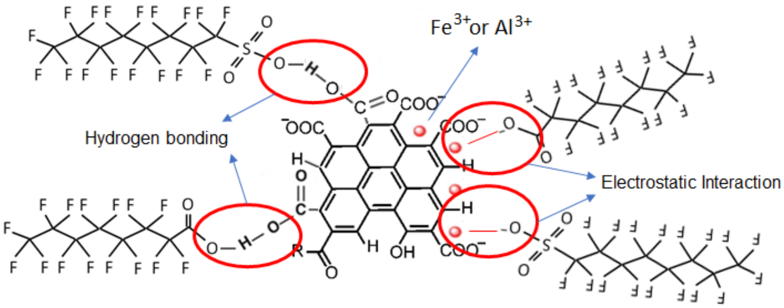

Figure 14. PFAS Adsorption to Biochar through Electrostatic Interactions and Hydrogen Bonding

Adsorption of PFAS onto CNT-coated biochar is attributed to reactions of PFAS carboxyl groups with CNC functional groups to adsorb ionizable PFAS molecules:

$$RCOO^{-} + H ++ \text{-O-CNTs}\ (RCOO\ldots H\ldots O\text{-CNTs})$$

The carboxyl, hydroxyl, and amine functional groups on the CNT surface also attract water molecules to promote hydrogen bonding. The hydrophobicity of the PFAS alkyl chain is directly related to PFAS adsorption, which increases with the increase of PFAS chain length. Again, long-chain PFAS have obvious adsorption. On the other hand, short-chain PFAS are hardly absorbed. Although electrostatic interaction exists during PFAS adsorption since PFAS exist in anionic forms, attractive hydrophobic interaction outweighs electrostatic interaction.

ΔG^0 was calculated using K_L for PFOA adsorption on engineered biochar based on isotherm experiments at different temperatures (Table 2). With a small $\Delta H^0 < 80$ kJ/mol and a positive ΔS^0, PFOA adsorption occurs on biochar as a chemisorption. Also, a slightly acidic condition is favorable for PFOA adsorption. Table 3 indicates that Fe-impregnation and CNC-coating significantly improve PFOA adsorption with decreased ΔG^0 values.

Table 2. Thermodynamic Parameters of PFOA Adsorption (Wu et al., 2022)

Biochar	ΔG^0 (kJ/mol) at 303.15K	ΔG^0 (kJ/mol) at 313.15K	ΔG^0 (kJ/mol) at 323.15K	ΔS^0 (kJ/mol/K)	ΔH^0 (kJ/mol)	R^2
SG-No*	-20.22	-18.78	-16.24	-0.20	-80.81	0.98
SG-Fe	-19.22	-15.59	-14.62	-0.23	-88.50	0.93
SG-CNT	-19.34	-19.44	-13.42	-0.30	-110.10	0.79
WO-No	-17.53	-15.68	-15.91	-0.08	-41.75	0.83
WO-Fe	-19.56	-16.12	-13.99	-0.28	-103.83	0.99
WO-CNT	-19.78	-20.53	-22.51	0.14	21.75	0.85
BS-No	-17.75	-14.04	-15.62	-0.11	-49.15	0.51
BS-Fe	-18.64	-16.90	-19.67	0.05	-2.37	0.37
BS-CNT	-13.83	-16.31	-14.74	0.05	-0.68	0.43

* SG, WO, and BS denote feedstocks of switchgrass, water oak, and biosolids. No, Fe, and CNT denote non-engineered biochar and biochar engineered with Fe and carbon nanotubes, respectively.

2.6.4 PFAS removal by foam fractionation

PFAS are surface-active compounds and tend to attach to the air-water interface (Brusseau and Van Glubt, 2019). Subsequently, PFAS compounds have higher concentrations on the air-water interface. PFAS can thus be removed by enriching PFAS at the air-water interface through the aeration of gas bubbles. Using N_2 gas bubbles, PFAS can accumulate at the surface and enrich after the bubbles eventually collapse. Decreased pH increases PFAS enrichment due to the enhanced attachment at the air-water interface. Increasing the air flow rate, ionic strength, and the concentration of co-existing surfactant can all promote PFAS attachment and removal.

The gas bubble size is significant for PFAS enrichment and removal by the gas bubbles. Assuming spherical diffusion, the diffusion flux of PFAS from the surrounding solution to the bubble surface is inversely proportional to the bubble radius. When concentrating PFAS using gas bubbles, aerosols may be formed with sizes of one magnitude smaller than those of the gas bubbles. It is assumed that the transition of PFAS concentration on gas bubbles to PFAS concentration in the aerosol droplets depends on the bubble radius. Subsequently, PFAS enrichment by gas bubbling can be described as:

$$\frac{\partial R}{\partial h} = a \frac{D_{PFASs}}{r_{bubble}^4}$$

where R is the enrichment factor defined as the ratio of PFAS concentration on aerosol to that of the bulk solution, h is the bubble transport length, D_{PFAS} is the PFAS diffusion coefficient, and a is a constant.

3. Materials and Methods

3.1 Characterization of PFAS release from PFAS-containing waste

For a typical landfill, around 3.75 g/d mass flux of PFASs was generated, which included 0.15 g/d PFOA and 0.3 g/d PFOS. In the leachate, the average mass flux of PFASs was 2.7 g/d. The specific PFASs that are of interest are summarized in Table 3.

Table 3. Target PFAS Compounds of the Research

Substances	Acronym	Range of $\mathrm{LogK_{oc}}$ (L/Kg)
Pentafluorobenzoic acid	PFBA	1.88
Perfluoropentanoic acid	PFPeA	1.37
Perfluorohexanoic acid	PFHxA	1.91
Perfluoroheptanoic acid	PFHpA	2.19
Perfluorooctanoic acid	PFOA	2.35
Perfluorononanoic acid	PFNA	2.39
Perfluorodecanoic acid	PFDA	2.76
Perfluoroundecanoic acid	PFUdA	3.3
Perfluorobutanesulfonic acid	PFBS	1
Perfluorohexanesulphonic acid	PFHxS	1.78
Perfluorooctanesulfonic acid	PFOS	3
6:2 Fluorotelomer sulfonic acid	6:2 FTS	2.43
8:2 Fluorotelomer sulfonic acid	8:2 FTS	3.84

It was expected that variable C-F chains of PFAAs as well as PFAA precursors summarized in Table 4 were contained in the waste. Solid waste including paper cups, paper plates, instant noodle bowls, and food packaging paper were tested for PFAS release. They were cut into pieces of 2 cm to 5 cm and introduced to thermal reactors for PFAS leaching (Figure 15). To characterize leached PFASs, the leachate was neutralized with glacial acetic acid and added C18 and primary and secondary amine (PSA) to remove interfering compounds.

Figure 15. Thermal Reactor for PFAS Release Experiments

For this research, the target PFASs were typical PFAAs including PFCAs, PFSAs, and PFAA precursors. The PFCAs included perfluorinated carbons with carbon numbers ranging from 3 to 10 and PFSAs included perfluorinated carbons with carbon numbers of 4, 6 and 8 (Figure 16). PFAS compounds such as PFOA, PFOS, PFHxS, PFBS, PFHpA, PFHxA, PFPeA, PFBA, etc. were quantified by liquid chromatography-tandem mass spectrometry (LC-MS/MS) following the EPA SW-846 and Method 537 for PFAS extraction and measurements. Special attention was paid to PFCAs with variable perfluoroalkyl chain lengths such as PFBA (4C), PFPeA (5C), PFHxA

(6C), PFHpA (7C), PFOA (8C), PFNA (9C), PFDA (10C), and PFUdA (11C) as well as PFSAs with variable perfluoroalkyl chain lengths such as PFBS (4C), PFHxS (6C), and PFOS (8C).

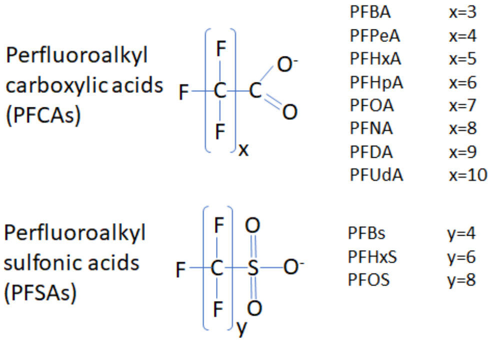

Figure 16. Targeted PFCAs and PFSAs

3.2 Saturated PFAS transport

Experimental investigation of the impact of perfluoroalkyl chain length on PFAS transport under saturated conditions was conducted in acrylic columns (0.75-inch diameter × 12-inch length) in sand (Figure 17). Before the experiments, the sand was soaked in concentrated hydrochloric acid overnight to minimize the influence of inorganic and organic impurities on the surface. The pretreated sand was sequentially rinsed with tap water and deionized water, then dried at 105 ˚C and stored in a glass bottle for usage. The sand was uniformly wet packed in columns according to our past procedures. The porosity of the packed columns was approximately 0.40. Before starting each experiment, 10 pore volumes (PVs) of PFCA-free background solution were eluted through the columns to reach equilibrium. The hydrodynamic properties of the sand columns were characterized via a nonreactive tracer of NaBr.

Following the tracer test, a pulse of 3 PVs of PFASs with target pH (adjusted using 0.1 M HCl and 0.1 M NaOH) and ionic strengths (adjusted by dilute NaCl and $CaCl_2$ stock solutions) was injected to columns in upward mode by a peristaltic pump (Masterflex L/S, Cole Parmer Instrument, USA) at a steady rate of 0.5 mL/min. Then, several PVs of background solution were pumped through columns at the same velocity until the background signal was detected. Effluent solutions were collected continuously in polypropylene tubes using a fraction collector (Spectra/Chrom CF-2, Spectrum Chemical Mfg. Corp., USA) and then transferred into chromatography vials for PFCA concentration quantification.

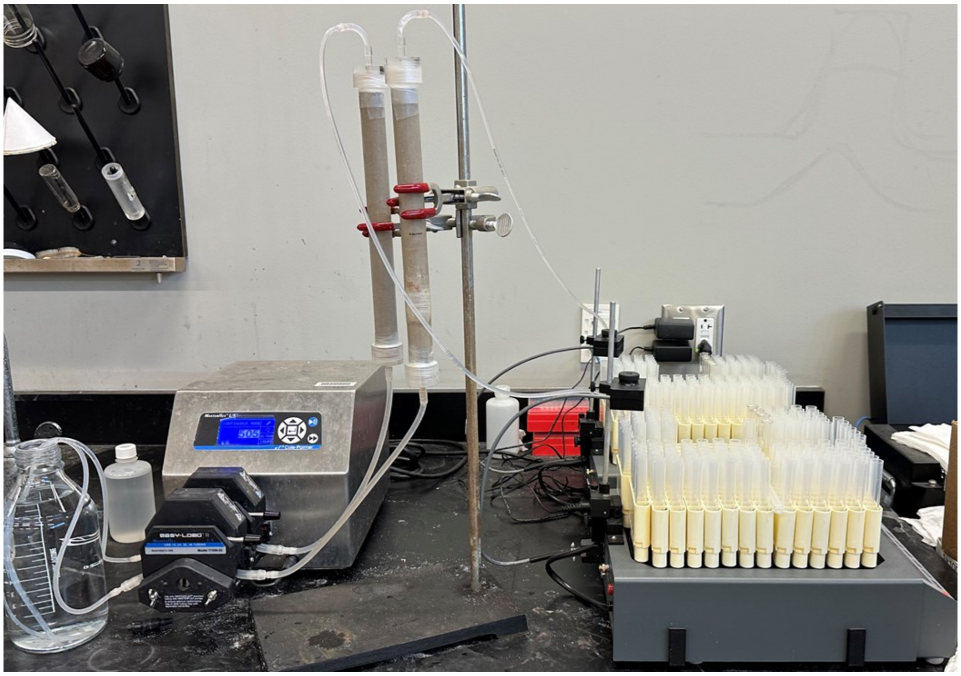

Figure 17. Saturated Column Experimental Setup

We tested four perfluoroalkyl sulfonates (PFSAs) with different carbon chain lengths, including perfluorobutanesulfonic acid (PFBS), perfluoropentanesulfonic acid (PFPeS), perfluorohexanesulfonic acid (PFHxS) and perfluorooctanesulfonic acid (PFOS) for this part of research (Table 4).

Table 4. Characteristics of Study PFASs

Chemicals	Acronym	Molecular formula	Molecular weight **(g/mol)**	CAS
Perfluorobutanes ulfonic acid	PFBS	$C_4F_9SO_3H$	300.10	375-73-5
Perfluoropentane sulfonic acid	PFPeS	$C_5F_{11}SO_3H$	350.11	2706-91-4
Perfluorohexane sulfonic acid	PFHxS	$C_6F_{13}SO_3H$	400.1	355-46-4
Perfluorooctanes ulfonic acid	PFOS	$C_8F_{17}SO_3H$	500.1	1763-23-1

Liquid samples were filtered through a 0.2 μm pore-size nylon membrane (Acrodisc, Pall Laboratory) before quantification. Then, filtered samples were analyzed by a high-performance liquid chromatography tandem mass spectrometry (LC-MS/MS) (TSQ Quantis Triple Quadrupole Mass Spectrometer, Thermo Scientific, USA) in electrospray ionization negative (ESI) mode. The chromatography was performed with an Agilent InfinityLab Poroshell 120 Bonus-RP analytical column (2.1 × 100 mm, 120 Å, 2.7 μm) and a Thermo Scientific Acclaim 120-C18 isolator column (4.6 × 100 mm, 120 Å, 5 μm). The mobile phase eluent A was water containing 2 mM ammonium acetate, 2% methanol, and 0.1% acetic acid, while eluent B was methanol containing 2 mM ammonium acetate, 2% water, and 0.1% acetic acid. Detailed information about the LC/ MS/MS system parameters is provided in Table 6 and Table 7. Bromide concentration was measured by an Ion Chromatography (IC) system (Model Dionex ICS-900, Dionex Corp., Sunnyvale, USA). The breakthrough tracer data were fitted with the convection-dispersion equation to obtain the dispersion coefficients in the media.

Table 5. HPLC Mobile Phase Gradient

Time	Mobile phase A (%)	Mobile phase B (%)
0.0	30	70
1.0	30	70
8.0	100	0
10.5	100	0
12	30	70
16	30	70

Table 6. Monitored SRM Transition

Compound	Precursor (m/z)	Product (m/z)	Collision energy (V)	RF Lens (V)
PFPeA	262.976	219.042	9	31
PFHxA	312.973	268.970	9	39
PFOA	412.966	369.042	10.23	74
PFDA	512.960	469.042	10.23	84

3.3 Unsaturated PFAS transport

PFAS transport under unsaturated conditions was evaluated using unsaturated intact column (5 cm ID × 30 cm length) (Figure 18). The column was vertically oriented, and inflow was applied from the top using a sprinkler consisting of 12 hypodermic needles (30-gauge) by a peristaltic pump (Thermo Scientific, Waltham, MA). The bottom of the column was equipped with two layers of a nylon membrane (500 mesh, 25 mm pore opening, Gilson Company, Lewis Center, OH). The nylon membrane had a bubbling pressure of -75 cm-H2O. A constant tension of -10 cm-H_2O was maintained at the bottom of the column using a hanging water column. The column itself was mounted on an electronic load-cell to monitor the overall gravimetric water content. Along the depth of the column, five time-domain reflectometry (TDR) probes and tensiometer (PX170-28DV, Omega Engineering, Inc., Stamford, CT) probes were arranged and connected to the TDR 100 system and CR-7X data logger (Campbell Scientific, Inc., Logan UT). The effluent was collected and analyzed for PFASs. The experimental setup is illustrated in Figure 19 and the actual setup is shown in Figure 20.

Figure 18. Unsaturated Column Setup

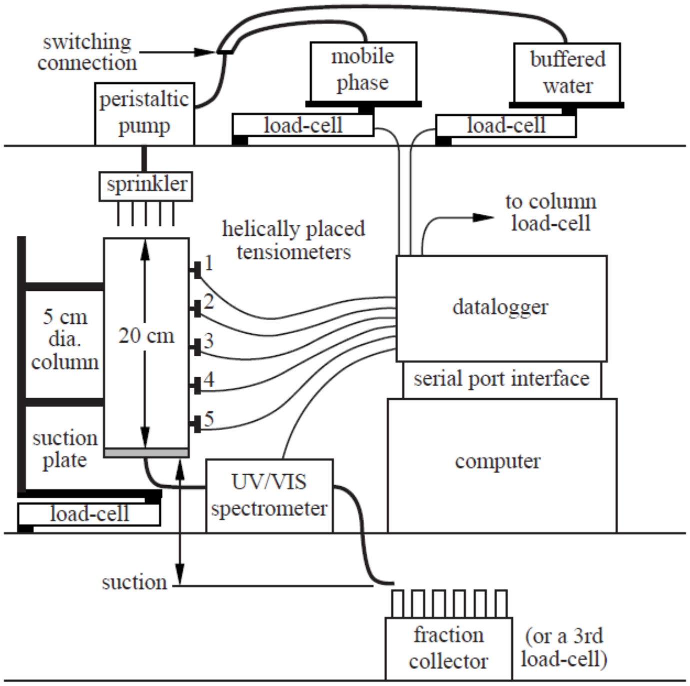

Figure 19. Unsaturated Column Experimental Design

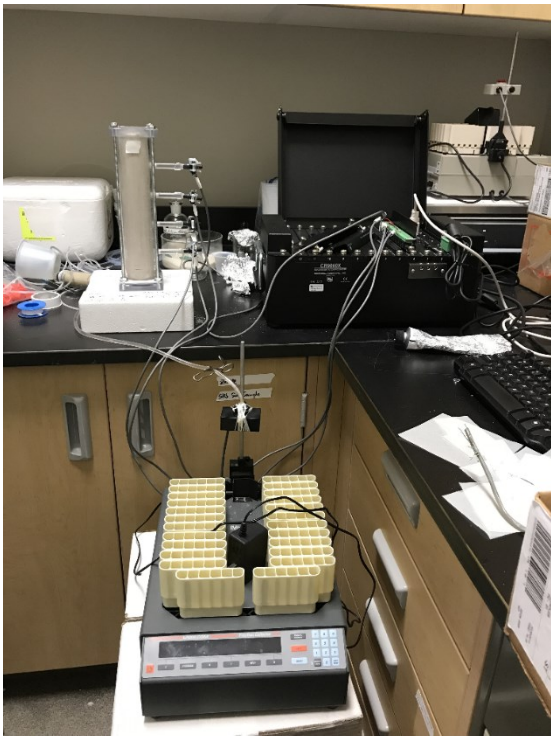

Figure 20. Unsaturated Column Experiments

The tensiometer assembly is illustrated in Figure 21. The tensiometer reading was related to the water content in the column following the van Genuchten equation (Figure 22):

$$\theta_{v,pred} = \theta_r + \frac{\theta_s - \theta_r}{[1+(\alpha h)^n]^{(1-n^{-1})}}$$

where $\theta_{v,\,pred}$ is the predicted volumetric water content, h is the measured average water suction, θ_s is the saturated volumetric water content, θ_r is the residual volumetric water content, α is the parameter that accounts the inverse of air entry suction, and n is the pore size distribution parameter.

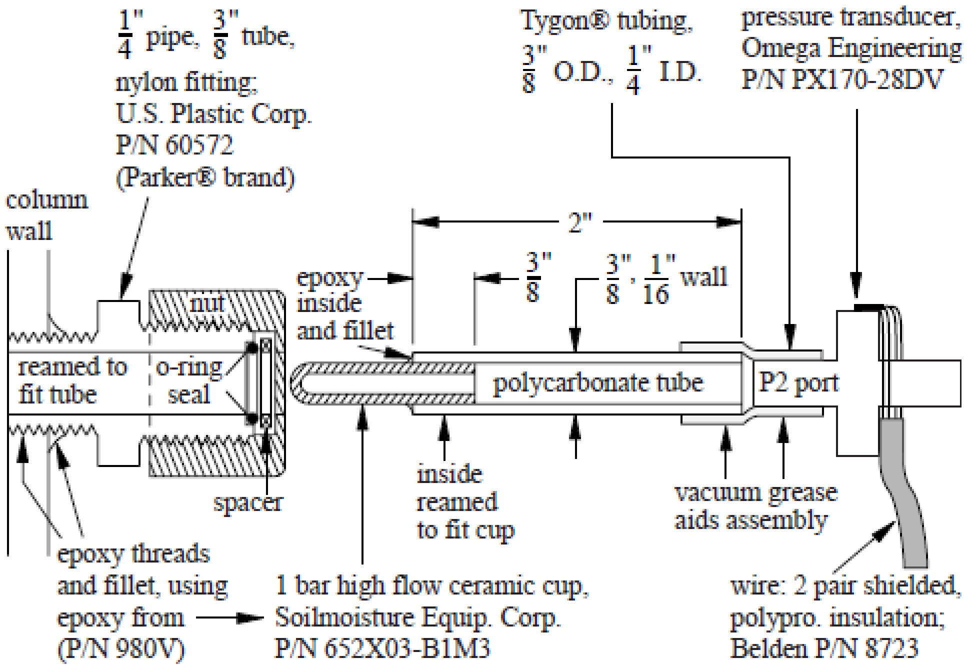

Figure 21. Tensiometer Assembly

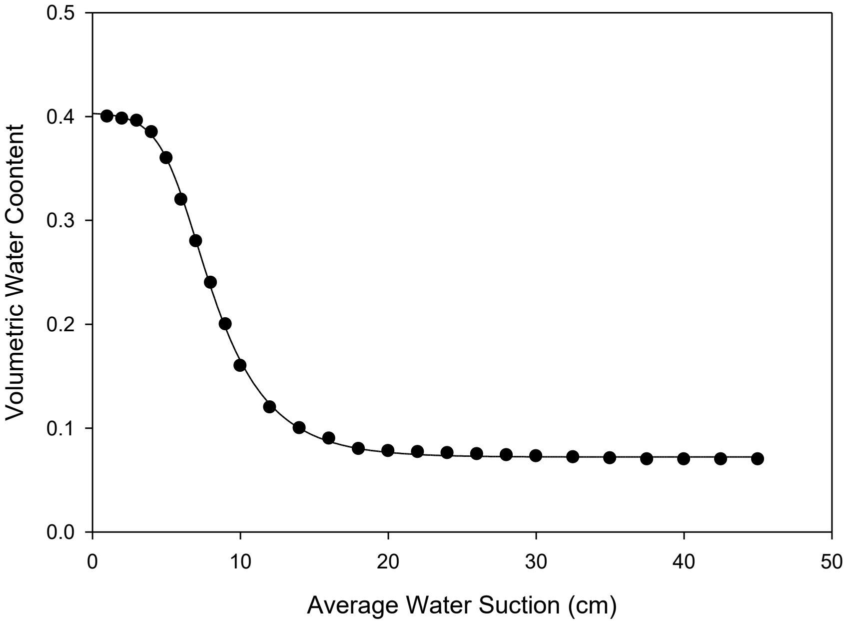

Figure 22. Water Retention Curves Simulated Using the van Genuchten Equation

At the bottom of the column, Teflon end pieces and 25 µm pore size frits (Omnit, Cambridge, UK) were used as the suction plate to retain the soil and discharge the excess liquid (Figure 23). The suction plate was designed to maintain saturated conditions to prevent gas escape from this region. The calibration of the tensiometers and pressure plate was conducted to ensure the tensiometer readings were sensitive to the moisture content change in the column (Figure 24). Under unsaturated conditions, air was trapped in the porous media. The presence of the air-water interface was important for PFAS attachment, which subsequently affected PFAS transport. The air-water interface was estimated based on the following equation:

$$S = \frac{\rho g}{\alpha \gamma} \int_{\theta}^{\theta_0} [(\frac{\theta}{\theta_0})^{\frac{n}{1-n}} - 1]^{\frac{1}{n}} d\theta$$

where S is the air-water interfacial area, ρ is the water density, g is the gravitational constant, γ is the water surface tension, and θ_0 is the porous media volume fraction of pore space.

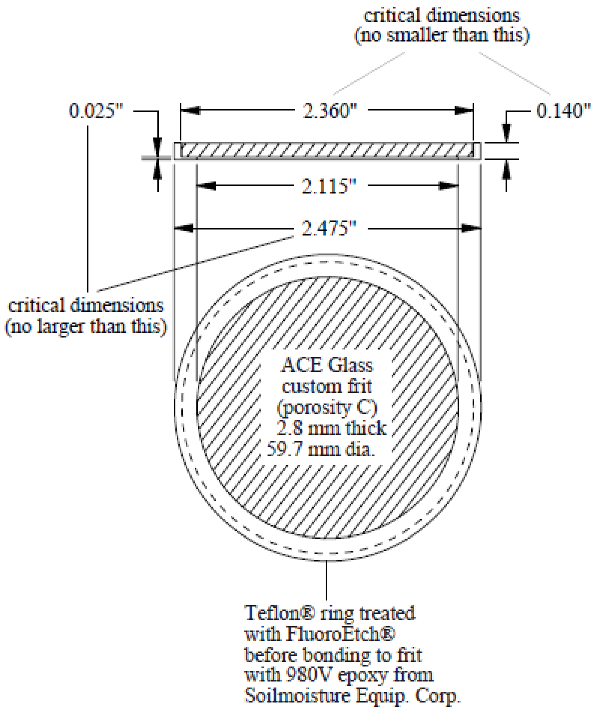

Figure 23. Suction Plate Assembly

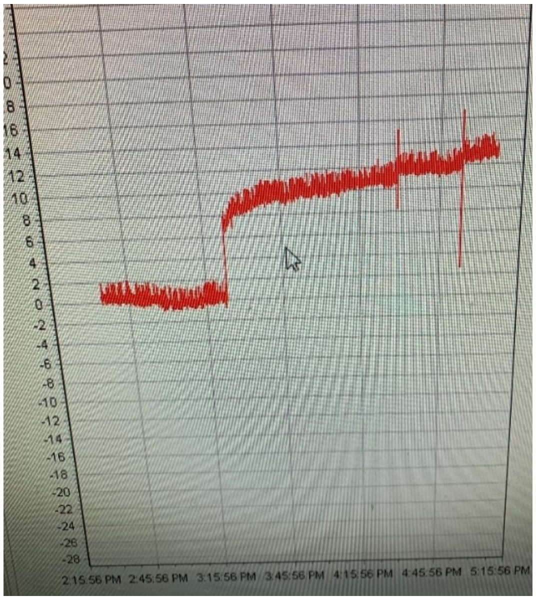

Figure 24. Tensiometer Calibration

PFPeA (Perfluoropentanoic acid, CAS 2706-90-3), PFHxA (Perfluorohexanoic acid, 307-24-4), PFOA (Perfluorooctanoic acid, CAS 335-67-1), and PFDA (Perfluorodecanoic acid, 335-76-2) were used for the unsaturated transport, which were purchased from Sigma–Aldrich (St. Louis, MO, USA). Comprehensive description of their physicochemical properties, including chemical formula, molecular weight, water solubility, and pKa is summarized in Table 9. HPLC-grade reagents (methanol and water) for liquid chromatography tandem mass spectrometry (LC-MS/MS) analysis were obtained from Fisher Scientific. All PFAS stock solutions were prepared in 50% methanol (v/v) and diluted with deionized water (~18.2 MΩ cm) to reach the final concentration of 100 μg/L.

Table 7. Physicochemical Properties of Study PFASs

Chemicals	Acronym	Molecular formula	Molecular weight (g/mol)	pKa	Water solubility (g/L)
Perfluoropentanoic acid	PFPeA	C_4F_9COOH	264.1	-0.1	120
Perfluoroheptanoic acid	PFHxA	$C_5F_{11}COOH$	314.1	-0.16	29.5
Perfluorooctanoic acid	PFOA	$C_7F_{15}COOH$	414.1	-0.2	1.74
Perfluorodecanoic acid	PFDA	$C_9F_{19}COOH$	514.1	-0.21	0.03

3.4 Cationic PFAS transport

PFASs are a diverse class of anionic, zwitterionic, and cationic compounds present in aqueous film-forming foam (AFFF) as well as other industrial and consumer applications. Although PFAS fate and transport have been extensively investigated, zwitterions and cations are typically excluded. PFASs present in landfills are diverse and include a broad array of polyfluorinated substances—particularly zwitterionic and cationic compounds. To investigate the impact of PFAS functional groups on PFAS transport, transport experiments of cationic PFASs were conducted in acrylic columns (0.75-inch diameter × 12-inch length) in sand under saturated conditions. PFASs with cationic and zwitterionic functional groups were tested. The tested PFAS information and chemical structure are presented in Table 8 and Figure 25.

Table 8. Information of Cationic and Zwitterionic PFASs

Chemicals	Acronym	Molecular formula	Molecular weight (g/mol)	CAS
Perfluorooctaneamide betaine	PFOAB	$C_{15}H_{15}F_{15}N_2O_3$	556.27	90179-39-8
Perfluorooctaneamido ammonium	PFOAAmS	$C_{14}H_{16}F_{15}N_2O^+$	513.27	45305-66-6

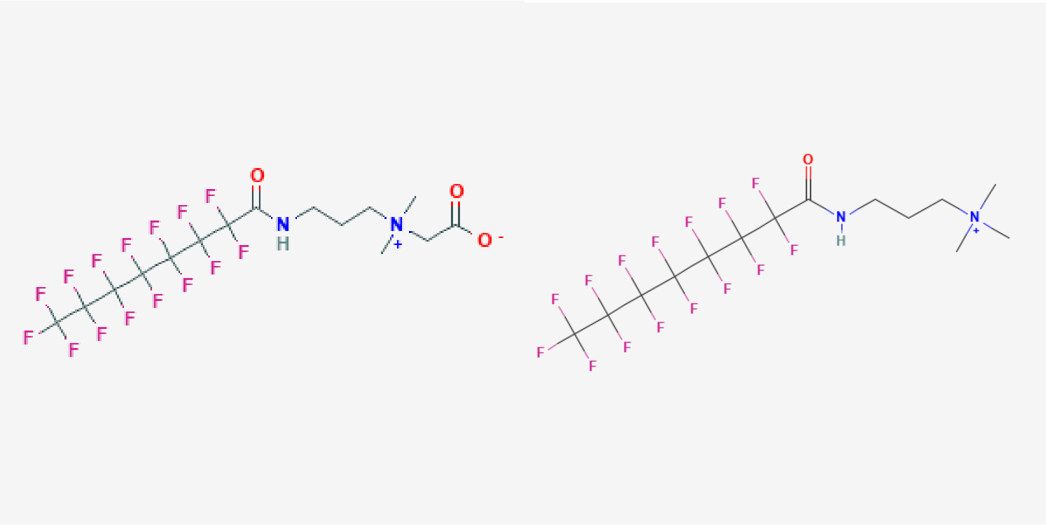

Figure 25. Chemical Structure of PFOAB (Left) and PFOAAmS (Right)

4. Results

4.1 PFAS release

Our results indicated that the concentrations of PFASs found in solid waste, including carpet, paper cups, paper plates, instant noodle bowls, and food packaging paper, were below the limit of detection (LOD). This meant PFAS levels in these wastes fell beneath the threshold for precise quantification, although several studies described the potential release of PFASs from PFAS-impregnated carpet and food packaging, with up to 33% of extractable PFASs on the surface of food contact materials. Subsequently, the PFASs in landfills were likely to have stemmed from the large volumes of the chemicals in aqueous film-forming foam (AFFF), which were used for firefighting to fight fuel-based fires. During training and response exercises, these PFAS chemicals were mainly dumped into the local landfills.

PFASs were used in many industrial and consumer applications. Aqueous film forming foam (AFFF) and other fluorinated Class B firefighting foams were another important source of PFAS to the environment. Tallahassee Fire Training Division located at 2964 Municipal Way, Tallahassee, FL is used for firefighting training programs and was formerly a part of the Dale Mabry Army Airfield, which operated from 1928 to 1961. A site assessment conducted on June 12, 2019 indicated that concentrations of perfluorooctanoate acid (PFOA) and perfluorooctane sulfonate (PFOS) in groundwater were above the provisional Groundwater Cleanup Target Level. Concentrations of PFOA and PFOS in soil were also above provisional soil cleanup target levels. These wastes from this location and other firefighting related events were deposited in the local landfills, which contributed the major PFASs in the landfill.

4.2 Transport of short-chain and long-chain PFASs

The observed breakthrough curves of two short-chain and two long-chain PFASs and nonreactive tracer transport in 10 mM NaCl solution at pH 7.2 are presented in Figure 30. The breakthrough curves of PFPeA, PFHxA, and PFOA were similar to that of the tracer, whereas PFDA was asymmetrical and displayed some delay. The column experiment results indicated that PFPeA, PFHxA, and PFOA were slightly retarded upon passing through the sand column, while PFDA exhibited enhanced retardation due to sorption to the minerals.

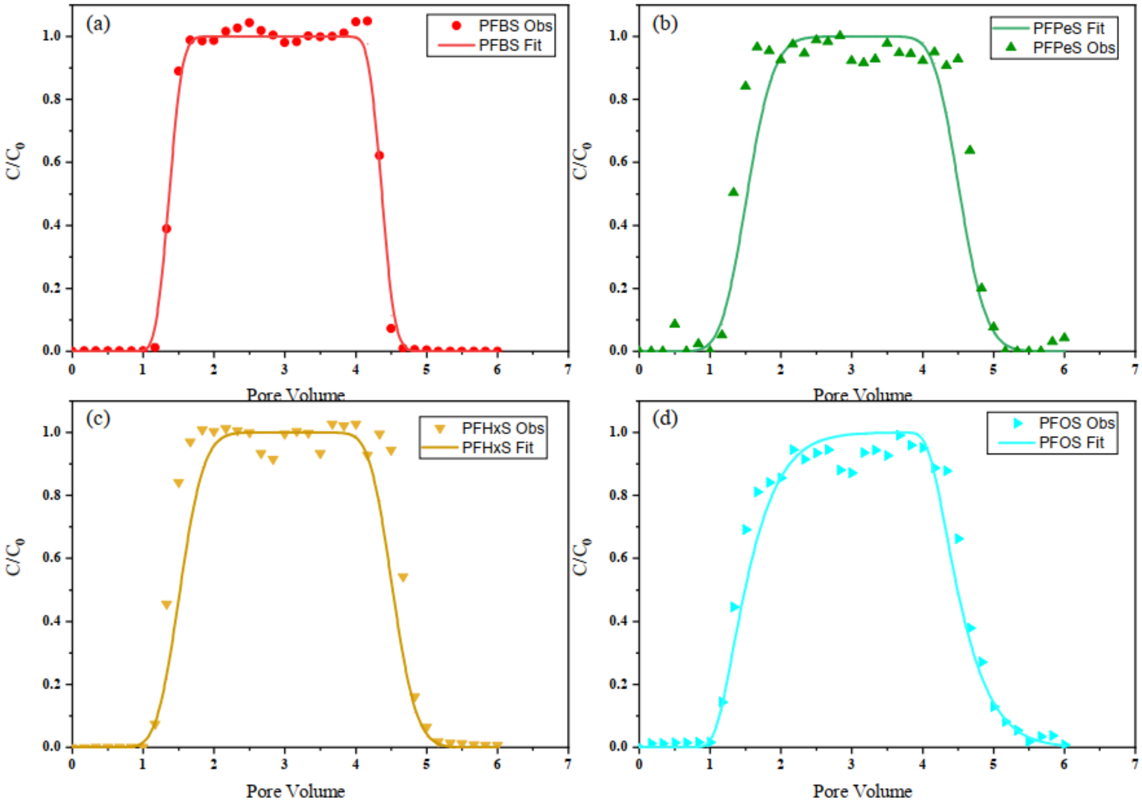

Figure 26. PFSA Breakthrough Curves

4.3 Effect of solution chemistry on PFAS transport

4.3.1 Effect of pH on PFAS transport

Under saturated conditions, the starting elution time of PFPeA, PFHxA, and PFOA slightly increased as the pH increased from 5.6 to 7.2, and then 9.2 (Figure 31). In the meantime, the normalized peak concentration of PFDA was significantly enhanced from around 0.67, 0.83, to a plateau of 0.94. The breakthrough curves in Figure 3 showed that increasing pH had a relatively minor effect on the transport of PFPeA, PFHxA, and PFOA. On the other hand, an increase in pH yielded a substantially higher migration of PFDA in saturated porous media. It is worth noting that there was a downward trend in fitted retardation factors of all PFAS with pH increased, implying that higher pH would promote the mobility of PFAS in sand columns.

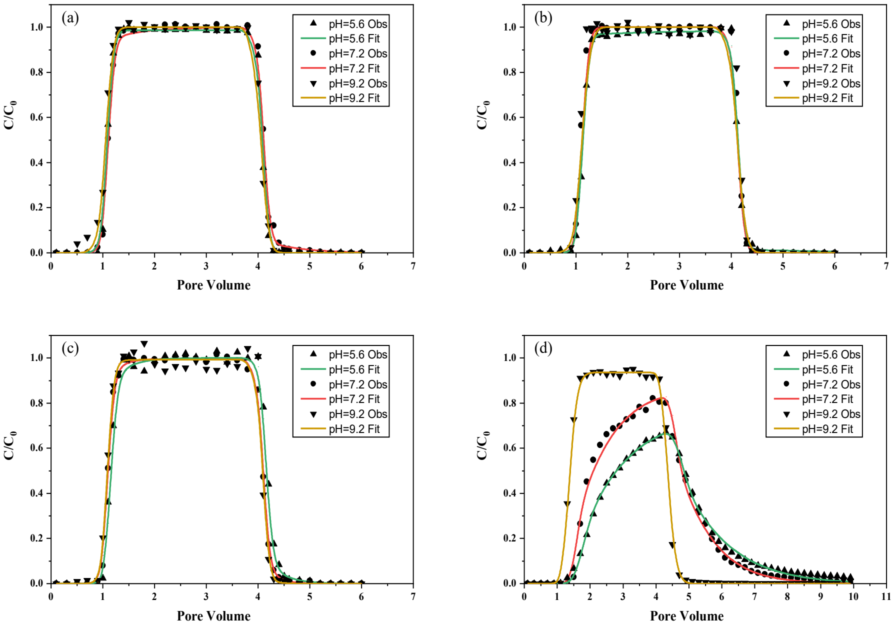

Figure 27. Breakthrough Curves of (a) PFPeA, (b) PFHxA, (c) PFOA and (d) PFDA in 10 mM NaCl at Different pH (Symbols and lines represents observed data and model fitting)

The one dimensional steady-state equilibrium convection–dispersion equation with two-site nonequilibrium transport model was used to simulate the transport of four PFASs in water-saturated sand columns (Toride et al., 1995) (Figure 32):

$$\beta R\frac{\partial C_1}{\partial T}=\frac{1}{P}\frac{\partial^2 C_1}{\partial Z^2}-\frac{\partial C_1}{\partial Z} \quad -\omega(C_1-C_2)-\mu_1 C_1$$

$$(1-\beta)R\frac{\partial C_2}{\partial T}=\omega(C_1-C_2)-\mu_2 C_2$$

where C_1 and C_2 are the dimensionless PFAS concentration in the solution and on the soil surface, respectively,β is the partition coefficient, R is the retardation factor ($R=1+\rho_b\frac{K_d}{\theta}$, where ρ_b is the media bulk density, K_d is the partition coefficient of PFASs between the solution and media, and θ is the porosity), T is the dimensionless time, P is the Peclet number ($P=\frac{vL}{D}$, where v is the interstitial pore-water velocity, L is the length of the column, and D is the dispersion coefficient), Z is the dimensionless axial coordinate, ω is the dimensionless mass transfer coefficient, and μ_1 and μ_2 are the dimensionless deposition coefficient in the solution and on the soil surface, respectively.

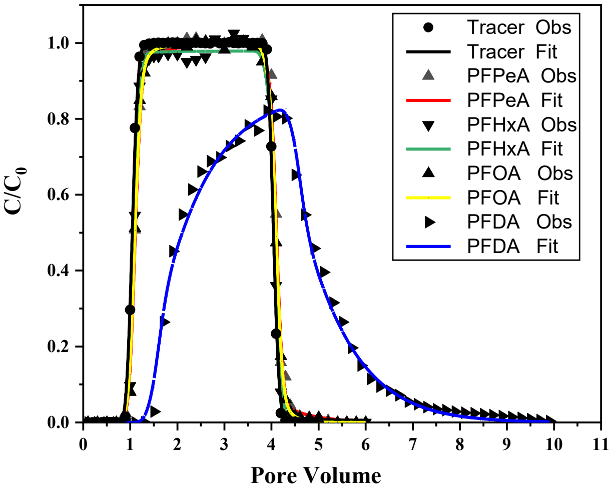

Figure 28. Breakthrough Curves of PFPeA, PFHxA, PFOA, PFDA and Tracer (Bromide) in 10 mM NaCl at pH 7.2 (Symbols and lines represents observed data and model fitting)

4.3.2 Effect of ionic strength on PFAS transport

Compared to PFPeA, PFHxA, and PFOA, the breakthrough curves of PFDA exhibited a noticeable difference under given ionic strengths (Figure 33). As the ionic strength was raised from 1 mM to 100 mM, the maximum relative effluent PFDA concentration decreased, indicating stronger retention of PFDA at high ionic strength conditions. On the other hand, PFPeA, PFHxA, and PFOA transport were less impacted by solution ionic strength than PFDA, with elution time only slightly delayed, even at higher electrolyte concentrations. This observation was attributed to the fact that electrostatic interaction was one of the main underlying mechanisms controlling PFDA's transport, but it was relatively less important in determining the transport of PFPeA, PFHxA, and PFOA in saturated sand columns.

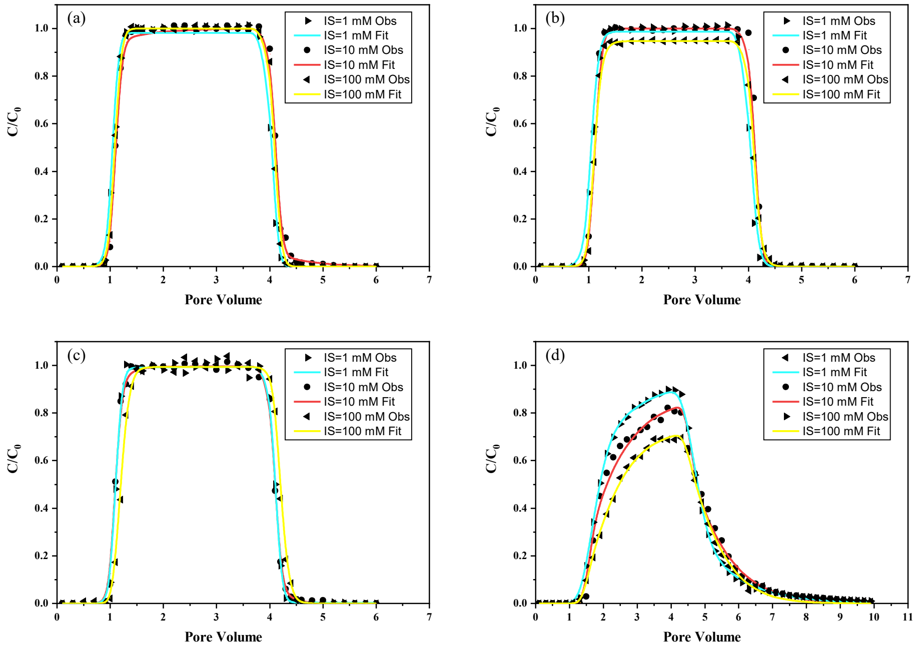

Figure 29. Breakthrough Curves of (a) PFPeA, (b) PFHxA, (c) PFOA and (d) PFDA at Different Ionic Strengths (1, 10, and 100 mM) and pH 7.2 (IS = Ionic Strength)

4.3.3 Effect of divalent cation on PFAS transport

At the same ionic strength, the transport of four PFCAs displayed retardation in $CaCl_2$ as compared to that of NaCl (Figure 34). Specifically, the relative concentration (C/C_0) plateau of PFPeA, PFHxA, and PFOA declined from approximately 1 in NaCl to 0.91, 0.95, and 0.87 in $CaCl_2$, respectively. Similarly, the maximum normalized effluent concentrations (C/C_0) of PFDA were reduced from 0.83 to 0.65 when switched from NaCl to $CaCl_2$. The results indicated that PFCAs mobility was strongly influenced by the solute.

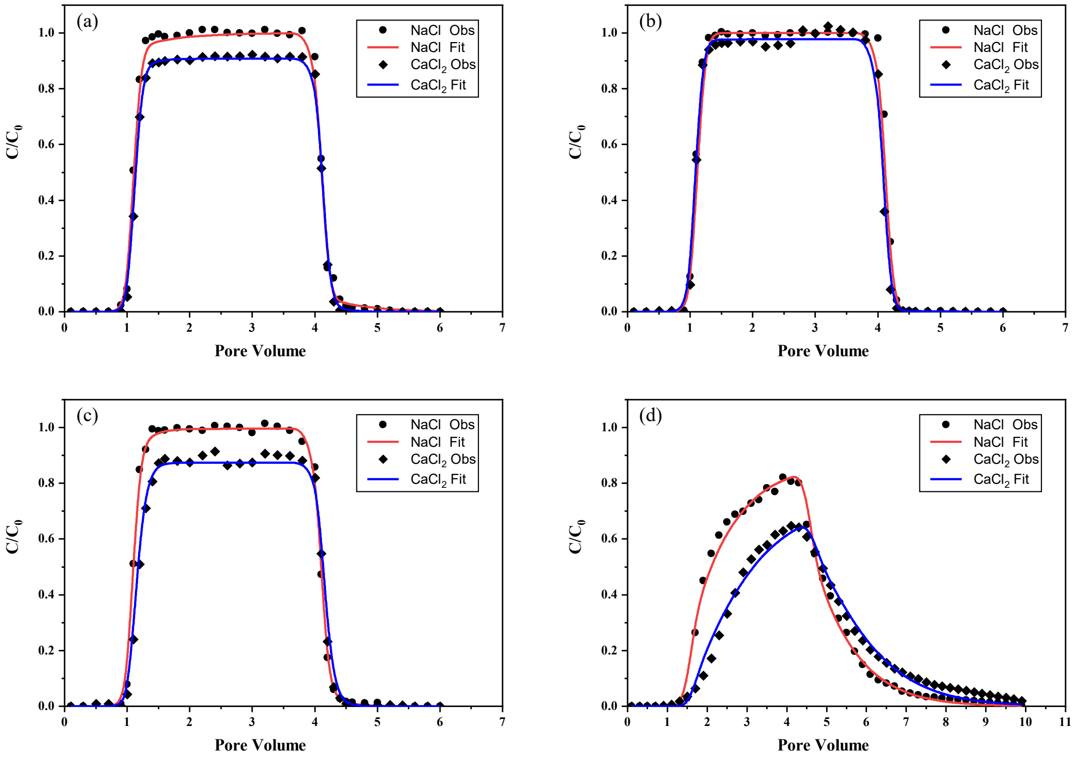

Figure 30. Breakthrough Curves of (a) PFPeA, (b) PFHxA, (c) PFOA and (d) PFDA at 10mM Ionic Strengths in NaCl and $CaCl_2$ and pH=7.2 (Symbols and lines represents observed data and model fitting)

Retardation factor was reported to be smaller for short-chain PFASs than that of long-chain PFASs (Ateia et al., 2019; Stebel et al., 2019). In addition, the solution chemistry might impact PFAS transport in terms of retardation. Specifically, when the fluorocarbon chains contained eight or less carbons, the impact of solution chemistry had minimal impact on their transport. However, when the fluorocarbon chains contained carbon numbers greater than eight, such as PFDA, the retardation became significant. In addition, the presence of the divalent cation of Ca^{2+} inhibited the transport of both short-chain and long-chain PFASs, which was more pronounced for the long-chain ones.

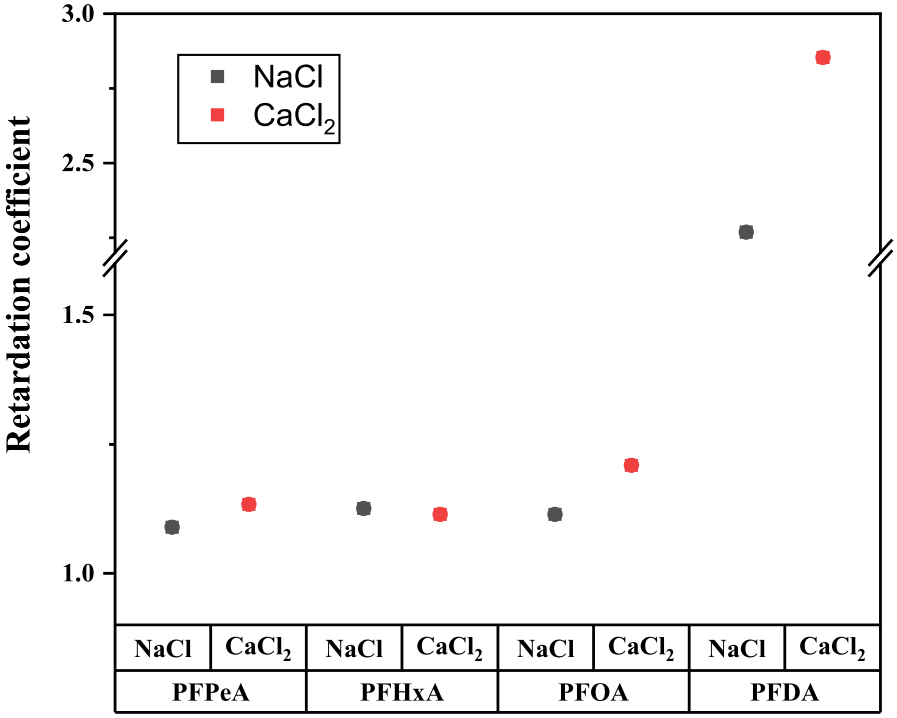

Figure 31. Retardation Factor of Four PFCAs at 10mM Ionic Strengths in NaCl and $CaCl_2$ and pH=7.2

4.4 Effect of surface coating on PFAS transport

PFASs exist in numerous ionic states (i.e., anionic, cationic, or zwitterionic). Thus, electrostatic interactions play a significant role in PFAS transport. In typical environmental conditions, many PFASs are in anionic forms, resulting in attraction to positively charged soil and sediment. Although most sediment surfaces are negatively charged, positively charged soils are common when the soil contains oxidized iron components. For this part of research, transport of PFASs in uncoated sand, iron oxide-coated sand, and manganese oxide-coated sand was investigated (Figure 36). Iron and manganese oxides are ubiquitous in soils and sediments, and their formation and conversion processes affect the migration and transformation of subsurface pollutants. Especially, Mn^{2+} was found to affect the formation of iron oxides from Fe^{2+} oxidation.

Figure 32. Uncoated Sand, Iron Oxide-Coated Sand and Manganese Oxide-Coated Sand

The observed breakthrough curves of PFOA in four PFSA compounds in uncoated sand, iron oxide-coated sand, and manganese oxide-coated sand are presented in Figure 33. It seemed that PFOA broke through uncoated sand, iron oxide-coated sand, and manganese oxide-coated sand with minimal differences. Specifically, the retention of PFOA followed manganese oxide-coated sand, iron oxide-coated sand, and uncoated sand, in the increasing order. For this part of experiment, the retention of PFOA was attributed to the electrostatic interactions between PFOA and the porous media since PFOA was negatively charged and iron oxide-coated sand and manganese oxide-coated sand were positively charged. The observations indicated that the attractive electrostatic interactions contributed to a less significant extent to PFOA retention as compared to the hydrophobic interactions attributed to the C-F chain. The results of the observations made it clear that the carbon chain, which introduced hydrophobic interaction, played an important role in the retention of PFOA in the porous media.

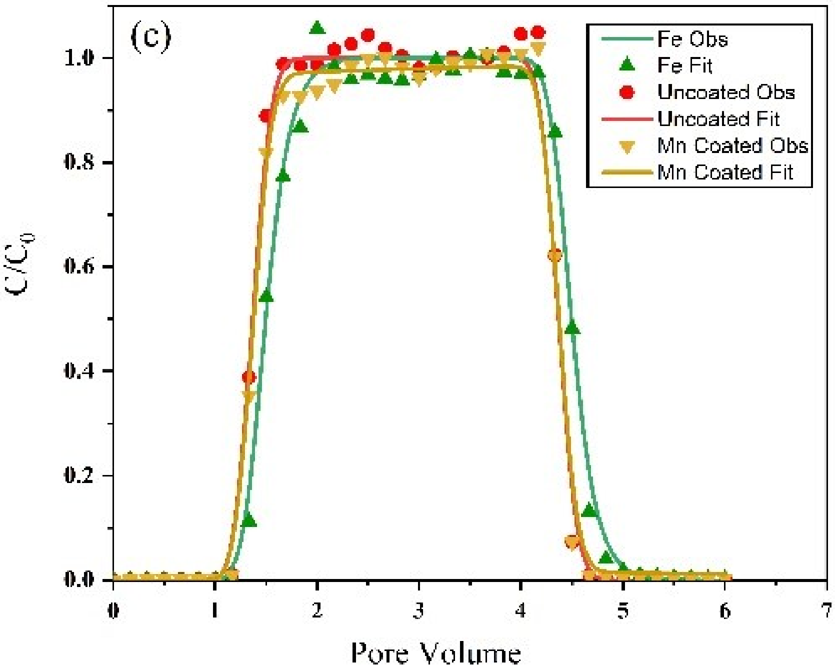

Figure 33. Breakthrough Curves of PFOA in Uncoated Sand, Iron Oxide-Coated Sand and Manganese Oxide-Coated Sand at 10mM Ionic Strengths and pH=7.2

4.5 PFAS transport under unsaturated conditions

The breakthrough curves of PFBS, PFPeS, PFHxS, and PFOS under saturated, high saturation and low saturation conditions are presented in Figure 34. Compared to saturated transport, all the study PFAS compounds exhibited different breakthrough observations corresponding to different saturation conditions.

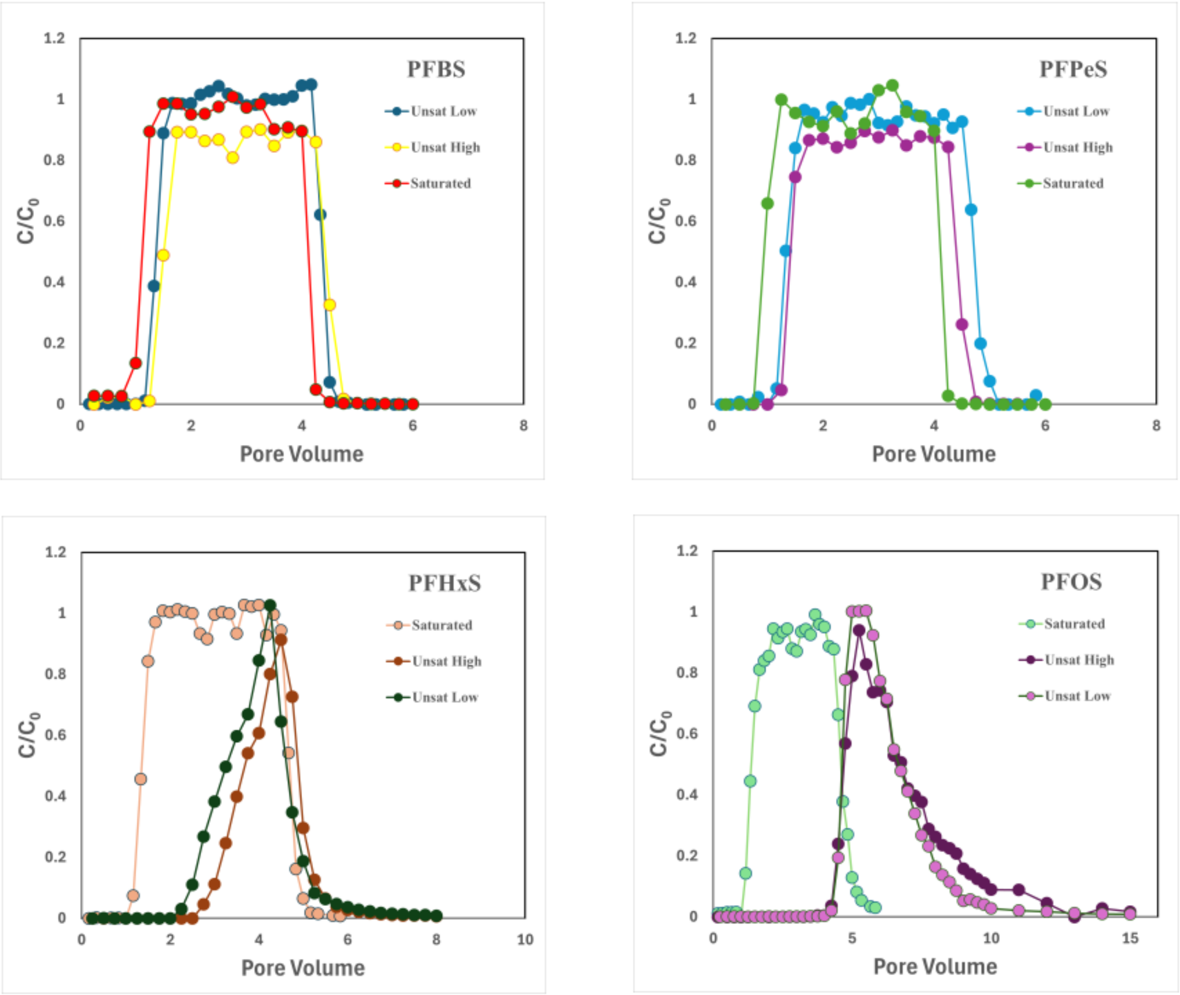

Figure 34. Breakthrough Curves of (a) PFBS, (b) PFPeS, (c) PFHxS, and (d) PFOS under Saturated, High Saturation, and Low Saturation Conditions

Under unsaturated conditions, PFBS still showed symmetric breakthrough curves. In addition, there was minimal difference of PFBS breakthrough under saturated and high saturation conditions. For instance, PFBS retention was a lit bit higher under low saturation conditions as demonstrated by the slightly lower breakthrough peaks. PFPeS had similar observations, but a slightly higher retention was observed for high saturation. Overall, the change of saturation conditions did not make significant differences for PFBS and PFPeS breakthroughs. For PFHxS and PFOS, obvious delays were observed under unsaturated conditions. In addition, by integrating the breakthrough curves, there was obvious retention of these two PFAS compounds under unsaturated conditions.

By plotting the breakthrough curves in terms of saturation, the different observations of the breakthrough of these four PFAS compounds were more obvious (Figure 35). Under saturated conditions, there was minimal difference of these four compounds (left image of Figure 35). Under high saturation conditions, breakthrough delays were observed for PFHxS and PFOS, which was more pronounced for PFOS as compared to PFHxS (right image of Figure 35). Under low saturation conditions, similarly, breakthrough delays were observed for PFHxS and PFOS with PFOS more pronounced (middle image of Figure 35). PFOS and PFHxS had the same functional group, i.e., sulfonic acid functional group, but different perfluoroalkyl chain lengths, i.e., 8C and 6C. The delays of the breakthrough curves of PFOS and PFHxS clearly indicated that the perfluoroalkyl chain length played significant roles of PFAS retention in the porous media, with enhanced effects with increased C-F chain length. The results also indicated that the impact of C-F chain length on PFAS retention started to be observed with C-F chain length greater than 6.

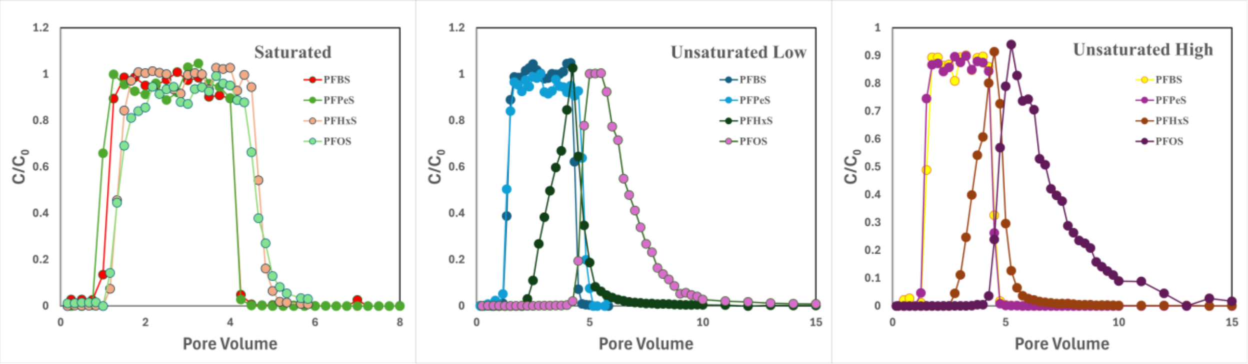

Figure 35. Breakthrough Curves of (a) PFBS, (b) PFPeS, (c) PFHxS, and (d) PFOS under Saturated, High Saturation, and Low Saturation Conditions

4.6 Impact of PFAS functional groups on their transport

Cationic (positively charged) and zwitterionic (variably charged) PFAS have not received as much attention as their anionic counterparts. Prior research showed that cationic PFAA precursor compounds, such as 6:2 fluorotelomer sulfonamidoamine (6:2 FtSaAm), and zwitterionic PFAA precursor compounds, such as fluorotelomer sulfonamido betaines (FtSaB), could be retained in porous media via electrostatic interactions when compared to anionic fluorotelomer sulfonates (FtS). Similar findings were observed for cationic perfluorooctaneamido ammonium salt (PFOAAmS) and zwitterionic perfluorooctaneamido betaine (PFOAB) when compared to PFOA. Cationic PFOAAmS and zwitterionic PFOAB and 6:2 fluorotelomer sulfonamido betaine (6:2 FTAB) were also found to adsorb more readily than their anionic counterparts PFOA and PFOS due to electrostatic interactions, which were influenced by differences in dissociation constants (pKa) of the select PFAS compounds. It was also observed that the presence of pyrogenic carbonaceous material enhanced the adsorption of cationic and zwitterionic compounds. In this research, when PFOAB was introduced to the column at 400 ppb, breakthrough ocuured at pore volume of 3, indicating an obvious delay (Figure 35).

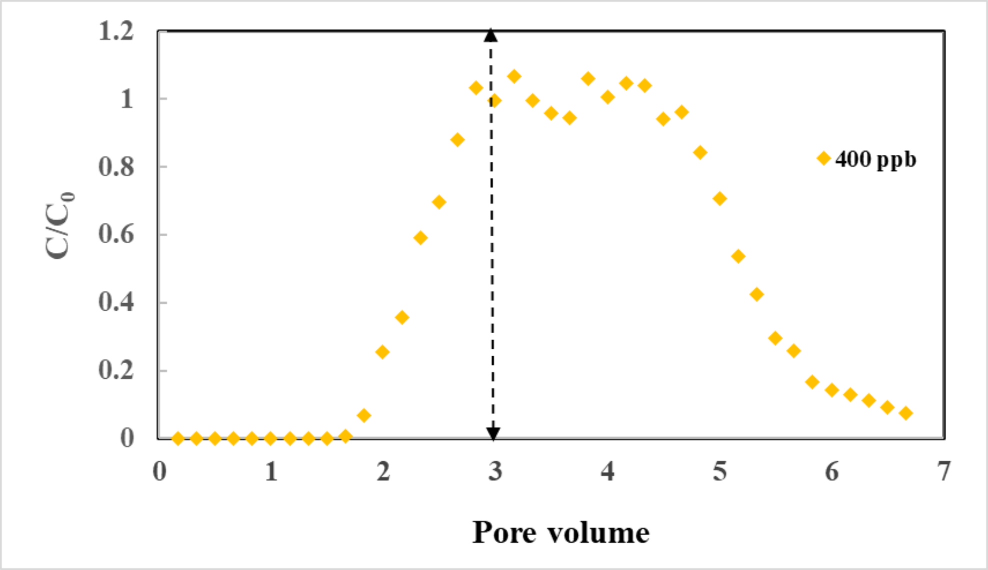

Figure 36. PFOAB Breakthrough Curve

PFOAAmS breakthrough was not observed at low concentrations. But with increased input concentrations, breakthrough started to occur (Figure 37). This was because PFASs had surfactant properties. With increased input concentration, PFASs formed micelles or hemi-micelles, which promoted PFAS transport in the form of micelles with the flowing solution, leading to advection. With no micelle formation, PFAS molecules tended to accumulate at the surface of porous media. In addition, at high concentrations, the interfacial adsorption sites were exhausted by PFAS molecules, and PFASs started to breakthrough the column in the form of micelles in the liquid phase.

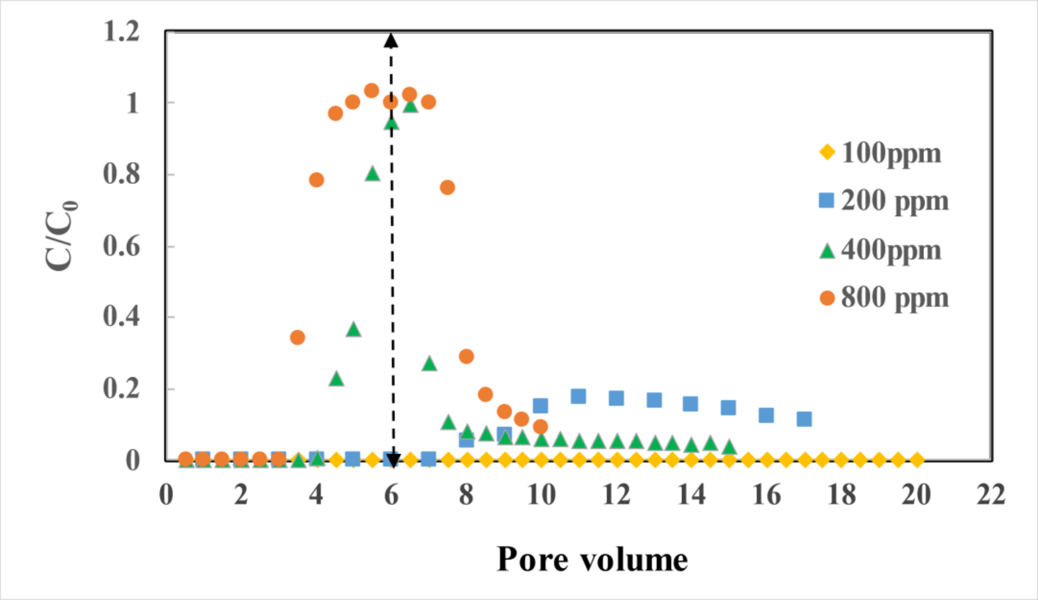

Figure 37. PFOAAmS Breakthrough Curve at Different Initiation Concentrations (i.e., 100 ppm, 200 ppm, 400 ppm, and 800 ppm)

5. Discussion

5.1 PFAS adsorption in soil matrices

In the subsurface soil, PFASs tend to absorb the soil matrices, which is attributed to the interactions between soil properties, PFAS properties, and environmental conditions. Soil properties, encompassing organic matter content, clay mineralogy, pH levels, and cation exchange capacity, exert significant influence over the extent of PFAS adsorption. PFAS properties, including their molecular structure, chain length, and functional groups, further influence their interactions with the soil environment. Environmental conditions such as temperature fluctuations, pH variations, ionic strength, and the presence of competing ions also play pivotal roles in shaping the adsorption process. These factors collectively contribute to the overall efficacy of PFAS remediation strategies within soil matrices, highlighting the importance of considering the complex interplay between soil characteristics, PFAS properties, and environmental conditions for successful mitigation efforts.

As discussed before, adsorption of PFASs can be explained by three mechanisms: 1) hydrophobic interactions of the fluorinated carbon tail with the organic carbon fraction of the sorbent, 2) electrostatic interactions of the polar head group with the sorbent charged fraction, and 3) hydrogen bonding of the acidic head group with functional groups such as carboxylic on the sorbent surfaces (Bresnahan et al., 2023; Dong et al., 2024; Lei et al., 2023; Zhang et al., 2024). Within the PFASs, carbon-fluorine chain is hydrophobic, and the functional groups (e.g., sulfonate, carboxyl, etc.) are hydrophilic. PFASs of concern, i.e., PFAAs, including PFCAs, PFSAs, perfluoroalkyl phosphonic acids (PFPAs), perfluoroalkyl phosphonic acids (PFPiAs), etc., all contain hydrophobic perfluoroalkyl chains and hydrophilic functional groups. The hydrophilic functional groups exist in equilibrium between the neutral and the anionic forms, influencing their solubility in water. Typically, the anionic form leads to greater water solubility than the neutral form.

The perfluoroalkyl chain length of PFASs largely determines their solubility, and the hydrophobic property of the perfluoroalkyl chain also make PFASs adsorb to the organic fraction of the soil matrices (Pauletto and Bandosz, 2022; Wang et al., 2021; Zhang et al., 2024). In the subsurface soil, three phases coexist, i.e., a solution phase, a solid phase, and an air phase. It should be noted that the air phase interacts with liquid and solid phases to form air-water interface, sediment-air interface, and sediment-air-water three-phase interface. Since most PFASs display amphiphilic properties owing to the hydrophobic C-F chain and a hydrophilic polar functional head group, they tend to attach to the air-water interface as well as the sediment surface in the soil matrices (Guo et al., 2020). Again, since the adsorption of PFASs to the sediment and air-water interface depends on the perfluoroalkyl chain length and functional groups, different types of PFASs would exhibit different fate and transport behaviors (Silva et al., 2022; Wallis et al., 2022).

5.2 Hydrophobic interaction

The perfluoroalkyl chain length of PFAS affects PFAS adsorption. Typically, PFASs with low perfluoroalkyl chain lengths tend to be soluble and mobile. On the contrary, PFASs with high perfluoroalkyl chain lengths tend to be insoluble and adsorbed in the subsurface soil. There is a general trend that the hydrophobicity of PFASs increases with the increase of the carbon numbers in the C-F chain and the PFAS adsorption capacity. It should be noted that although the interaction of C-F chain with water is more attractive than that of C-H chain with water, the fluorocarbon surfaces are more hydrophobic than those of the corresponding hydrocarbons because of the enhanced hydrophobicity of fluorinated surfaces (Dalvi and Rossky, 2010). The fluorocarbons have a molecular cross-section of 28.3 $Å^2$ and occupy sufficiently more volume and surface area in water than the corresponding hydrocarbons with a molecular cross-section of 18.9 $Å^2$. Subsequently, fluorocarbons pack less densely on the surface, leading to poorer van der Waals interaction with water. Long-chain PFAS are easier to adsorb than those of short-chain PFAS because of the greater decrease of the cross-section area after adsorption (i.e., greater decrease of Gibbs free energy). Branched isomers have less sorption than linear ones because of the reduction of the contact area (Brendel et al., 2018).

Recognizing the key role that the C-F chain plays in the hydrophobic interaction, theories have been developed to account for PFAS adsorption to the hydrophobic interaction free energy change in terms of the C-F chain (Cai et al., 2022a; Silva et al., 2021):

$$\Delta G_{hydrophobic} = m \cdot \Delta G_{CF_2}$$

where m is the number of carbon atoms on the C-F chain of the PFAS compound and ΔG_{CF_2} represents the hydrophobic free energy contribution of each CF_2 group. An increase in the perfluoroalkyl chain length will increase their hydrophobic interaction. The increase of the hydrophobic interaction, i.e., a greater decrease in the free energy of the hydrophobic interaction, displays a nearly linear relationship with the increase of the C-H chain (Figure 38).

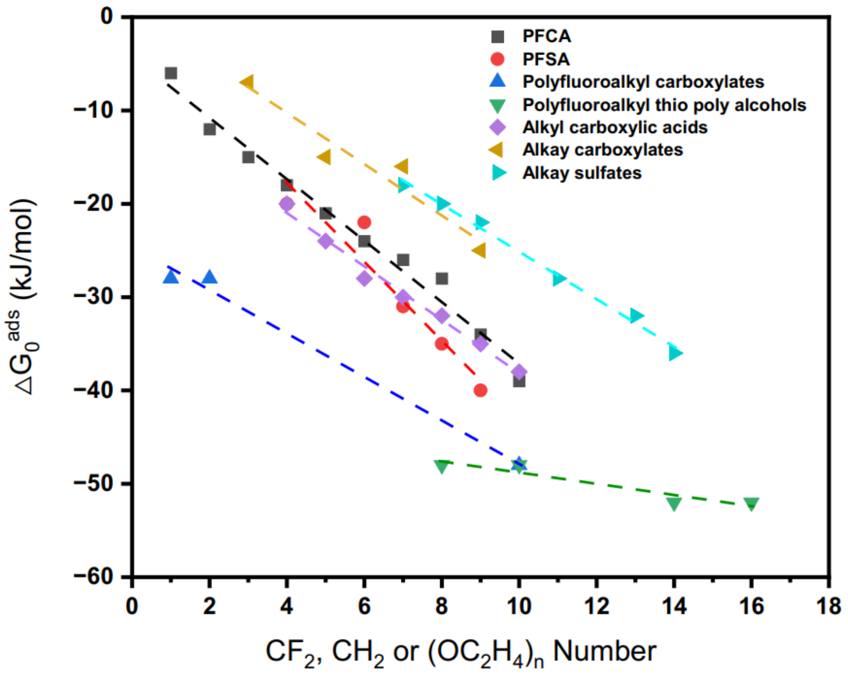

Figure 38. Free Energy Change of Hydrophobic Interaction as a Function of C-H Chain (Le et al., 2021)

The adsorption of PFASs to the organic fraction of the sediment is described by the adsorption coefficient, K_{oc}. Research demonstrated a general increase of K_{oc} with the chain length increase (Figure 39) (Anderson et al., 2019). This also indicates greater leaching potentials of short-chain PFAS under equilibrium conditions. Among PFASs, a significant difference in K_{oc} exists between PFASs with fewer than 8 perfluorinated carbons and those with 8 or more. As demonstrated in this study, PFBS and PFPeS breakthroughs were quite different from those of PFHxS and PFOS. The difference in the relative partitioning affinity of the PFASs with variable chain lengths also reflected that hydrophobicity played a key role in PFAS retention in the subsurface. In other words, the partition of PFASs to the organic fraction of the sediment controlled PFAS transport, which depended on the perfluorinated chain length. The typical K_{oc} values for typical PFASs with variable perfluorinated carbons are summarized in Table 9.

Table 9. K_{oc} Values of Typical PFASs

PFAS	Full Name	Formular	CMC (mM)	K_{oc}
PFDA	Perfluorodecanoic acid	$C_{10}HF_{19}O_2$	1.5	575.44
PFNA	Perfluorononanoic acid	$C_9HF_{17}O$	3.1	245.47
PFHpA	Perfluoroheptanoic acid	$C_7HF_{13}O_2$	9	7.94
PFPeA	Perfluoropentanoic acid	$C_5HF_9O_2$	250	0.79
PFOS	Perfluorooctanesulfonic acid	$C_8HF_{17}O_3S$	3.1	3.89×10^{-4}
PFHxS	Perfluorohexanesulfonic acid	$C_6HF_{13}O_3S$	12	3.55×10^{-4}
PFBS	Perfluorobutanesulfonic acid	$C_4HF_9O_3S$	22	1.14×10^{-4}

It should be noted that although 8 perfluorinated carbons are mentioned as the threshold between short- and long-chain PFAS, the actual threshold of perfluorinated carbons is less clear. For instance, PFOA (8 perfluorinated carbons) and PFHxS (6 perfluorinated carbons) were typically considered “long-chain” PFAS, although they partitioned to organic fractions similarly to conventional short-chain PFAS (lower than 6 perfluorinated carbons).

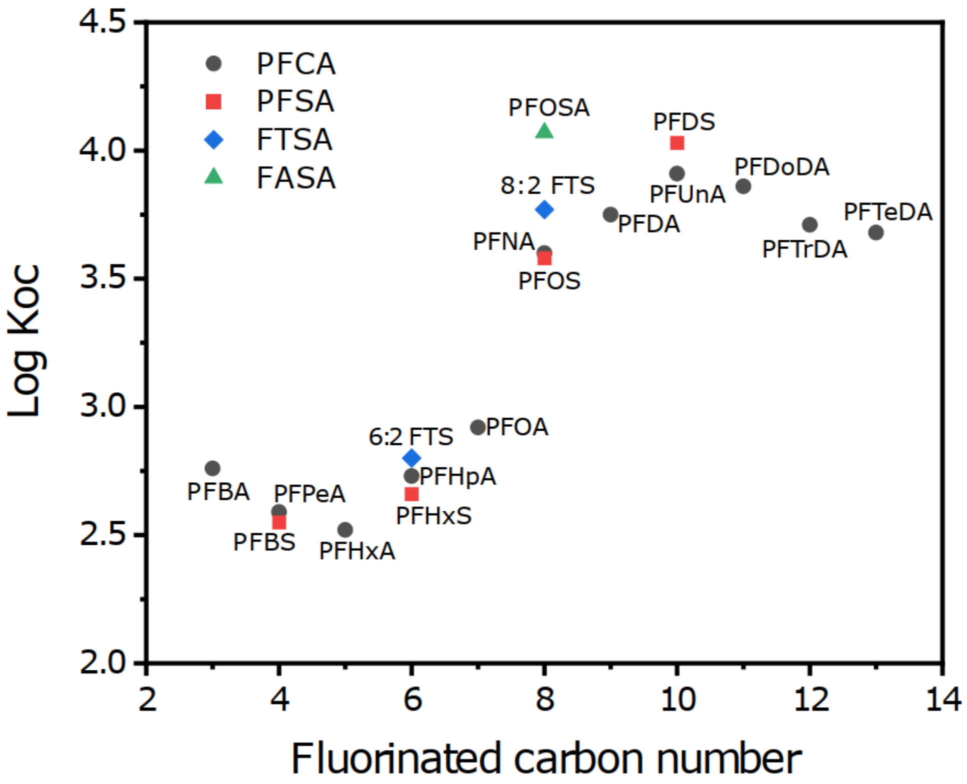

Figure 39. Log(K_{oc}) of Different PFAS (Anderson et al., 2019)

The simultaneous hydrophobicity and oleophobicity characteristics specific to perfluorinated chain compounds creates a paradoxical scenario within two-phase environments where aqueous and organic phases coexist. These attributes would counterbalance each other, yet adsorbents, particularly those of a carbon-based nature, demonstrate amphiphilic traits capable of adsorbing oleophobic PFASs. The observation of PFOS absorption on diesel oil surfaces in aqueous environments illustrates PFOS's hydrophobic dominance over its oleophobic tendencies, leading to its settlement in the organic phase despite the presence of negatively charged organic molecules. The octanol-water partition coefficient, K_{ow}, typically measures hydrophobicity. However, obtaining

K_{ow} values for PFASs via experimental methods remains challenging due to their low solubility in octanol, which poses significant challenges in developing alternative measurement techniques, especially considering PFAS's amphiphilic nature.

PFSAs partition to the organic fraction to a greater extent than PFCAs of equal C-F chain-length. To explain this observation, the strength of PFSA hydrophobic adsorption is explained by the octanol-water distribution ratio, D_{ow} (Figure 6) (Park et al., 2020):

For acids:

$$logD_{ow} = logK_{ow} - \log\left[1 + 10^{(pH - pK_a)}\right]$$

For bases:

$$logD_{ow} = logK_{ow} - \log\left[1 + 10^{(pK_a - pH)}\right]$$

where K_{ow} is the octanol/water partition coefficient, which is the measure of the distribution of dissociated and non-dissociated species in octanol and water as a function of pH, and K_a is the acid dissociation constant. When comparing the two acidic functional groups, sulfonic PFSAs have a greater hydrophobicity at the given pH (higher $logD_{ow}$) than carboxylic ones (PFCAs) with the same number of carbons, even though their octanol-water partition coefficients ($logK_{ow}$) are similar. For instance, PFOS (a PFSA compound) has a higher $logD_{ow}$ than PFOA (a PFCA compound) (i.e., $3.05 > 1.58$). Subsequently, PFSAs have more retention or are less mobile than PFCAs. It should be noted that this difference is attributed by the hydrophobicity of the C-F chain through the impact of the functional groups.

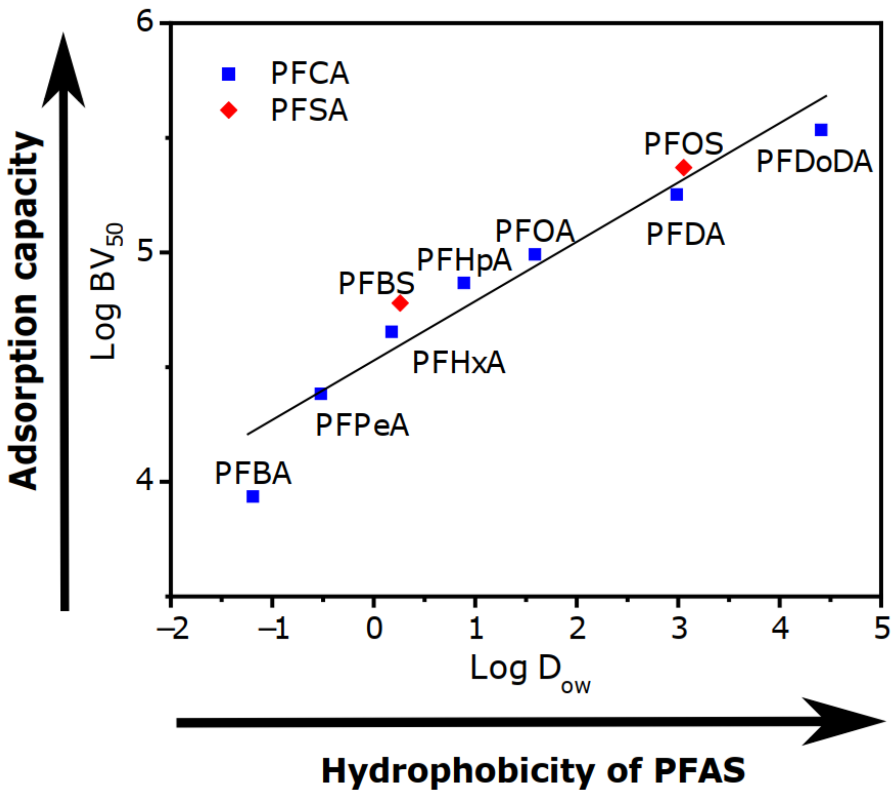

Figure 40. PFAS Adsorption Capacity and D_{ow} (Park et al., 2020)

5.3 Electrostatic interaction

The adsorption of PFASs is a function of molecular interactions between PFASs and soil matrices. The thermodynamics of PFASs and the sorbent can explain the adsorption process by quantifying the interactions during the adsorption (Cai et al., 2022b). Specifically, thermodynamics is used to characterize the driving forces, including hydrophobic interaction, electrostatic interaction, and hydrogen bonding in terms of $\Delta G_{electrostatic}$, $\Delta G_{hydrophobic}$, and $\Delta G_{hydogen}$. The total Gibbs free energy change during PFAS adsorption is thus calculated as:

$$\Delta G_{adsorption} = \Delta G_{hydrophobic} + \Delta G_{electrostatic} + \Delta G_{hydrogen\ bonding}$$

PFAS adsorption changes the system's Gibbs free energy due to the change of the surfaces (i.e., PFAS-water and sediment-water interface becomes PFAS-sediment interface by adhesion), which is related to interfacial surface tensions (Chen and Zhu, 2005; van Oss, 1994):

$$\Delta G_{adsorption} = (\gamma_{ps} - \gamma_{pl} - \gamma_{sl})A$$

where $\Delta G_{adsorption}$ is the system's Gibbs free energy change due to adhesion, γ_{ps}, γ_{pl}, and γ_{sl} are PFAS-sediment, PFAS-water, and sediment-water interfacial tensions, respectively, and A is the adhesion area. Changes in solution chemistry will lead to variations of γ_{ps}, γ_{pl}, and γ_{sl}, which eventually result in different adhesion.

The electrostatic interaction between the conjugate bases of PFASs and charges on the sediment can be calculated by (Zhao et al., 2015):

$$F^{el} = kT\sum_i (C_i(z) - C_{i,\infty}) - \frac{\varepsilon\varepsilon_0}{2}\left(\frac{d\psi}{dz}\right)^2$$

where k is the Boltzmann constant, T is the absolute temperature, $C_i(z)$ is the ion concentration for species i at distance z, $C_{i,\infty}$ is the bulk concentration of the corresponding ion, ε and ε_0 are the relative dielectric permittivity of water and permittivity under vacuum, respectively, and ψ is the surface potential. The first term is the contribution due to osmotic repulsion caused by local variation of ion concentration and the second one is due to direct electrostatic interactions, which can be attractive or repulsive depending on sediment surface charges. ψ is calculated by (Dukhin, 1993):

$$\psi = \xi\left(1 + \frac{z}{R}\right)\exp(\kappa z)$$

where z is the distance from the surface to the slip plane, R is the radius of the PFAS molecule, and $1/\kappa$ is the Debye-Hückel length, which is also an estimation of the effective thickness of the electrical double layer. κ is estimated by (Schiessl et al., 2012; Zhou et al., 2005; Zhu and Hang, 2017):

$$\kappa = \sqrt{4\pi e^2 \sum_i \frac{v_i^2 n_i^2}{\varepsilon \varepsilon_0 kT}}$$

where e is the charge of the electron, v_i is the valence of each ionic species, and n_i is the number concentration of ions of each species in the bulk liquid. ξ-potential can be quantified from its electrophoretic mobility by dynamic light scattering.

Solution chemistry is important in terms of pH and ionic strength for electrostatic interactions. At the environmental pH values, PFASs exist primarily as anions, making them potentially water-soluble (Le et al., 2021). At these pH values, PFASs likely adsorb strongly to positively charged materials by electrostatic interactions. In the subsurface, increases in pH cause minerals such as goethite and kaolinite to become negatively charged, decreasing PFAS adsorption. As pH rises, the surface charges of the affinity molecule tend to become more negative or less positive, affecting attraction or repulsion towards PFAS's negatively charged functional head. On the other hand, greater acidity increases the potential magnitude of PFAS adsorption by electrostatic attraction (Nguyen et al., 2020). Similarly, different ionic strengths lead to variable electrical double-layer thickness, and eventually electrostatic interactions between PFASs and the sorbent. Higher ionic strength leads to lower electrostatic interactions and, subsequently, less adsorption. Divalent cations like Mg^{2+} and Ca^{2+} can neutralize negative charges, promoting electrostatic attraction (Cai et al., 2022c). Moreover, interference from organic matter in clay and sediments reduces PFAS adsorption capacities due to repulsive forces generated between the adsorbent and anionic PFASs, which is linked to the drop in pH of zero point of charge (Jeon et al., 2011). Different PFASs display different adsorption under the same water chemistry conditions. For instance, PFSAs adsorb more strongly than PFCAs through electrostatic interactions.

5.4 Hydrogen Bonding

The polarity of the H−O bonds plays the key role for the formation of the hydrogen bonds as the hydrogen bonding arises from the attraction between electron-deficient hydrogen atoms (i.e., δ^+) and lone pairs of electrons on oxygen atoms (i.e., δ^-), which are sufficiently electronegative to withdraw electron density in the H−O bonds away from the hydrogen atoms, resulting in the hydrogen atoms being attracted to the lone pairs (Angelina et al., 2013; Guillaumes et al., 2014). Carboxylic acids are weak acids. Subsequently, deprotonation due to the strong stabilizing resonance formed by two oxygen atoms, releasing H^+ cations and $RCOO^-$ anions in neutral aqueous solvents such as water (Chen et al., 2016). $[H^+]_0$ deviates from the bulk concentration $[H^+]_\infty$, which is fixed by the pH, i.e., pH = $-\log[H+]_\infty$. $[H^+]_0$ is assumed to follow the Boltzmann distribution (Shear, 1973):

$$[H^+]_0 = [H^+]_\infty e^{-e\psi_0/k_B T}$$

where e is the charge of the electron, ψ_0 is the potential measured at the surface, k_B is the Boltzmann constant, and T is the absolute temperature.

The surface carboxyl functional groups favor adsorption of weak acids through formation of hydrogen-bonds. Hydrogen-bond donors (D-H) are acids (A-H, i.e., PFAS) with dissociation constant $K_a = K^0_{AH}$. Hydrogen-bond acceptors (:A) are bases (B, i.e., carboxyl functional groups) with dissociate constant $K_a = K^0_{BH^+}$ (Gilli et al., 2009; Meot-Ner, 2005):

$$AH(H_2O) + H_2O \overset{K^0_{AH}}{\Longleftrightarrow} H_3O^+(H_2O) + A^-(H_2O)$$

$$BH^+(H_2O) + H_2O \overset{K^0_{BH^+}}{\Longleftrightarrow} H_3O^+(H_2O) + B(H_2O)$$

Hydrogen bonds are formed as D-H···: A and the difference in the acidity constants, ΔpK_a, is calculated as:

$$\Delta pK_a(D - H \cdots : A) = pK_a(D - H) - pK_a(A - H^+)$$

ΔpK_a is negative or positive according to whether the $D:^- \cdots H - A^+$proton transfer occurs.

The strength of hydrogen bonds is determined by $|\Delta pK_a|$. The smaller the $|\Delta pK_a|$ is, the shorter and stronger the hydrogen bonds are. Hydrogen bonds between carboxyl functional groups and weak acids should have a $|\Delta pK_a|$ value of ~16 – 18 based on the fundamental force of dipole-dipole interactions (Gilli et al., 2009; Meot-Ner, 2005). Accordingly, the hydrogen bond strength is ~ 4 – 17 kJ/mole. The acidic head group of PFASs can form hydrogen bonding with functional groups (e.g., -NH, -OH and -COOH) on porous media.

Hydrogen bonds can be formed between PFASs and functional groups including hydroxyl, carbonyl, and carboxyl groups, etc., which commonly exist on sediment surfaces (Lutskii, 1976; Paoloni et al., 1975; Pauwels and Huyskens, 1974). The hydroxyl group, denoted by -OH, consists of a hydrogen atom covalently bonded to an oxygen atom and is present in alcohols and carboxylic acid molecules. The carbonyl group contains a covalent C=O double bond and is present in aldehydes, ketones, esters, anhydrides, and carboxylic acids. The carboxyl group is the monovalent group of -COOH, consisting of a carbonyl group bound to a hydroxyl group and is the main functional group in organic acids (i.e., carboxylic acids) (Laurence et al., 1985). Carboxylic acids also form hydrogen bonds with each other.

5.5 PFAS adhesion at the air-water interface

In water, water molecules are attracted to each other by forming hydrogen bonds, which are initiated by attractive interactions between the hydrogen atoms and the oxygen atoms (Campbell, 1952). In such systems, each water molecule has four hydrogen bonding arms, with each arm having the capacity to form a single hydrogen bond and adopt a continuum of orientations (Lu et al., 2008). The oxygen atom of a water molecule is located at the center of the symmetric tetrahedral configuration with the inter-arm angle equal to 109°. For water molecules to form hydrogen bonds with each other, the tips of two hydrogen atoms are positioned towards one oxygen atom with the length of the hydrogen bonding-arms equal to the hydrogen bond length, which is assumed to be independent of whether the water molecules are in the bulk or at the surface (Brini et al., 2017).

At the air-water interface, water molecules are subject to interactions in three directions instead of four (i.e., no interactions in the direction of the air). The thus unbalanced interactions lead to the establishment of stronger hydrogen bonds at the water surface, resulting in the formation of the surface tension, which makes the surface area as small as possible to minimize the required work (Claussen, 1967). Similarly to the air-water interface, when two different phases (i.e., gas/liquid, liquid/liquid, gas/solid, or liquid/solid) are in contact with each other, interfaces are formed. At the interfaces, the molecules experience imbalanced forces, leading to an accumulation of free energy. The excess free energy is usually quantified by the measurement of the energy to area ratio or the energy required to increase the unit area of the interface (Kuchek and Gribanova, 2007; Popov and Witten, 2001). Another way to describe the above phenomena is through interfacial tension. The interfacial tension or the excess free energy at the interface, which is also called adhesion force, is attributed to the interactions between different molecules (Kronberg et al., 2014; Miller et al., 1992).

The charge at the air-water interface is negative as measured by electrophoresis on air bubbles, which arises from an excess of OH^- as a result of the preferential orientation of water molecules at the air-water interface (Flury and Aramrak, 2017; Wan and Tokunaga, 1998). The ζ-potential of the air-water interface ranges from -110 mV at pH 10.5 to 20 mV at pH of 2 or 3 with a typical ζ-potential value of -65 mV commonly used for neutral water. There is a general trend of negative ζ-potential at higher pH and positive ζ-potential at low pH. The ζ-potential is also influenced by ionic strength. High ironic strength compresses the double layer and decreases the ζ-potential (Wan and Tokunaga, 2002). The ζ-potential plays the key role for repulsive interactions between the air-water interface and negatively charged PFASs.

The air-water interface is responsible for PFAS adhesion owing to the surfactant characteristics of PFASs, which can be explained by the thermodynamic quantification in terms of Gibbs free energy change. PFAS adhesion to the air-water interface attributes mainly to hydration forces, specific interactions in close proximity to the air-water interface, which reflect the potential bonding induced by the electron-donor (i.e., hydrogen-acceptor) and electron-acceptor (i.e., hydrogen-donor). Owing to the accumulation of OH^- groups at the air-water interface, the air-water interface serves as the electron-donor (i.e., hydrogen-acceptor) and PFASs serve as the electron-acceptor (i.e., hydrogen-donor). The hydration forces are strong enough to establish stable PFAS attachment. Moving air-water interfaces also mobilize the attached PFASs.

In the subsurface soil, the air-water interface is created by the trapped air in the pore space, which plays an important role in the fate and transport of PFASs, which serves as an extra sink to adsorb PFASs (Lazouskaya et al., 2011). The degree of adhesion at the air-water interface is controlled by PFAS hydrophobicity, solution ionic strength, and surface charges, etc. PFAS adhesion increases with the increase of C-F chain length. In addition, positively charged PFASs have strong affinity to the air-water interface since the air-water interface is negatively charged (Hanni-Ciunel et al., 2009). Similarly to adhesion of hydrophobic substances at the air-water interface, adhesion of PFASs to the air-water interface is essentially irreversible.

The air-water interface complicates the fate and transport of PFASs in the subsurface soil. Since the very specific molecular properties of the air-water interface differ from those of the bulk solution, air-water interface retains PFASs by acting like a flat hydrophobic surface. The water surface tension is influenced by pH. The electrokinetic data indicate that the isoelectric point of the air-water interface is pH 3.8, at which the air-water interface exhibits a minimum surface tension (Colussi, 2018). Also, ions are not distributed equally between the air-water interface and the bulk solution. At the air-water interface, a significantly higher concentration of ions accumulates as compared to the bulk phase, which is reflected by the ionization equilibrium constant obtained from the surface and electrokinetic potential data (D'Auria and Tobias, 2009). Specifically, hydrogen and hydroxide ions have higher tendency to accumulate at the air-water interface than in the bulk solution, with hydroxide ions being more pronounced.

At the air-water interface, free O-H groups of water account for 28% of the interfacial water (Hsieh et al., 2013; Tang et al., 2018), and lack of polarizability at the air-water interface induces the accumulation of PFASs. High ionic strength increases surface tension (Bulavin et al., 1998). In addition, anions adsorb more strongly to the air-water interface than their counterpart cations. Subsequently, electrical double layer is formed near the interface, with the anions residing in or near the topmost layer of the solution and the cations residing below the anions (Clavero and Rodriguez, 2011; Rosen and Kunjappu, 2012). The free energy changes due to anion adsorption at the air-water interface is dominated by a balance between favorable cavitation and unfavorable desolvation, which moves an anion from bulk to the air-water interface. The shift of anions also reduces the favorable interactions of the anion with the solvation shell (Casey et al., 2016). In salt solutions that contain alkali metal cations, the cations are excluded from the topmost layer

(Jungwirth and Tobias, 2002). Compared with anions, adsorption of cations is less pronounced and its effects on the air-water interface property are generally weak. However, cations affect the strength of the electrical double layer, which, in turn, influences the ion distribution at the air-water interface (Clavero and Rodriguez, 2011).

5.6 Performance of PFASs with high concentrations

Adhesion theory can also be applied to adhesion of PFASs at the air-water interface at high concentrations. PFASs preferably adsorb at the interfaces energetically, which decreases the interfacial tension. The more the PFASs are adsorbed at the interface, the greater the decrease of the interfacial tension is (Fainerman and Miller, 1995). Once the interface is saturated with PFASs, the interfacial tension will not be decreased any further. Instead, PFASs form micelles in the solution phase (Povkh et al., 1978). The self-association or micellization is initiated by the amphiphilic character of PFASs, whereby the hydrophobic portion forms the micelle core (known as normal micelle) and the polar head groups form the micelle-water interface. Micelles are formed when PFAS concentrations are greater than the critical micelle concentration (CMC), which is a function of PFAS structure, composition, temperature, ionic strength, and the presence and types of organic additives in the solution (Povkh et al., 1978).

The minimization of the unfavorable contact between nonpolar PFAS chains and the polar solvent compensates the loss of entropy by micelle formation (Lu et al., 1993). In addition to the normal micelles, inverse micelles also exist which cluster their headgroups and orient their chains towards a surrounding nonpolar phase. The interfacial activity and amphiphilic nature of the PFAS molecules render them adsorbable to the air-water interface, reducing the interfacial tension.

6. Conclusions

In this study, transport of PFASs with variable chain lengths was investigated. The transport of PFPeA, PFHxA, and PFOA were similar to that of the tracer, whereas PFDA was asymmetrical and displayed delays, indicating that PFPeA, PFHxA, and PFOA were slightly retarded upon passing through the sand column, while PFDA exhibited enhanced retardation due to sorption to the minerals. Under saturated conditions, increasing pH had a relatively minor effect on the transport of PFPeA, PFHxA, and PFOA. On the other hand, an increase in pH yielded a substantially higher mitigation of PFDA transport. Retardation factor was observed to be smaller for short-chain PFASs than that of long-chain PFASs. When the fluorocarbon chains contained eight or less carbons, the impact of solution chemistry had minimal impact on their transport. However, when the fluorocarbon chains contained carbon numbers greater than eight, such as PFDA, the retardation became significant. In addition, the presence of the divalent cation of Ca^{2+} inhibited the transport of both short-chain and long-chain PFASs, which was more pronounced for the long-chain ones.

Observation of PFAS transport in uncoated sand, iron oxide-coated sand, and manganese oxide-coated sand indicated that the attractive electrostatic interactions contributed to a less significant extent to PFOA retention as compared to the hydrophobic interactions attributed to the C-F chain. Subsequently, the C-F chain, which introduced hydrophobic interaction, played an important role in the retention of PFOA in the porous media.

Under saturated conditions, there was minimal difference of PFBS, PFPeS, PFHxS, and PFOS. Under high saturation conditions, breakthrough delays were observed for PFHxS and PFOS, which was more pronounced for PFOS as compared to PFHxS. Under low saturation conditions, similarly, breakthrough delays were observed for PFHxS and PFOS with PFOS more pronounced. The delays of the breakthrough curves of PFOS and PFHxS clearly indicated that the perfluoroalkyl chain length played significant roles of PFAS retention in the porous media, with enhanced effects with increased C-F chain length. The results also indicated that the impact of C-F chain length on PFAS retention started to be observed with C-F chain length greater than 6.

With increased input concentration, PFASs formed micelles or hemi-micelles, which promoted PFAS transport in the form of micelles with the flowing solution, leading to advection. With no micelle formation, PFAS molecules tended to accumulate at the surface of porous media. In addition, at high concentrations, the interfacial adsorption sites were exhausted by PFAS molecules, and PFASs started to breakthrough the column in the form of micelles in the liquid phase.

7. Future Work

We plan to enhance adsorption of short-chain PFASs, which will be subsequently destructed with the sorbents by hydrothermal liquefaction to break the loop of PFAS cycling in landfills. PFAS concentration will be achieved using foam fraction. In this part of research, a batch-scaled column will be set up, consisting of an acrylic column, a centrifugal pump to circulate air flow, and a peristaltic pump to introduce the co-surfactant. The foam will be formed on the top of the bulk liquid, where biochar barrier will be introduced.

PFAS-saturated biochar will be subject to hydrothermal treatment. Hydrothermal reaction will be conducted stainless steel reactors. The formation of PFAS intermediate and released F-, different groups of fluoride will be examined using LC-MS/MS, ICP-OES, and 19F NMR, respectively. Alkaline condition may accelerate the destruction process because it catalyzes the PFAS destruction by raising pH in the reactor. Carbonaceous sorbent such as biochar accelerates the process of different thermal reactions.

8. Student Training

Two graduate students, Li Qi and Shahin Alam were trained in this project. Both of these two students are currently pursuing their PhDs in our laboratory. Lin Qi started his PhD study in the fall of 2019 and has authored and co-authored more than 5 papers during his study. Shahin Alam joined our laboratory in the fall of 2023 and authored and co-authored four papers. Based on this work, Li Qi was awarded the 2023 Future Faculty Award from the Department of Civil and Environmental Engineering at FAMU-FSU college of Engineering.

9. Acknowledgements

The work was supported by the Hinkley Center for Solid and Hazardous Waste Management through Grant SUB00003896 to Florida State University. We thank Bruce Marvin (Geosyntec Consultants), Chao Zhou (Geosyntec Consultants), Kevin Warner (Geosyntec Consultants), Gary Williams (Florida Rural Water Association), Paul E. Seaver (Palm Beach Springs Water Company Inc.), Sterling Carroll (Florida Rural Water Association), Owete S. Owete (WSP USA), Natalia Soares Quinete (Florida International University), Joseph Dertien (Florida Department of Environmental Protection), Shanin Speas-Frost (Florida Department of Environmental Protection), Walsta Jean-Baptiste (Florida Department of Environmental Protection) for serving on the TAG committee. They provided invaluable advice on improving the laboratory design and data analysis.

9.1 Peer-Reviewed Journal Paper Publication:

Qi, L., Alam, S. and Chen, G., 2024, PFAS Adhesion to Porous Media: A Surface Thermodynamic Exploration, in Kash Mittal (Editor), Progress in Adhesion and Adhesives, Scrivener Publishing LLC.

Alam, S. and Chen, G., 2024, PFAS research trend, concern and removal from the environment: A review, Environmental Science and Pollution Research, under review.

Alam, S. and Chen, G., 2024, PFAS health impacts of humans and ecosystem emerging contaminants: A review, Emerging Contaminants, under review.

9.2 Conference Presentation:

Chen, G., 2024, Fate and transport of PFASs in the landfill — Impact of the perfluoroalkyl chain length, Food-Energy-Water-Climate Nexus, July 2-4, Durban, South Africa.

10. References

Adachi S., Panintrarux C., Matsuno R. (1997) Methods for Estimating the Parameters of Nonlinear Adsorption Isotherms of Langmuir and Freundlich Types from a Response Curve of Pulse Input of an Adsorbate. Biosci Biotechnol Biochem 61:1626-33. DOI: 10.1271/bbb.61.1626.

Alves A.V., Tsianou M., Alexandridis P. (2020) Fluorinated Surfactant Adsorption on Mineral Surfaces: Implications for PFAS Fate and Transport in the Environment. Surfaces 3:516-566.

Aly Y.H., McInnis D.P., Lombardo S.M., Arnold W.A., Pennell K.D., Hatton J., Simcik M.F. (2019) Enhanced adsorption of perfluoro alkyl substances for in situ remediation. Environmental Science-Water Research & Technology 5:1867-1875. DOI: 10.1039/c9ew00426b.

Anderson R.H., Adamson D.T., H.F. S. (2019) Partitioning of poly- and perfluoroalkyl substances from soil to groundwater within aqueous film-forming foam source zones. Journal of Contaminant Hydrology 220:59-65.

Angelina E.L., Duarte D.J., Peruchena N.M. (2013) Is the decrease of the total electron energy density a covalence indicator in hydrogen and halogen bonds? J Mol Model 19:2097-106. DOI: 10.1007/s00894-012-1674-y.

Ateia M., Maroli A., Tharayil N., Karanfil T. (2019) The overlooked short- and ultrashort-chain poly- and perfluorinated substances: A review. Chemosphere 220:866-882. DOI: 10.1016/j.chemosphere.2018.12.186.

Benskin J.P., Li B., Ikonomou M.G., Grace J.R., Li L.Y. (2012) Per- and polyfluoroalkyl substances in landfill leachate: patterns, time trends, and sources. Environ Sci Technol 46:11532-40. DOI: 10.1021/es302471n.

Bigler M., He X., Brusseau M.L. (2024) PFAS transport under lower water-saturation conditions characterized with instrumented-column systems. Water Res 260:121922. DOI: 10.1016/j.watres.2024.121922.

Boone J.S., Vigo C., Boone T., Byrne C., Ferrario J., Benson R., Donohue J., Simmons J.E., Kolpin D.W., Furlong E.T., Glassmeyer S.T. (2019) Per- and polyfluoroalkyl substances in source and treated drinking waters of the United States. Science of the Total Environment 653:359-369. DOI: 10.1016/j.scitotenv.2018.10.245.

Brendel S., Fetter E., Staude C., Vierke L., Biegel-Engler A. (2018) Short-chain perfluoroalkyl acids: environmental concerns and a regulatory strategy under REACH. Environmental Sciences Europe 30. DOI: ARTN 9
10.1186/s12302-018-0134-4.

Bresnahan C.G., Schutt T.C., Shukla M.K. (2023) Exploration of functionalizing graphene and the subsequent impact on PFAS adsorption capabilities via molecular dynamics. Chemosphere 345:140462. DOI: 10.1016/j.chemosphere.2023.140462.

Brini E., Fennell C.J., Fernandez-Serra M., Hribar-Lee B., Luksic M., Dill K.A. (2017) How Water's Properties Are Encoded in Its Molecular Structure and Energies. Chemical Reviews 117:12385-12414. DOI: 10.1021/acs.chemrev.7b00259.

Brusseau M.L. (2018a) Assessing the potential contributions of additional retention processes to PFAS retardation in the subsurface. Science of the Total Environment 613:176-185. DOI: 10.1016/j.scitotenv.2017.09.065.

Brusseau M.L. (2018b) Assessing the potential contributions of additional retention processes to PFAS retardation in the subsurface. Sci Total Environ 613-614:176-185. DOI: https://doi.org/10.1016/j.scitotenv.2017.09.065.

Brusseau M.L. (2019) Estimating the relative magnitudes of adsorption to solid-water and air/oil-water interfaces for per- and poly-fluoroalkyl substances. Environmental Pollution 254. DOI: UNSP 113102
10.1016/j.envpol.2019.113102.

Brusseau M.L., Guo B. (2022) PFAS concentrations in soil versus soil porewater: Mass distributions and the impact of adsorption at air-water interfaces. Chemosphere 302. DOI: 10.1016/j.chemosphere.2022.134938.

Brusseau M.L., Guo B. (2023a) Revising the EPA dilution-attenuation soil screening model for PFAS. Journal of Hazardous Materials Letters 4. DOI: 10.1016/j.hazl.2023.100077.

Brusseau M.L., Guo B. (2023b) Revising the EPA Dilution-Attenuation Soil Screening Model for PFAS. J Hazard Mater Lett 4. DOI: 10.1016/j.hazl.2023.100077.

Brusseau M.L., Van Glubt S. (2019) The influence of surfactant and solution composition on PFAS adsorption at fluid-fluid interfaces. Water Res 161:17-26. DOI: 10.1016/j.watres.2019.05.095.

Brusseau M.L., Van Glubt S. (2021) The influence of molecular structure on PFAS adsorption at air-water interfaces in electrolyte solutions. Chemosphere 281:130829. DOI: 10.1016/j.chemosphere.2021.130829.

Buck R.C., Franklin J., Berger U., Conder J.M., Cousins I.T., de Voogt P., Jensen A.A., Kannan K., Mabury S.A., van Leeuwen S.P. (2011) Perfluoroalkyl and polyfluoroalkyl substances in the environment: Terminology, classification, and origins. Integrated Environmental Assessment and Management 7:513-541. DOI: https://doi.org/10.1002/ieam.258.

Bulavin L.A., Garamus V.M., Karmazina T.V., Pivnenko E.N. (1998) Measurements of structural and electrostatic parameters and surface tension of micelles of an ionic surfactant versus concentration, ionic strength of solution and temperature by small-angle neutron scattering. Colloids and Surfaces a-Physicochemical and Engineering Aspects 131:137-144. DOI: Doi 10.1016/S0927-7757(96)03882-4.

Burgisser C.S., Cernik M., Borkovec M., Sticher H. (1993) Determination of Nonlinear Adsorption-Isotherms from Column Experiments - an Alternative to Batch Studies. Environmental Science & Technology 27:943-948.

Cai W., Navarro D., Du J., Ying G., Yang B., McLaughlin M.J., Kookana R.S. (2022a) Increasing ionic strength and valency of cations enhance sorption through hydrophobic interactions of PFAS with soil surfaces. Science of The Total Environment 817:152975.

Cai W., Navarro D.A., Du J., Ying G., Yang B., McLaughlin M.J., Kookana R.S. (2022b) Increasing ionic strength and valency of cations enhance sorption through hydrophobic interactions of PFAS with soil surfaces. Sci Total Environ 817:152975. DOI: 10.1016/j.scitotenv.2022.152975.

Cai W., Navarro D.A., Du J., Ying G., Yang B., McLaughlin M.J., Kookana R.S. (2022c) Increasing ionic strength and valency of cations enhance sorption through hydrophobic interactions of PFAS with soil surfaces. Sci Total Environ:152975.

Campbell E.S. (1952) Hydrogen Bonding and the Interactions of Water Molecules. Journal of Chemical Physics 20:1411-1420. DOI: Doi 10.1063/1.1700772.

Capozzi S.L., Leang A.L., Rodenburg L.A., Chandramouli B., Delistraty D.A., Carter C.H. (2023) PFAS in municipal landfill leachate: Occurrence, transformation, and sources. Chemosphere 334:138924. DOI: 10.1016/j.chemosphere.2023.138924.

Carter K.E., Farrell J. (2010) Removal of Perfluorooctane and Perfluorobutane Sulfonate from Water via Carbon Adsorption and Ion Exchange. Separation Science and Technology 45:762-767. DOI: Pii 920104553
10.1080/01496391003608421.

Casey J.R., Schwartz B.J., Glover W.J. (2016) Free Energies of Cavity and Noncavity Hydrated Electrons Near the Instantaneous Air/Water Interface. Journal of Physical Chemistry Letters 7:3192-3198. DOI: 10.1021/acs.jpclett.6b01150.

Chen G., Zhu H.L. (2005) Bacterial adhesion to silica sand as related to Gibbs energy variations. Colloids and Surfaces B-Biointerfaces 44:41-48. DOI: DOI 10.1016/j.colsurfb.2005.05.012.

Chen H., Zhao L.J., Wang N., Yao Y.M., Sun H.W. (2019) Aerobic biotransformation of 6:2 fluorotelomer sulfonic acid in soil. Chinese Science Bulletin-Chinese 64:3441-3448. DOI: 10.1360/Tb-2019-0126.

Chen H.C., Mai F.D., Hwang B.J., Lee M.J., Chen C.H., Wang S.H., Tsai H.Y., Yang C.P., Liu Y.C. (2016) Creation of Electron-doping Liquid Water with Reduced Hydrogen Bonds. Sci Rep 6:22166. DOI: 10.1038/srep22166.

Claussen W.F. (1967) Surface tension and surface structure of water. Science 156:1226-7. DOI: 10.1126/science.156.3779.1226.

Clavero E., Rodriguez J. (2011) Ionic liquids at the air/water interface. Journal of Molecular Liquids 163:64-69. DOI: 10.1016/j.molliq.2011.07.014.

Coffin E.S., Reeves D.M., Cassidy D.P. (2023) PFAS in municipal solid waste landfills: Sources, leachate composition, chemical transformations, and future challenges. Current Opinion in Environmental Science & Health 31. DOI: ARTN 100418
10.1016/j.coesh.2022.100418.

Coggan T.L., Moodie D., Kolobaric A., Szabo D., Shimeta J., Crosbie N.D., Lee E., Fernandes M., Clarke B.O. (2019) An investigation into per- and polyfluoroalkyl substances (PFAS) in nineteen Australian wastewater treatment plants (WWTPs). Heliyon 5. DOI: ARTN e02316
10.1016/j.heliyon.2019.e02316.

Colussi A.J. (2018) Can the pH at the air/water interface be different from the pH of bulk water? Proceedings of the National Academy of Sciences of the United States of America 115:E7887-E7887. DOI: 10.1073/pnas.1811632115.

Coppola G., Polesello S., Ferrario C., Peruzzo M., Lava R., Mazzola M. (2022) Does the partitioning of perfluoroalkyl acids to soil depend on their chain length? Integr Environ Assess Manag 18:1747-1749. DOI: 10.1002/ieam.4681.

D'Auria R., Tobias D.J. (2009) Relation between surface tension and ion adsorption at the air-water interface: a molecular dynamics simulation study. J Phys Chem A 113:7286-93. DOI: 10.1021/jp810488p.

Dalvi V.H., Rossky P.J. (2010) Molecular origins of fluorocarbon hydrophobicity. Proceedings of the National Academy of Sciences of the United States of America 107:13603-13607. DOI: 10.1073/pnas.0915169107.

de Vries P., Slijkerman D.M.E., Kwadijk C., Kotterman M.J.J., Posthuma L., de Zwart D., Murk A.J., Foekema E.M. (2017) The toxic exposure of flamingos to per- and

Polyfluoroalkyl substances (PFAS) from firefighting foam applications in Bonaire. Mar Pollut Bull 124:102-111. DOI: 10.1016/j.marpolbul.2017.07.017.

Dombrowski P.M., Kakarla P., Caldicott W., Chin Y., Sadeghi V., Bogdan D., Barajas-Rodriguez F., Chiang S.Y. (2018) Technology review and evaluation of different chemical oxidation conditions on treatability of PFAS. Remediation-the Journal of Environmental Cleanup Costs Technologies & Techniques 28:135-150. DOI: 10.1002/rem.21555.

Dong Q., Min X., Zhao Y., Wang Y. (2024) Adsorption of per- and polyfluoroalkyl substances (PFAS) by ionic liquid-modified clays: Effect of clay composition and PFAS structure. J Colloid Interface Sci 654:925-934. DOI: 10.1016/j.jcis.2023.10.112.

Dukhin S.S. (1993) Nonequilibrium Electric Surface Phenomena. Advances in Colloid and Interface Science 44:1-134.

Eriksson U., Haglund P., Karrman A. (2017) Contribution of precursor compounds to the release of per- and polyfluoroalkyl substances (PFASs) from waste water treatment plants (WWTPs). Journal of Environmental Sciences 61:80-90. DOI: 10.1016/j.jes.2017.05.004.

Fainerman V.B., Miller R. (1995) Dynamic Surface Tensions of Surfactant Mixtures at the Water-Air Interface. Colloids and Surfaces a-Physicochemical and Engineering Aspects 97:65-82. DOI: Doi 10.1016/0927-7757(94)03069-C.

Flury M., Aramrak S. (2017) Role of air-water interfaces in colloid transport in porous media: A review. Water Resources Research 53:5247-5275. DOI: 10.1002/2017wr020597.

Francis B.R., Watkins K., Kubelka J. (2017) Double Hydrogen Bonding between Side Chain Carboxyl Groups in Aqueous Solutions of Poly (beta-L-Malic Acid): Implication for the Evolutionary Origin of Nucleic Acids. Life-Basel 7. DOI: ARTN 35
10.3390/life7030035.

Furlow B. (2024) US EPA sets historic new restrictions on toxic PFAS in drinking water. Lancet Oncol 25:e181. DOI: 10.1016/S1470-2045(24)00215-8.

Gagliano E., Sgroi M., Falciglia P.P., Vagliasindi F.G.A., Roccaro P. (2020) Removal of poly- and perfluoroalkyl substances (PFAS) from water by adsorption: Role of PFAS chain length, effect of organic matter and challenges in adsorbent regeneration. Water Res 171:115381. DOI: 10.1016/j.watres.2019.115381.

Gilli P., Pretto L., Bertolasi V., Gilli G. (2009) Predicting Hydrogen-Bond Strengths from Acid-Base Molecular Properties. The pK(a) Slide Rule: Toward the Solution of a Long-Lasting Problem. Accounts of Chemical Research 42:33-44. DOI: 10.1021/ar800001k.

Gluge J., Scheringer M., Cousins I.T., DeWitt J.C., Goldenman G., Herzke D., Lohmann R., Ng C.A., Trier X., Wang Z. (2020) An overview of the uses of per- and polyfluoroalkyl substances (PFAS). Environ Sci Process Impacts 22:2345-2373. DOI: 10.1039/d0em00291g.

Guillaumes L., Salvador P., Simon S. (2014) A fuzzy-atom analysis of electron delocalization on hydrogen bonds. J Phys Chem A 118:1142-9. DOI: 10.1021/jp4119869.

Guo B., Saleem H., Brusseau M.L. (2023) Predicting Interfacial Tension and Adsorption at Fluid-Fluid Interfaces for Mixtures of PFAS and/or Hydrocarbon Surfactants. Environ Sci Technol 57:8044-8052. DOI: 10.1021/acs.est.2c08601.

Guo B., Zeng J., Brusseau M.L. (2020) A Mathematical Model for the Release, Transport, and Retention of Per- and Polyfluoroalkyl Substances (PFAS) in the Vadose Zone. Water Resour Res 56. DOI: 10.1029/2019wr026667.

Hajratwala B.R. (1982) Potential errors in determining Freundlich and Langmuir constants from adsorption isotherms. J Pharm Sci 71:125-6. DOI: 10.1002/jps.2600710133.

Hamdani S.S., Elkholy H.M., Alford A., Jackson K., Naveed M., Wyman I., Wang Y., Li K., Haider S.W., Rabnawaz M. (2024) Synthesis of Water-Dispersible Poly(dimethylsiloxane) and Its Potential Application in the Paper Coating Industry as an Alternative for PFAS-Coated Paper and Single-Use Plastics. Polymers (Basel) 16. DOI: 10.3390/polym16071006.

Hamid N., Junaid M., Sultan M., Yoganandham S.T., Chuan O.M. (2024) The untold story of PFAS alternatives: Insights into the occurrence, ecotoxicological impacts, and removal strategies in the aquatic environment. Water Res 250:121044. DOI: 10.1016/j.watres.2023.121044.

Hanni-Ciunel K., Schelero N., von Klitzing R. (2009) Negative charges at the air/water interface and their consequences for aqueous wetting films containing surfactants. Faraday Discussions 141:41-53. DOI: 10.1039/b809149h.

Herath M.B., Creager S.E., Kitaygorodskiy A., DesMarteau D.D. (2010) Effect of perfluoroalkyl chain length on proton conduction in fluoroalkylated phosphonic, phosphinic, and sulfonic acids. J Phys Chem B 114:14972-6. DOI: 10.1021/jp107190q.

Hilton W.D.W.W. (1972) Request for Toxicological Information - 'Teflon' Division Chemicals. pp. 6.

Hoisaeter A., Pfaff A., Breedveld G.D. (2019) Leaching and transport of PFAS from aqueous film-forming foam (AFFF) in the unsaturated soil at a firefighting training facility under cold climatic conditions. J Contam Hydrol 222:112-122. DOI: 10.1016/j.jconhyd.2019.02.010.

Hsieh C.S., Campen R.K., Okuno M., Backus E.H.G., Nagata Y., Bonn M. (2013) Mechanism of vibrational energy dissipation of free OH groups at the air-water interface.

Proceedings of the National Academy of Sciences of the United States of America 110:18780-18785. DOI: 10.1073/pnas.1314770110.

ITRC. (2024) Firefighting Foams.

Jeon J., Kannan K., Lim B.J., An K.G., Kim S.D. (2011) Effects of salinity and organic matter on the partitioning of perfluoroalkyl acid (PFAs) to clay particles. J Environ Monit 13:1803-10. DOI: 10.1039/c0em00791a.

Jungwirth P., Tobias D.J. (2002) Ions at the air/water interface. Journal of Physical Chemistry B 106:6361-6373. DOI: 10.1021/jp020242g.

Kancharla S., Alexandridis P., Tsianou M. (2022) Sequestration of per- and polyfluoroalkyl substances (PFAS) by adsorption: Surfactant and surface aspects. Current Opinion in Colloid & Interface Science 58:101571.

Krahn K.M., Cornelissen G., Castro G., Aro H.P.H., Asimakopoulos A.G., Wolf R.E., Holmstad R., Zimmerman A.R., Sormo E. (2023a) Sewage sludge biochars as effective PFAS-sorbents. Journal of Hazardous Materials 445:130449.

Krahn K.M., Cornelissen G., Castro G., Arp H.P.H., Asimakopoulos A.G., Wolf R., Holmstad R., Zimmerman A.R., Sormo E. (2023b) Sewage sludge biochars as effective PFAS-sorbents. J Hazard Mater 445:130449. DOI: 10.1016/j.jhazmat.2022.130449.

Kronberg B., Holmberg K., Lindman B. (2014) Surface and Interfacial Tension. Surface Chemistry of Surfactants and Polymers:231-249. DOI: Book_Doi 10.1002/9781118695968.

Kuchek E., Gribanova E.V. (2007) The acid-base characteristics of the surface of alpha-Al2O3: Potentiometry and wetting methods. Russian Journal of Physical Chemistry A 81:387-389. DOI: 10.1134/S0036024407030156.

Lang J.R., Allred B.M., Field J.A., Levis J.W., Barlaz M.A. (2017) National Estimate of Per- and Polyfluoroalkyl Substance (PFAS) Release to US Municipal Landfill Leachate. Environmental Science & Technology 51:2197-2205. DOI: 10.1021/acs.est.6b05005.

Laurence C., Berthelot M., Helbert M. (1985) The Stereochemistry of Hydrogen-Bonds on Carbonyl Groups. Spectrochimica Acta Part a-Molecular and Biomolecular Spectroscopy 41:883-892. DOI: Doi 10.1016/0584-8539(85)80220-8.

Lazouskaya V., Wang L.P., Gao H., Shi X.Y., Czymmek K., Jin Y. (2011) Pore-Scale Investigation of Colloid Retention and Mobilization in the Presence of a Moving Air-Water Interface. Vadose Zone Journal 10:1250-1260. DOI: 10.2136/vzj2011.0003.

Le S.T., Kibbey T.C.G., Weber K.P., Glamore W.C., O'Carroll D.M. (2021) A group-contribution model for predicting the physicochemical behavior of PFAS components for understanding environmental fate. Sci Total Environ 764:142882. DOI: 10.1016/j.scitotenv.2020.142882.

Lei X., Lian Q., Zhang X., Karsili T.K., Holmes W., Chen Y., Zappi M.E., Gang D.D. (2023) A review of PFAS adsorption from aqueous solutions: Current approaches, engineering applications, challenges, and opportunities. Environ Pollut 321:121138. DOI: 10.1016/j.envpol.2023.121138.

Lenard P., von Dallwitz-Wegener R., Zachmann E. (1924) Surface tension measurement, especially following the separation methods, and the surface tension of water. Annalen Der Physik 74:381-404.

Li S., Chen G. (2018) Thermogravimetric, thermochemical, and infrared spectral characterization of feedstocks and biochar derived at different pyrolysis temperatures. Waste Management 78:198-207.

Li S., Harris S., Anandhi A., Chen G. (2019) Predicting biochar properties and functions based on feedstock and pyrolysis temperature: A review and data syntheses. Journal of Cleaner Production 215:890-902.

Liu Y., Mendoza-Perilla P., Clavier K.A., Tolaymat T.M., Bowden J.A., Solo-Gabriele H.M., Townsend T.G. (2022) Municipal solid waste incineration (MSWI) ash co-disposal: Influence on per- and polyfluoroalkyl substances (PFAS) concentration in landfill leachate. Waste Manag 144:49-56. DOI: 10.1016/j.wasman.2022.03.009.

Liuzza S. (2024) History and Development of Firefighting Foams.

Lu H.G., Wang Y.K., Wu Y.B., Yang P., Li L.M., Li S.D. (2008) Hydrogen-bond network and local structure of liquid water: An atoms-in-molecules perspective. Journal of Chemical Physics 129. DOI: Artn 124512
10.1063/1.2985605.

Lu J.R., Simister E.A., Thomas R.K., Penfold J. (1993) Structure of the Surface of a Surfactant Solution above the Critical Micelle Concentration. Journal of Physical Chemistry 97:13907-13913. DOI: DOI 10.1021/j100153a074.

Lukic Bilela L., Matijosyte I., Krutkevicius J., Alexandrino D.A.M., Safarik I., Burlakovs J., Gaudencio S.P., Carvalho M.F. (2023) Impact of per- and polyfluorinated alkyl substances (PFAS) on the marine environment: Raising awareness, challenges, legislation, and mitigation approaches under the One Health concept. Mar Pollut Bull 194:115309. DOI: 10.1016/j.marpolbul.2023.115309.

Lutskii A.E. (1976) Conjugation Properties of Functional-Groups, Participating in Formation of Intramolecular Hydrogen-Bond. Zhurnal Obshchei Khimii 46:1368-1372.

Lyu Y., Brusseau M.L., Chen W., Yan N., Fu X., Lin X. (2018) Adsorption of PFOA at the air–water interface during transport in unsaturated porous media. Environ Sci Technol 52:7745-7753.

Manciu M., Ruckenstein E. (2012) Ions near the air/water interface: I. Compatibility of zeta potential and surface tension experiments. Colloids and Surfaces a-Physicochemical and Engineering Aspects 400:27-35. DOI: 10.1016/j.colsurfa.2012.02.038.

Manya J.J. (2012) Pyrolysis for Biochar Purposes: A Review to Establish Current Knowledge Gaps and Research Needs. Environmental Science & Technology 46:7939-7954. DOI: Doi 10.1021/Es301029g.

McFarlan E.L., Lemke L.D. (2024) Per- and polyfluoroalkyl substances (PFAS) fate and transport across a groundwater-surface water interface. Sci Total Environ 951:175672. DOI: 10.1016/j.scitotenv.2024.175672.

Menger F.M., Shi L., Rizvi S.A. (2009) Re-evaluating the Gibbs analysis of surface tension at the air/water interface. J Am Chem Soc 131:10380-1. DOI: 10.1021/ja9044289.

Meot-Ner M. (2005) The ionic hydrogen bond. Chemical Reviews 105:213-284. DOI: 10.1021/cr9411785.

Merino N., Qu Y., Deeb R.A., Hawley E.L., Hoffmann M.R., Mahendra S. (2016) Degradation and Removal Methods for Perfluoroalkyl and Polyfluoroalkyl Substances in Water. Environmental Engineering Science 33:615-649. DOI: 10.1089/ees.2016.0233.

Miller R., Hofmann A., Hartmann R., Schano K.H., Halbig A. (1992) Measuring Dynamic Surface and Interfacial-Tensions. Advanced Materials 4:370-374. DOI: DOI 10.1002/adma.19920040513.

Mukherjee A., Zimmerman A.R. (2013) Organic carbon and nutrient release from a range of laboratory-produced biochars and biochar-soil mixtures. Geoderma 193:122-130. DOI: 10.1016/j.geoderma.2012.10.002.

Nguyen T.M.H., Braunig J., Thompson K., Thompson J., Kabiri S., Navarro D.A., Kookana R.S., Grimison C., Barnes C.M., Higgins C.P., McLaughlin M.J., Mueller J.F. (2020) Influences of Chemical Properties, Soil Properties, and Solution pH on Soil-Water Partitioning Coefficients of Per- and Polyfluoroalkyl Substances (PFASs). Environ Sci Technol 54:15883-15892. DOI: 10.1021/acs.est.0c05705.

Niarchos G., Ahrens L., Kleja D.B., Fagerlund F. (2022) Per- and polyfluoroalkyl substance (PFAS) retention by colloidal activated carbon (CAC) using dynamic column experiments. Environmental Pollution 308. DOI: 10.1016/j.envpol.2022.119667.

Panieri E., Baralic K., Djukic-Cosic D., Buha Djordjevic A., Saso L. (2022) PFAS Molecules: A Major Concern for the Human Health and the Environment. Toxics 10. DOI: 10.3390/toxics10020044.

Paoloni L., Patti A., Mangano F. (1975) Hydrogen-Bond with Carbonyl Groups - Theoretical-Study of Correlation between X-H Stretching Frequency-Shift and C=O Group Properties. Journal of Molecular Structure 27:123-137. DOI: Doi 10.1016/0022-2860(75)85130-1.

Park M., Wu S., Lopez I.J., Chang J.Y., Karanfil T., Snyder S.A. (2020) Adsorption of perfluoroalkyl substances (PFAS) in groundwater by granular activated carbons: Roles of hydrophobicity of PFAS and carbon characteristics. Water Res 170:115364. DOI: 10.1016/j.watres.2019.115364.

Pauletto P.S., Bandosz T.J. (2022) Activated carbon versus metal-organic frameworks: A review of their PFAS adsorption performance. J Hazard Mater 425:127810. DOI: 10.1016/j.jhazmat.2021.127810.

Pauwels H., Huyskens P. (1974) Polarity of Hydrogen-Bonds on Carbonyl Groups. Bulletin of the Psychonomic Society 83:427-441.

Pinkard B., Sharp N., Strathmann T., Novosselov I., Deeb R., Major D. (2021) Bridging the gap - University, startup, and industry partnership to destroy per- and polyfluoroalkyl substance (PFAS) forever chemicals. iScience 24:102904. DOI: 10.1016/j.isci.2021.102904.

Popov Y.O., Witten T.A. (2001) Characteristic angles in the wetting of an angular region: Surface shape. European Physical Journal E 6:211-220. DOI: DOI 10.1007/s101890170003.

Povkh I.L., Kucher R.V., Shevchuk I.A., Serdyuk A.I., Vashun Z.M., Lvov V.G. (1978) Critical Micelle Concentrations of Aqueous-Solutions of a Surfactant. Journal of Applied Chemistry of the Ussr 51:1006-1009.

Qi L., Li R., Wu Y., Lin X., Chen G. (2022) Effect of solution chemistry on the transport of short-chain and long-chain perfluoroalkyl carboxylic acids (PFCAs) in saturated porous media. Chemosphere 303:135160. DOI: 10.1016/j.chemosphere.2022.135160.

Rayne S., Forest K. (2009) Congener-specific organic carbon-normalized soil and sediment-water partitioning coefficients for the C1 through C8 perfluoroalkyl carboxylic and sulfonic acids. J Environ Sci Health A Tox Hazard Subst Environ Eng 44:1374-87. DOI: 10.1080/10934520903217229.

Robey N.M., da Silva B.F., Annable M.D., Townsend T.G., Bowden J.A. (2020) Concentrating Per- and Polyfluoroalkyl Substances (PFAS) in Municipal Solid Waste Landfill Leachate Using Foam Separation. Environ Sci Technol 54:12550-12559. DOI: 10.1021/acs.est.0c01266.

Rosen M.J., Kunjappu J.T. (2012) Adsorption of Surface-Active Agents at Interfaces: The Electrical Double Layer. Surfactants and Interfacial Phenomena, 4th Edition:39-122. DOI: Book_Doi 10.1002/9781118228920.

Ross I., McDonough J., Miles J., Storch P., Kochunarayanan P.T., Kalve E., Hurst J., Dasgupta S.S., Burdick J. (2018) A review of emerging technologies for remediation of PFASs. Remediation-the Journal of Environmental Cleanup Costs Technologies & Techniques 28:101-126. DOI: 10.1002/rem.21553.

Scher D.P., Kelly J.E., Huset C.A., Barry K.M., Hoffbeck R.W., Yingling V.L., Messing R.B. (2018) Occurrence of perfluoroalkyl substances (PFAS) in garden produce at homes with a history of PFAS-contaminated drinking water. Chemosphere 196:548-555. DOI: 10.1016/j.chemosphere.2017.12.179.

Schiessl K., Babick F., Stintz M. (2012) Calculation of double layer interaction between colloidal aggregates. Advanced Powder Technology 23:139-147. DOI: 10.1016/j.apt.2011.01.005.

Schymanski E.L., Zhang J., Thiessen P.A., Chirsir P., Kondic T., Bolton E.E. (2023) Per- and polyfluoroalkyl substances (PFAS) in PubChem: 7 million and growing. Environ Sci Technol 57:16918-16928.

Sepulvado J.G., Blaine A.C., Hundal L.S., Higgins C.P. (2011) Occurrence and fate of perfluorochemicals in soil following the land application of municipal biosolids. Environ Sci Technol 45:8106-12. DOI: 10.1021/es103903d.

Shear D.B. (1973) The generalized Boltzmann distribution. J Theor Biol 39:165-9. DOI: 10.1016/0022-5193(73)90211-7.

Shimoaka T., Sonoyama M., Amii H., Takagi T., Kanamori T., Hasegawa T. (2017) Study of Perfluoroalkyl Chain-Specific Band Shift in Infrared Spectra on the Chain Length. J Phys Chem A 121:8425-8431. DOI: 10.1021/acs.jpca.7b08940.

Silva J.A.K., Martin W.A., McCray J.E. (2021) Air-water interfacial adsorption coefficients for PFAS when present as a multi-component mixture. J Contam Hydrol 236:103731. DOI: 10.1016/j.jconhyd.2020.103731.

Silva J.A.K., Simunek J., McCray J.E. (2022) Comparison of methods to estimate air-water interfacial areas for evaluating PFAS transport in the vadose zone. J Contam Hydrol 247:103984. DOI: 10.1016/j.jconhyd.2022.103984.

Simunek J., Van Genuchten M.T., Sejna M. (2005) The HYDRUS-1D software package for simulating the one-dimensional movement of water, heat, and multiple solutes in variably-saturated media. University of California-Riverside Research Reports 3:1-240.

Solo-Gabriele H.M., Jones A.S., Lindstrom A.B., Lang J.R. (2020) Waste type, incineration, and aeration are associated with per- and polyfluoroalkyl levels in landfill leachates. Waste Manag 107:191-200. DOI: 10.1016/j.wasman.2020.03.034.

Sorengard M., Ostblom E., Kohler S., Ahrens L. (2020) Adsorption behavior of per- and polyfluoralkyl substances (PFASs) to 44 inorganic and organic sorbents and use of dyes as proxies for PFAS sorption. Journal of Environmental Chemical Engineering 8:103744.

Stebel E.K., Pike K.A., Nguyen H., Hartmann H.A., Klonowski M.J., Lawrence M.G., Collins R.M., Hefner C.E., Edmiston P.L. (2019) Absorption of short-chain to long-chain perfluoroalkyl substances using swellable organically modified silica. Environmental Science-Water Research & Technology 5:1854-1866. DOI: 10.1039/c9ew00364a.

Sun M., Arevalo E., Strynar M., Lindstrom A., Richardson M., Kearns B., Pickett A., Smith C., Knappe D. (2016a) Legacy and Emerging Perfluoroalkyl Substances Are Important Drinking Water Contaminants in the Cape Fear River Watershed of North Carolina. Environ. Sci. Technol. Lett. 3:415-419.

Sun M., Arevalo E., Strynar M., Lindstrom A., Richardson M., Kearns B., Pickett A., Smith C., Knappe D.R.U. (2016b) Legacy and Emerging Perfluoroalkyl Substances Are Important Drinking Water Contaminants in the Cape Fear River Watershed of North Carolina. Environmental Science & Technology Letters 3:415-419. DOI: 10.1021/acs.estlett.6b00398.

Sun R., Babalol S., Ni R., Dolatabad A.A., Cao J., Xiao F. (2024) Efficient and fast remediation of soil contaminated by per- and polyfluoroalkyl substances (PFAS) by high-frequency heating. J Hazard Mater 463:132660. DOI: 10.1016/j.jhazmat.2023.132660.

Sundstrom M., Bogdanska J., Pham H.V., Athanasios V., Nobel S., McAlees A., Eriksson J., DePierre J.W., Bergman A. (2012) Radiosynthesis of perfluorooctanesulfonate (PFOS) and perfluorobutanesulfonate (PFBS), including solubility, partition and adhesion studies. Chemosphere 87:865-71. DOI: 10.1016/j.chemosphere.2012.01.027.

Tang F.J., Ohto T., Hasegawa T., Xie W.J., Xu L.M., Bonn M., Nagata Y. (2018) Definition of Free O-H Groups of Water at the Air-Water Interface. Journal of Chemical Theory and Computation 14:357-364. DOI: 10.1021/acs.jctc.7b00566.

Teflon™. (2024) The History of Teflon™ Fluoropolymers.

Tolaymat T., Robey N., Krause M., Larson J., Weitz K., Parvathikar S., Phelps L., Linak W., Burden S., Speth T., Krug J. (2023) A critical review of perfluoroalkyl and polyfluoroalkyl substances (PFAS) landfill disposal in the United States. Sci Total Environ 905:167185. DOI: 10.1016/j.scitotenv.2023.167185.

Toride N., Leij F., Van Genuchten M.T. (1995) The CXTFIT code for estimating transport parameters from laboratory or filed tracer experiments US Salinity Laboratory Riverside, CA.

Tuller M., Or D., Hillel D. (2004) Retention of water in soil and the soil water characteristic curve. Encyclopedia of Soils in the Environment 4:278-289.

Unice K.M., Logan B.E. (2000) Insignificant role of hydrodynamic dispersion on bacterial transport. Journal of Environmental Engineering-Asce 126:491-500. DOI: Doi 10.1061/(Asce)0733-9372(2000)126:6(491).

USEPA. (2009) Provisional Health Advisories for Perfluorooctanoic Acid (PFOA) and Perfluorooctane Sulfonate (PFOS)

USEPA. (2016) Drinking Water Health Advisories for PFOA and PFOS.

USEPA. (2023) Per- and Polyfluoroalkyl Substances (PFAS); Proposed PFAS National Primary Drinking Water Regulation.

van Oss C.J. (1994) Interfacial Forces in Aqueous Media Marcel Dekker, New York.

Viticoski R.L., Wang D., Feltman M.A., Mulabagal V., Rogers S.R., Blersch D.M., Hayworth J.S. (2022) Spatial distribution and mass transport of Perfluoroalkyl Substances (PFAS) in surface water: A statewide evaluation of PFAS occurrence and fate in Alabama. Sci Total Environ 836:155524. DOI: 10.1016/j.scitotenv.2022.155524.

Vo P.H.N., Buckley T., Xu X.Y., Nguyen T.M.H., Rudolph V., Shukla P. (2023) Foam fractionation of per- and polyfluoroalkyl substances (PFASs) in landfill leachate using different cosurfactants. Chemosphere 310. DOI: ARTN 136869
10.1016/j.chemosphere.2022.136869.

Wallis I., Hutson J., Davis G., Kookana R., Rayner J., Prommer H. (2022) Model-based identification of vadose zone controls on PFAS mobility under semi-arid climate conditions. Water Res 225:119096. DOI: 10.1016/j.watres.2022.119096.

Wan J.M., Tokunaga T.K. (1998) Measuring partition coefficients of colloids at air-water interfaces. Environmental Science & Technology 32:3293-3298.

Wan J.M., Tokunaga T.K. (2002) Partitioning of clay colloids at air-water interfaces. Journal of Colloid and Interface Science 247:54-61. DOI: 10.1006/jcis.2001.8132.

Wang F., Lu X.W., Li X.Y., Shih K.M. (2015) Effectiveness and Mechanisms of Defluorination of Perfluorinated Alkyl Substances by Calcium Compounds during Waste Thermal Treatment. Environmental Science & Technology 49:5672-5680. DOI: 10.1021/es506234b.

Wang M., Orr A.A., Jakubowski J.M., Bird K.E., Casey C.M., Hearon S.E., Tamamis P., Phillips T.D. (2021) Enhanced adsorption of per- and polyfluoroalkyl substances (PFAS) by edible, nutrient-amended montmorillonite clays. Water Res 188:116534. DOI: 10.1016/j.watres.2020.116534.

Wei C.L., Song X., Wang Q., Hu Z.H. (2017) Sorption kinetics, isotherms and mechanisms of PFOS on soils with different physicochemical properties. Ecotoxicology and Environmental Safety 142:40-50. DOI: 10.1016/j.ecoenv.2017.03.040.

Wu Y., Qi L., Chen G. (2022) A mechanical investigation of perfluorooctane acid adsorption by engineered biochar. Journal of Cleaner Production 340:130742.

Yan N., Ji Y., Zhang B., Zheng X., Brusseau M.L. (2020) Transport of GenX in Saturated and Unsaturated Porous Media. Environ Sci Technol 54:11876-11885. DOI: 10.1021/acs.est.9b07790.

Yi S., Harding-Marjanovic K.C., Houtz E.F., Gao Y., Lawrence J.E., Nichiporuk R.V., Iavarone A.T., Zhuang W.Q., Hansen M., Field J.A., Sedlak D.L., Alvarez-Cohen L. (2018) Biotransformation of AFFF Component 6:2 Fluorotelomer Thioether Amido Sulfonate Generates 6:2 Fluorotelomer Thioether Carboxylate under Sulfate-Reducing Conditions. Environmental Science & Technology Letters 5:283-288. DOI: 10.1021/acs.estlett.8b00148.

Yu H. (2020) Destruction of PFAS and Organic Co-Occurring Chemicals in Water and Soil Present in Investigation-Derived Waste Using Novel Adsorbent and Ultrasound, SERDP Project ER18-1652.

Zhang M., Zhao X.D., Zhao D.Y., Soong T., Tian S.T. (2023a) Poly- and Perfluoroalkyl Substances (PFAS) in Landfills: Occurrence, Transformation and Treatment. Waste Management 155:162-178. DOI: 10.1016/j.wasman.2022.10.028.

Zhang Y., Thomas A., Apul O., Venkatesan A.K. (2023b) Coexisting ions and long-chain per- and polyfluoroalkyl substances (PFAS) inhibit the adsorption of short-chain PFAS by granular activated carbon. J Hazard Mater 460:132378. DOI: 10.1016/j.jhazmat.2023.132378.

Zhang Y., Wang B., Ma S., Zhang Q. (2024) Adsorption of per- and polyfluoroalkyl substances (PFAS) from water with porous organic polymers. Chemosphere 346:140600. DOI: 10.1016/j.chemosphere.2023.140600.

Zhao C.L., Ebeling D., Siretanu I., van den Ende D., Mugele F. (2015) Extracting local surface charges and charge regulation behavior from atomic force microscopy measurements at heterogeneous solid-electrolyte interfaces. Nanoscale 7:16298-16311. DOI: 10.1039/c5nr05261k.

Zhou H., Preston M.A., Tilton R.D., White L.R. (2005) Calculation of the dynamic impedance of the double layer on a planar electrode by the theory of electrokinetics. Journal of Colloid and Interface Science 292:277-289. DOI: 10.1016/j.jcis.2005.05.037.

Zhu X.L., Hang C.Z. (2017) Theoretically evaluating the electric property of electric double layer at electrode/electrolyte interfaces with heterogeneous dielectric properties. 2017 International Conference on Sensing, Diagnostics, Prognostics, and Control (Sdpc):504-509. DOI: 10.1109/Sdpc.2017.101.

Zhu Y., Ro A., Bartell S.M. (2021) Household low pile carpet usage was associated with increased serum PFAS concentrations in 2005-2006. Environ Res:110758. DOI: 10.1016/j.envres.2021.110758.